Title
Low-Temperature Processing of Poly(3,4-ethylenedioxythiophene):poly(styrenesulfonate) Hydrogels for Biomedical Applications

Author
Chen, Yihang

Publication Date
2020

Peer reviewed|Thesis/dissertation

UNIVERSITY OF CALIFORNIA

Los Angeles

Low-Temperature Processing of Poly(3,4-ethylenedioxythiophene):poly(styrenesulfonate) Hydrogels for Biomedical Applications

A thesis submitted in partial satisfaction

of the requirements for the degree Master of Science

in Materials Science and Engineering

by

Yihang Chen

2020

ABSTRACT OF THE THESIS

Low-Temperature Processing of Poly(3,4-ethylenedioxythiophene):poly(styrenesulfonate) Hydrogels for Biomedical Applications

by

Yihang Chen

Master of Science in Materials Science and Engineering

University of California, Los Angeles, 2020

Professor Ximin He, Chair

There is an increasing need to develop conducting hydrogels for biomedical applications. In particular, poly(3,4-ethylenedioxythiophene):poly(styrenesulfonate) (PEDOT:PSS) hydrogels have been viewed as optimal materials due to their excellent biocompatibility, stability and softness. However, low-temperature-processable PEDOT:PSS hydrogels, which are needed for biomedical applications have rarely been reported. Such low-temperature processability grant the hydrogels with the capability to in situ engineer the seamless, chronic and strain-free biointerface.

This thesis explores the low-temperature processing of PEDOT:PSS hydrogels for biomedical applications. We first investigated the mechanism for low-temperature and room-temperature gelation of PEDOT:PSS. We demonstrated that by simply injecting the precursor via syringe at

room temperature with no additional treatment, the in situ formed PEDOT:PSS hydrogels are highly desirable for minimally invasive biomedical therapeutics with smaller footprints. We found that the room-temperature-formed PEDOT:PSS hydrogels show superior swelling properties after rehydrating, and therefore demonstrated their potential for self-healing hydrogel electronics. Fiber has favorable structures with ultrahigh aspect ratios that are useful for minimally invasive therapeutics. Advanced by the injectability of PEDOT:PSS hydrogels, we developed a facile strategy for large-scale production of injectable PEDOT:PSS hydrogel fibers at room temperature. As a potential application, we exploited the possibility of using the fabricated PEDOT:PSS hydrogel fibers as channel materials for organic bioelectronic devices, such as organic electrochemical transistors (OECTs), which have been widely used for in vivo bioelectronics studies.

The thesis of Yihang Chen is approved.

Alireza Khademhosseini

Paul S. Weiss

Ximin He, Committee Chair

University of California, Los Angeles

2020

Table of Contents

List of Figures

List of Tables

Acknowledgments

I am grateful for all the support, guidance and help that I have received at UCLA.

First and foremost, I have a lifetime debt to my parents, who support me the opportunity to choose the lifestyle that I am interested in.

I would like to express my deep thanks to Prof. Ali Khademhosseini. He gave me the opportunities to join his lab in CNSI and present on the MRS conference sharing our recent work. I am especially thankful to Dr. Shiming Zhang for his great help and guidance. His passion for science helped me to overcome many difficult moments and shaped my vision toward organic bioelectronics. I am grateful to the lab members: Hao Liu, Zhikang Li, Haonan Ling, Martin Hartel, Wujin Sun, Xingwu Zhou, Moyuan Qu, Xing Jiang, Yumeng Xue, Canran Wang, Reihaneh Haghniaz, Tyler Hoffman, Peyton Tebon, etc. Although there were ups and downs, we shared the special 2 years in Khademhosseini lab. I am thankful to Prof. Zhen Gu and his group members. As neighbor at the same chamber in CNSI, the close academic and personal interactions constantly inspired me and made the 2 years of pleasure to work in CNSI. At Stanford, I am grateful to Prof. Guosong Hong for the opportunity to work in his labs, spend 3 months with him and his group, and learn about neurotechnology. I am thankful to Prof. Ximin He and Prof. Paul Weiss for supporting my thesis.

Chapter 1 Introduction

1.1 Poly(3,4-ethylenedioxythiophene):poly(styrenesulfonate) (PEDOT:PSS) and Hydrogels for Biomedical Engineering

The birth of organic conducting polymers has led the trend in exploring their exclusive properties for a wide range of applications[1]. Poly(3,4-ethylenedioxythiophene) polystyrene sulfonate (PEDOT:PSS), with its superior biocompatibility[2,3], low impedance[4,5], water-stability[6], solution-processability[7], and commercial availability[8,9], has attracted many research groups in extensively investigating its materials properties and potential applications. With interest in combining PEDOT:PSS with contemporary electronic industry, thin film processing methods, such as spin coating, are heavily investigated for roll-to-roll large-scale fabrication. There have been ground-breaking biomedical applications of PEDOT:PSS thin films, including bioactuators[10], strain sensors[11], haptic systems[12], ion pumps[13,14], neural probe coating[15], artificial synapses[16], and organic electrochemical transistors (OECTs)[17,18]. However, since PEDOT:PSS thin film devices requires rigid or flexible substrates whose Young's moduli are significantly higher than those of brain, spinal cord, or heart tissues, such thin-film-based devices exhibit their inherit limitations considering the mechanical mismatch[19].

Hydrogels, crosslinked three-dimensional (3D) polymeric network infiltrated with water (water content > 90% by weight), have been viewed as an optimal material class in seamlessly interfacing biological tissues due to their excellent mechanical, physical and chemical resemblance[20,21]. The tissue-level softness minimizes the mechanical mismatch. Comparing to elastomers whose Young's modulus is of MPa level and polymeric films whose Young's moduli are on the scale of GPa, hydrogels have dynamic, tunable mechanical properties with extremely low Young's moduli on the scale of kPa, which is comparable to biological tissue, for example,

brain tissue (1-4 kPa)[22]. The water-rich environment not only acts as a passive buffer to maintain physiological conduction, but also offers the opportunity to encapsulate hydrophilic drugs for delivery[23]. Moreover, the structural and compositional resemblance to natural extracellular matrix (ECM) also promotes hydrogels as a unique biocompatible materials for biomedical engineering[24]. Currently, hydrogels have been successfully translated for clinical and daily usage, for example, for manufacturing contact lenses, and hygiene products[25].

Given the aims of seamlessly integrating electronics with biological tissues, the combination of the two concepts above, hydrogel bioelectronics[20] shows great potentials to solve the technical problems for offering more accurate information about how biological systems work with minimized external irritations. Biocompatible and soft conducting polymer hydrogels represent a unique class of materials which have promising applications in flexible electronics and tissue engineering[26]. Conducting polymer hydrogels not only provide a suitable microenvironment for cellular growth, but also an electrically-conductive network that allows for easy investigation of cell activity under electrical stimulation, which is particularly beneficial when studying electroactive cells like cardiomyocytes, myocytes, and neurons[27]. Conducting polymer hydrogels have already been successfully demonstrated for in vivo studies, for example, in a heart patch that restores ventricular function[28]. Among these, PEDOT:PSS-based hydrogels have been extensively investigated due to their excellent electrical properties[29] and the technical challenges in manipulating PEDOT:PSS hydrogels for biomedical applications[30].

1.2 Motivations and Objectives of this Thesis

Science fiction has always been fertile land for scientific and engineering developments. Just as *Twenty Thousand Leagues Under the Sea* foreshadowed modern submarines, books including *Do Androids Dream of Electric Sheep?* (the movie, *Blade Runner*) and *Ghost in the Shell*, act as beacons for contemporary research interests. As an advanced form of human and artificial

component interaction, the interpretation of biointerfacing gradually shifts from simply adding materials to structurally support biological organs[31], for example, implanting metallic prosthesis, onto a more comprehensive concept, *cyborg*[32], where organisms and non-living machines could also be functionally bridged. Started by Italian scientist Luigi Galvani, electric, as a promising modality in either modulating or interrogating biological tissues, has been profoundly researched for two centuries[33]. Currently, building on the solid pre-knowledge on electrical engineering, bioengineering, and neuroengineering, an emerging field, bioelectronics, is rising as the biological-signal-transducer that interrogates or modulate cellular behaviors[34]. As one of the most important components, conductor is the key materials for realizing such seamlessly interfacing bioelectronics. Considering the mechanical and physiological requirements of targeted tissues to be interfaced, conducting polymer hydrogels, especially PEDOT:PSS hydrogels, are considered as more ideal chronic interfacing alternatives to biological tissues because of their water-rich nature and tissue-like mechanical properties. However, the resemblances to biological tissues accompany with technical issues. For example, to access the electrode to targeted tissue, traditionally the electrodes, such as tungsten probe[35], Michigan probe[36], Utah array[37], and Neuropixels[38], could be directly inserted into specific brain region after removing the scalp, since the electrode itself is stiff enough to penetrate the biological tissue. While granted as an overwhelming strength for minimizing the irritation during chronic interfacing, the extreme softness of hydrogels also becomes a lethal limitation for delivering them into body. One approach in tactically circumventing this issue would be locally synthesizing PEDOT:PSS *in vivo*[39]. On the contrary to conventional methods where the electronic devices, such as cuff electrodes[40], are pre-formed and then transfer to the targeted region and forcing the devices to comply to local geometry, *in situ* fabrication of PEDOT:PSS-based devices could not only minimize the inner strains of the interfacing device, preventing material detachment during “micromotions” during

body movements[41], but also potentially offer cell-type specificity in physically distinguishing the source of metabolic signals by specifically binding to targeted cells[42,43].

To gain the capability in patterning PEDOT:PSS hydrogels *in vivo*, the major challenges are that the synthesis conditions should be compatible with physiological surroundings. Among the aspects which could be toxic, temperature is one of the most important dimensions for forming a seamless biointerface. While most chemical or physical reactions require high temperature to decrease the Gibbs free energy and therefore thermodynamically driving the process, or kinetically accelerating the processes to result in the macroscopic phase change, the biological tissues could not tolerate high temperature, due to their temperature sensitivity. Hyperthermia kills the cells during exposure following the exponential trend depending on the temperature and length of exposure, resulting in additional trauma during therapeutics[44]. Meanwhile, such cytotoxicity of hyperthermia has also been actively utilized as a tool in cancer treatment, implying its significant damage to biological tissues[45]. Given the rapid growth of hydrogel bioelectronics, the administration of temperature would be a key concern to promote their integration with biological systems.

The primary objective of this thesis is to design, modify, and utilize PEDOT:PSS hydrogels that could seamlessly interface human with minimized irritations on normal metabolisms for biomedical engineering. Working toward this objective, it is of paramount importance to investigate the process of PEDOT:PSS hydrogels to achieve room-temperature-processability, injectability, and healability to develop next-generation hydrogel bioelectronics. Therefore, the main specific objectives of this thesis are:

(1) Processing PEDOT:PSS hydrogels at room temperature. By eliminating the need for elevating the temperature, approaches in realizing room-temperature-formed PEDOT:PSS hydrogels (RT-PEDOT:PSS hydrogels) are essential for enabling next-generation bioelectronics.

(2) Exploring the potentials of RT-PEDOT:PSS hydrogels for biomedical engineering in various scenarios. Considering the delivery process, since the hydrogels are of tissue level softness, it would be ideal if they could be simply injected into targeted area. Moreover, especially for the brain study where the access for further manipulation of the implanted devices is limited, it would be desirable to investigate and modify the RT-PEDOT:PSS hydrogels by granting them the capabilities to adjust the severe conditions *in vivo* and to heal on their own.

(3) Functionalizing RT-PEDOT:PSS hydrogels by fabricating hydrogel bioelectronics. Currently, most researches about hydrogels are merely limited to material level, however, to fully functionalize the biointerface, device-level applications are of significant importance.

In Chapter 2, the conducting mechanism, the thin film properties, and typical additives of PEDOT:PSS were illustrated to provide an objective-oriented background knowledge for this thesis. We then discussed the history, the approaches, and the temperature applied of PEDOT:PSS hydrogel synthesis. With the intention to achieve device-level hydrogel applications, OECTs, which has been widely used for *in vivo* bioelectronics studies, were discussed according to its working mechanism and typical applications.

Chapter 3 and 4 were extracted from the article:

Shiming Zhang,* **Yihang Chen**, Hao Liu, Zitong Wang, Haonan Ling, Changsheng Wang, Jiahua Ni, Betul Celebi Saltik, Xiaochen Wang, Xiang Meng, Han-Jun Kim, Avijit Baidya, Samad Ahadian, Nureddin Ashammakhi, Mehmet R. Dokmeci, Jadranka Travas-Sejdic, and Ali Khademhosseini*, Room-Temperature-Formed PEDOT:PSS Hydrogels Enable Injectable, Soft, and Healable Organic Bioelectronics, Advanced Materials, 2019, 1904752 (co-first author) [46].

In Chapter 3, the material-level researches on RT-PEDOT:PSS hydrogels were discussed. After evaluating the ability of room-temperature spontaneous gelation, we characterized the hydrogels for their mechanical robustness and biocompatibility. To further explore their potential in various

scenarios, we discussed RT-PEDOT:PSS hydrogels for injectable and healable biomedical engineering.

In Chapter 4, the large-scale production of RT-PEDOT:PSS hydrogel fibers as well as their capability in fabricating hydrogel bioelectronics, hydrogel-based OECTs were represented. By simply syringe-injecting one segment of RT-PEDOT:PSS hydrogel fibers between two metallic electrodes, followed by freezing drying, the OECTs could be fabricated and functionalize with high transconductance.

In Chapter 5, the conclusion of this thesis was summarized. A comprehensive outlook toward hydrogel bioelectronics for biomedical applications was discussed toward their promising developments in the future.

Chapter 2 Literature Review

2.1 Poly(3,4-ethylenedioxythiophene):poly(styrenesulfonate)

Since Shirakawa et al. reported the first highly electrically conductive iodine-doped polyacetylene[1], conducting polymers have drawn significant attentions due to their advantageous mechanical flexibility, cost-effectiveness and biocompatibility, which make them preferable materials for flexible electronics and biomedical sensors[47]. In the past years, we have witnessed the rapid development of different conducting polymers and their derivatives[48], for example, polyacetylenes (PA) and polydiacetylens (PDA), poly(paraphenylene) (PPP), polyfluorenes (PF), poly(paraphenylene vinylene) (PPV), polythiophenes (PTh), conjugated polymers containing N and Si, and conjugated small molecules, such as pentacene. Among these branches, polypyrrole (PPy), PTh, polyaniline (PANi) are the iconic materials that are frequently investigated due to their relatively good stability in air.

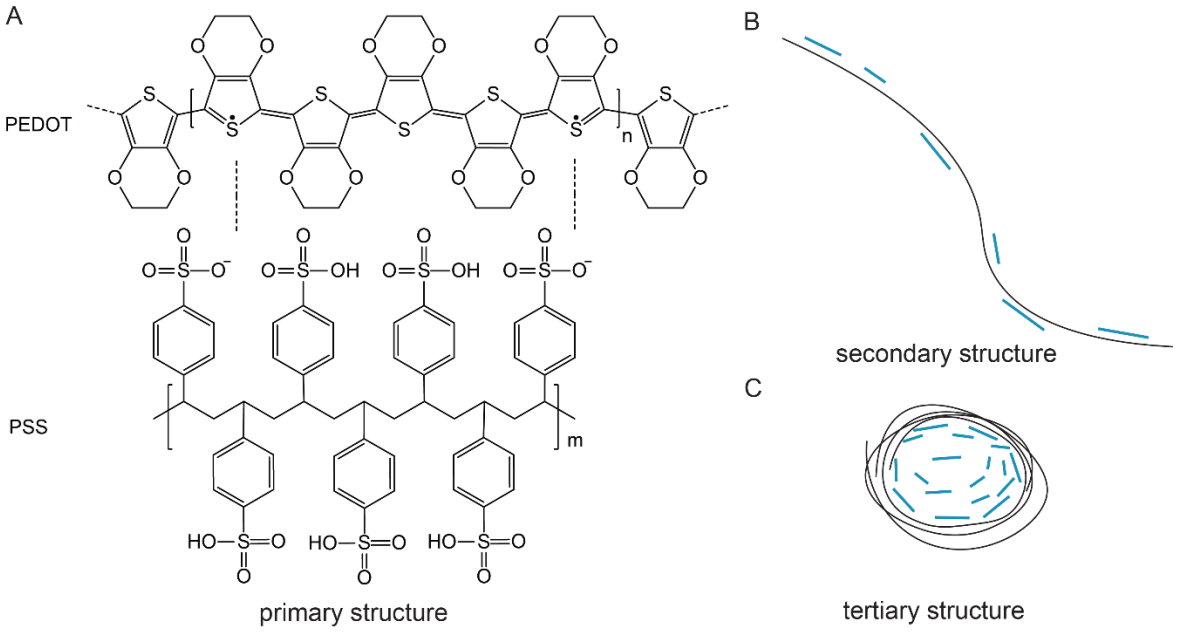

Figure 2-1 PEDOT:PSS. The primary (A), secondary (B), and tertiary (C) structures of PEDOT:PSS. The positive charges on the PEDOT are compensated by negative charges on the PSS chain. The blue bar indicates PEDOT chain; the black chain indicates PSS chain.

With the aim to further enhance the air stability as well as conductivity and to grant the materials with proper solution processability, Poly(3,4-ethylenedioxythiophene) (PEDOT) was synthesized and widely adopted as one of the most successful conducting polymers for contemporary organic electronics. By adding ethylenedioxy groups onto PTh main chains, PEDOT gains a moderate bandgap of 1.65 eV, low oxidation potential of 0.0 V comparing to SCE potential, enhanced chemical stability as well as optical transparency when oxidized (conducting state)[49].

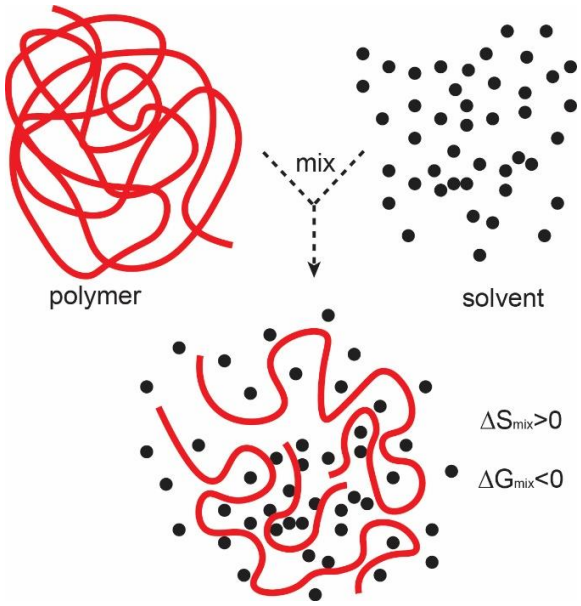

Figure 2-2 Solution processability of polymers.

As the initial goal, conducting polymer is designed to be "synthetic metal"[48] that can be processed as liquid conducting ink to support large scale roll-to-roll device fabrications. However, PEDOT itself, despite the excellent electrical and chemical properties, is insoluble in most solvents, which significantly undermines its ability in expected conducting polymer applications (Figure 2-2). This issue had not been successfully solved until the introduction of water-soluble counterion, PSS. Playing as a charge-compensating dopant, the long PSS chains could accommodate the short oxidized PEDOT chains via electrostatic interactions as shown in the primary and secondary

structures of PEDOT:PSS. Considering the Gibbs free energy changes ΔG_{mix} of the potential "dissolving" or mixing process:

$$\Delta G_{mix} = \Delta H_{mix} - T\Delta S_{mix}$$

, where is the ΔH_{mix}, ΔS_{mix} and T are the enthalpy, entropy changes during the process and the temperature, respectively. Since the entropy changes when mixing with specific solvents, for example, water, could be increased, because the soft PSS chains could lower steric hindrance, the Gibbs free energy changes could be more negative, pushing the physical process toward spontaneous mixing. Given the difference in hydrophilicity of the two chains, after mixing with solvent, for example, water, the chains would continue to transform in order to gain a lower Gibbs free energy state, by encapsulating most hydrophobic PEDOT chains within the PSS hydrophilic sheath, forming the tertiary structures of PEDOT:PSS water suspension. With the facile processes and excellent properties that sufficiently match blueprints of conducting polymers, PEDOT:PSS has undoubtable become the iconic polymer for organic electronics and bioelectronics. Advances in PEDOT:PSS have enabled its intensive applications in making various functional devices, such as solar cells[50], light-emitting diodes[51,52], electrochemical transistors[6,53,54], supercapacitors[55], transparent electrodes[56].

2.1.1 Conducting mechanism

The rapid developments of silicon industry have brought the society with numbers of priceless understanding toward the essence of materials. Conduction, from the perspective of silicon industry, could be interpreted as the microscopic Ohm's law:

$$\sigma = \frac{\vec{J}}{\vec{E}} = ne\mu_e + pe\mu_h$$

, where σ is the overall conductivity of the material, $\vec{J}$ is the current density, $\vec{E}$ is the applied electric field, e is the Coulomb constant, converting the number of charge carriers transported into

the amount of charge involved, n is the electron density in unit volume, μ_e is the electron mobility, p is the hole density, and μ_h is the hole mobility. Therefore, the conductivity of materials is proportional to the free carrier density and the free carrier mobility. Following similar logic, the conduction mechanism of conducting polymer could also be considered from the two dimensions.

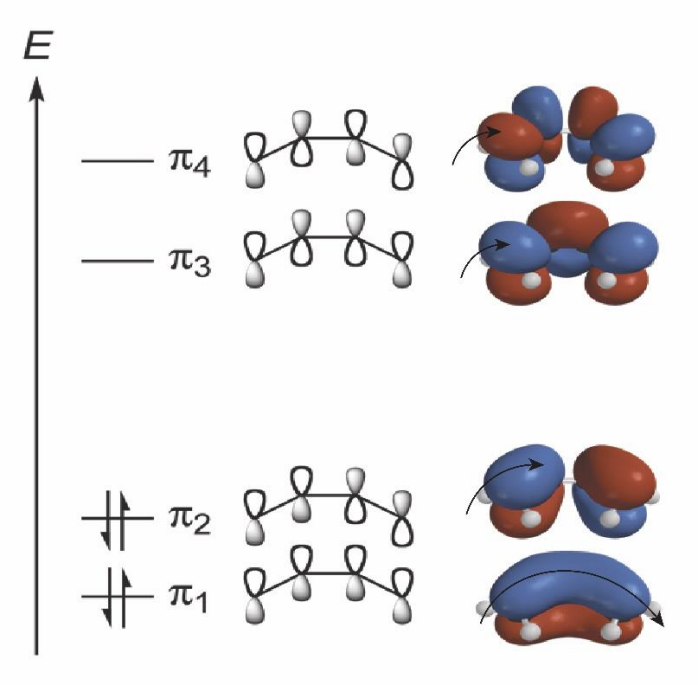

Figure 2-3 Illustrations of orbitals. The bottom one indicates the delocalized orbitals where electrons could transport with less hindrance.

In solid-state physics, the free carrier mobility indicates how fast the free carrier (electron or hole) can transport within metals or semiconductors when the external electrical field is applied. Mathematically written the expression of average drift mobility μ, the physical interpretation toward free carrier mobility is more obvious:

$$\mu = \frac{q}{m^*}\bar{\tau}$$

, where q is the elementary charge, m^* is the free carrier effective mass, and $\bar{\tau}$ is the average scattering time of the free carrier moving within the matrix materials. Therefore, to enhance the free carrier mobility is analogy to the idea in constructing roads between cities to avoid traffic jam

or in decreasing the size of vehicles to fit more vehicles into the same road. When the effective mass (vehicles size) of the free carriers is settled, the expression could also be understood as the connection (roads between cities) between the potential sites that could hold free carriers. If the connection is strong, the free carriers could bounce between potentials more easily and quickly. Following such understanding, in order to enable free carriers moving within polymers, the crucial task is to build roads within or across the polymeric chains. From the electron orbital perspectives, delocalized orbitals are needed to support the general transportation at least within the delocalized electron clouds. Taking *trans*-polyacetylene as an example given its structural simplicity, the backbone Carbon (C) has the electronic configuration of $(1s^2)2s^12p_x^12p_y^12p_z^1$ with three sp^2 hybrid orbitals and one $2p_z^1$ orbital[57]. Geometrically, the one remaining $2p_z^1$ orbital of the C atom overlaps sideway with the $2p_z^1$ orbitals of adjacent Cs forming one π bond, providing the chance for electron delocalization. PThs and PEDOT share the similar mechanism with *trans*-polyacetylene. Although PThs do not have degenerative states for free carriers as PA chains, the benzoid and quinoid states have similar energy level[58]. The benzoid and quinoid structures of PThs support the delocalized electron cloud for free carrier transportation. Moreover, the introduction of ethylenedioxy groups onto PTh main chains in PEDOT also increase the steric hindrances for the π-π conjugated planes from twisting, enhancing the coplanarity of the overall chain. However, in most cases, the single polymer chains aren't long enough to conduct a macroscopic current. Therefore, the thermally aided free carrier hopping between domains controls the overall conductivity. Predicted by the variable-range hopping (VRH) mechanism, the overall conductivity could be concluded as:

$$\sigma(T) = \sigma_0 e^{-(\frac{T_0}{T})^{\frac{1}{d+1}}}$$

, where d is the dimension, for 3-dimensional hopping, $d = 3$.

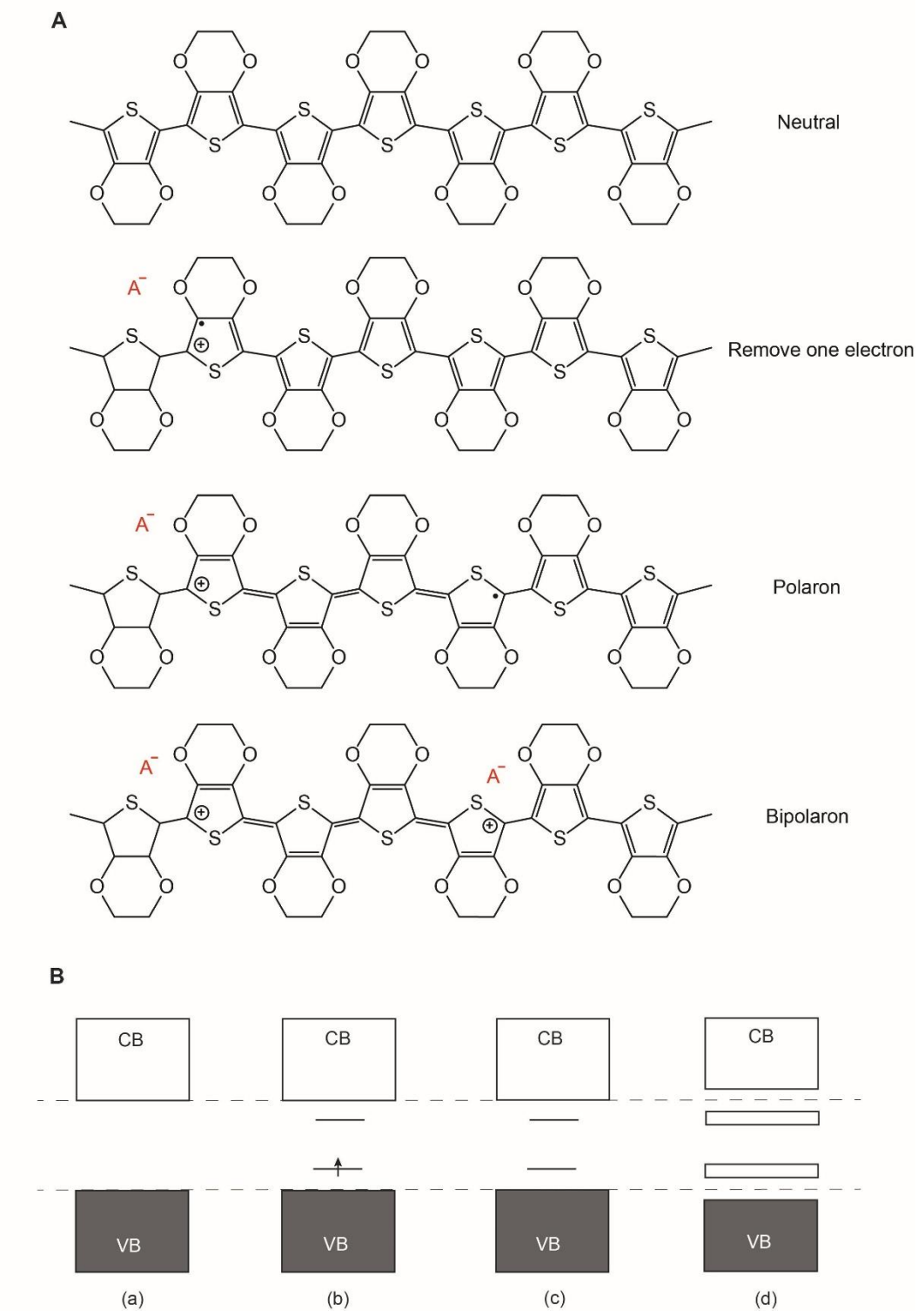

Figure 2-4 Evolution of PEDOT and PEDOT band structure upon doping. A. A demonstration of free carrier states change when doping PEDOT. A^- in red indicates the counterions of dopant. B. The PEDOT band structure evolution upon doping. (a) neutral PEDOT; (b) low doping level. Polaron formation; (c) moderate doping level, bipolaron formation; (d) high doping level, formation of bipolaron bands.

With proper roads (free carrier mobility), another aspect for connecting cities is to create or load vehicles (free carriers). Because of the charge neutrality of polymers, most conducting polymers have limited free charge carriers when untreated. Analog to the methods adopted in silicon industry, introducing dopants is a feasible way in creating defects and therefore the free carriers. However, on the contrary to inorganic cases where substitutional or interstitial impurity atoms (donors or acceptors) are introduced, doping process in conducting polymers normally refers to the phenomena where oxidizers strip electrons from polymeric chains. After the oxidation process, positively charged holes are left on the polymer backbones as free carriers. It's also worth noting that in PEDOT, the existence of ethylenedioxy groups alongside the benzoid and quinoid structures could further stabilize the free carriers within the chains. When an external electrical field is applied, the positively charged free carrier could transport within or across the delocalized π-π bonds, forming a persistent current as "synthetic metals".

2.1.2 Commercial poly(3,4-ethylenedioxythiophene):poly(styrenesulfonate) suspension

As discussed, the pristine PEDOT itself is not conductive and extremely hard to be processed given its poor solubility in most solvents. Therefore, the introduction of dopants (counterions) to form PEDOT:counterion polyelectrolyte complexes would be ideal for realizing pragmatic conducting polymers[59]. Poly(styrenesulfonate) (PSS) is the first counterion used to dissolve and dope PEDOT. And most importantly, PEDOT:PSS has been commercialized and remained the industrial standard ever since[60]. Besides PSS, there are also many other counterions that could form polyelectrolytes with PEDOT, such as, heparin[61], and BF_4[62]. Those counterions have their own benefits comparing to PSS, for example, enhanced biocompatibility. However, to acquire the PEDOT:heparin or PEDOT:BF_4 complex, extra polymerization processes are required. Considering the repeatability and the potentials in translating PEDOT biomedical devices, commercially available PEDOT:PSS is the exclusive candidate for organic bioelectronics.

Table 2-1 Database of commercial PEDOT:PSS in Clevios™

Name	PH1000	AI 4083	HTL Solar	HTL Solar 3
Resistivity (Ω*cm)	<0.0012	500-5000	1-10	5-500
Solvent	water	Water	Water	Toluene
Addition	5 v/v% DMSO	No addition	No addition	<0.5 v/v% water
Solid content (wt.%)	1.0-1.3	1.3-1.7	1.0-1.3	1.5-2.5
Viscosity (mPa*s)	<50	5-12	8-30	<10
PEDOT:PSS ratio	1:2.5	1:6	1:2.5	N/A
D_{50} (μm)	0.030	0.100	N/A	N/A
Work function (eV)	4.8-5.0	5-5.2	4.8-5.0	4.4-4.8

Note: D_{50} is a parameter characterizing the particle size distribution. D_{50} indicates that a 50% of the particles have size smaller that the value. (Data from Heraeus Clevios™)

Invented by Bayer AG and sold by two companies: Haraeus (formerly Baytron, Germany) and Agva Gevaert (Belgium), there are many standardized products of PEDOT:PSS with slight difference in composition, particle size distribution, working function, resistivity and viscosity, as shown in the Table 2-1. The significant difference among various products mainly originates from the composition difference. For example, since PEDOT:PSS forms polyelectrolyte complexes, the ratio of polycations and polyanions could affect the molecular arrangements of PEDOT:PSS complexes. Moreover, as shown in the tertiary structure of PEDOT:PSS complex, the interaction among hydrophobic PEDOT chains, hydrophilic PSS chains and water molecules spontaneously assembles PEDOT:PSS as microgels within water. Therefore, although certain publications named the complex as PEDOT:PSS solution, such expression is conceptually misleading, and the solution processable PEDOT:PSS complex should be always indicated as PEDOT:PSS dispersion or PEDOT:PSS suspension. Characterized by dynamic light scattering (DSL), the size distribution of PEDOT:PSS microgels is proved to be non-Gaussian, with D_{50} of 0.010 to 1 μm[59].

Considering the targeted applications for biomedical engineering, where PEDOT:PSS is normally used as conductors or active layers of OECTs, PEDOT:PSS (Clevios™ PH1000) purchased from Haraeus Electronic Materials is commonly adopted. Therefore, all PEDOT:PSS suspensions mentioned in this thesis are Clevios™ PH1000, if no specific explanation included.

2.1.3 Poly(3,4-ethylenedioxythiophene):poly(styrenesulfonate) thin film properties

PEDOT:PSS suspension is the mixture of PEDOT:PSS microgels and solvents. With the original intentions to replace silicon for semiconductor industry, PEDOT:PSS was first designed to be compatible with thin film applications following the two-dimensional logic of nanofabrication and microelectromechanical systems (MEMS). Guided by such layer-by-layer philosophy, PEDOT:PSS is normally deposited to form a thin film state via spin coating[17], screen printing[63], electrospinning[64], drop casting[65], slit coating[66], and bar coating[67]. Among these methods, spin coating, given its facile process and reliability, is most frequently adopted in PEDOT:PSS thin film deposition. By considering the viscosity of pre-mixed PEDOT:PSS mixture, and by controlling the spinning parameters (such as spinning steps, spinning speed, acceleration, and spinning time), PEDOT:PSS thin films could be uniformly and repeatedly produced. Heating is a crucial step to stabilize the structures. Besides the basic function in removing water, the heating steps could also removing certain conductivity enhancement agents whose boiling points are low[68]. Moreover, free PSSH chains may undergo temperature-induced fragmentation and be decomposed while leaving sodium salt (PSS^-Na^+) unaffected[69]. Although electropolymerization of 3,4-ethylenedioxythiophene (EDOT) is a feasible way in depositing PEDOT:PSS thin films on conducting substrates, for example, Si-based neural probe[70,71], in this thesis, we mainly discuss PEDOT:PSS thin films based on PEDOT:PSS suspension (Clevios™ PH1000).

2.1.3.1 Chemical properties

Stability is one of the major reasons that PEDOT:PSS is widely adopted in conducting polymer researches. Characterized by thermogravimetrical analysis (TGA), the thermal stability of PEDOT:PSS has been systematically investigated. Before 200 °C, the main weight loss is from water evaporation. Starting from 250 °C, the curve m/z=64 (Figure 2-5), initiates a spike which represents the SO_2 formation and releasing. Considering the PEDOT:PSS thin film systems, it indicates that from 250 °C, sulfur comes to become unstable in PEDOT:PSS, which might be caused by PSS chain fragmentation. According to the overall weight loss and ion current as functions of temperature, PEDOT:PSS thin films are thermally stable up to 200 °C[49]. PEDOT:PSS, similar to all organic materials, does suffer from degradation over time. The existence of oxygen might oxidize the thiophene group, therefore, stabilizers are needed for PEDOT:PSS thin films in long term usage (on the scale of days). PEDOT:PSS thin films are hygroscopic. A prebaked PEDOT:PSS thin films could spontaneously absorb water in ambient due to the existence of hydrophilic PSS chains.

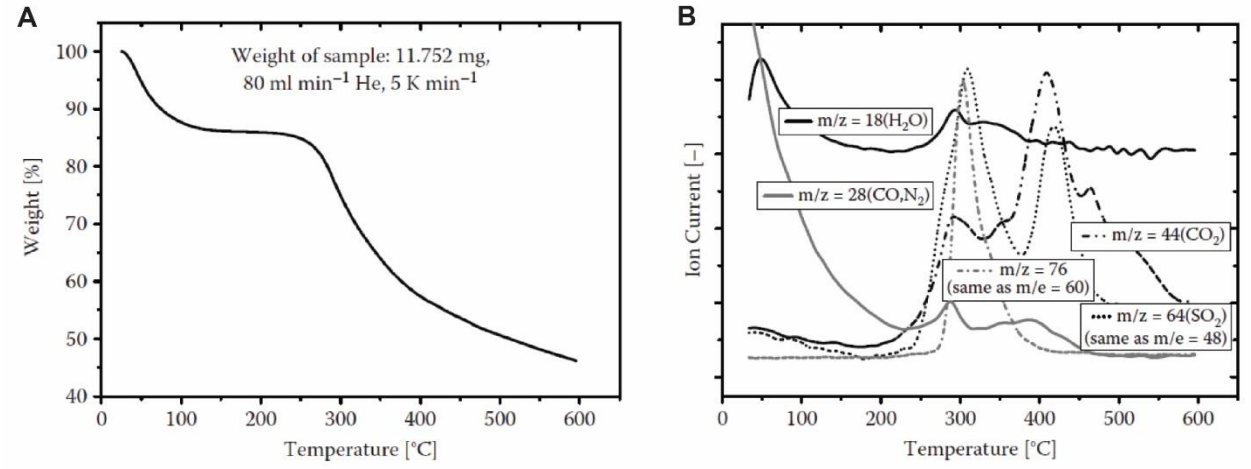

Figure 2-5 Thermal stability of PEDOT:PSS films characterized by TGA. A. The weight loss as function of heating temperature at constant heating rate (5 K/min) in helium; B. The ion currents of relevant masses recorded simultaneously as function of heating temperature (Data from Bayer Technology Services, Leverkusen, Germany).

2.1.3.2 Electrical properties

As discussed in the conducting mechanism section, PEDOT:PSS acts as synthetic metals with conductivity with free carriers. For PEDOT:PSS thin films, the conductivity is normally quantitively characterized by the sheet resistance R_{sq}:

$$R_{sq} = \frac{\rho}{d} = \frac{1}{\sigma \cdot d}$$

, where ρ is the resistivity, σ is the conductivity, and d is the PEDOT:PSS thin film thickness. In order to rule out the artefact introduced by contact resistance, four-point probes are normally used to measure the sheet resistance of PEDOT:PSS thin films. The conductivity of PEDOT:PSS thin films could be influence by many factors, including the PEDOT and PSS ratio, additions, pH and temperature. The PEDOT and PSS ratio directly reflects the density and morphology of PEDOT domains in the films, and therefore affects the overall conductivity. The addition of chemicals, such as high boiling point solvents, could increase the conductivity, supported by various theories[68,72,73] (details will be discussed in the typical additions section). Acidic (pH in the range between 0-3) and warm environments (better hopping conditions according to VRH model) are also favorable for PEDOT:PSS for conducting free carriers[74]. Since the gradual oxidative degradation might exist on sulfur at thiophene and α-carbon especially when exposed to light, the conductivity of PEDOT:PSS thin films would undergo continuous decrease over time in ambient atmosphere, which could be avoided by maintaining the thin film within inert atmosphere. It's also worth noting that PEDOT:PSS does exhibit no electron conductivity but hole conductivity since the injected electrons will immediately recombine with the holes at the oxidized PEDOT chains, hence electron transportation does not contribute to the overall current.

2.1.3.3 Mechanical properties

The Young's modulus of freestanding PEDOT:PSS thin films are systematically characterized by Lang et al.[75]. On the scale of GPa, the Young's moduli of PEDOT:PSS films are highly dependent

on the ambient humidity levels. The Young's modulus could shift from 0.9 GPa to 2.8 GPa by changing relative humidity (rH) level from 55% to 23%.

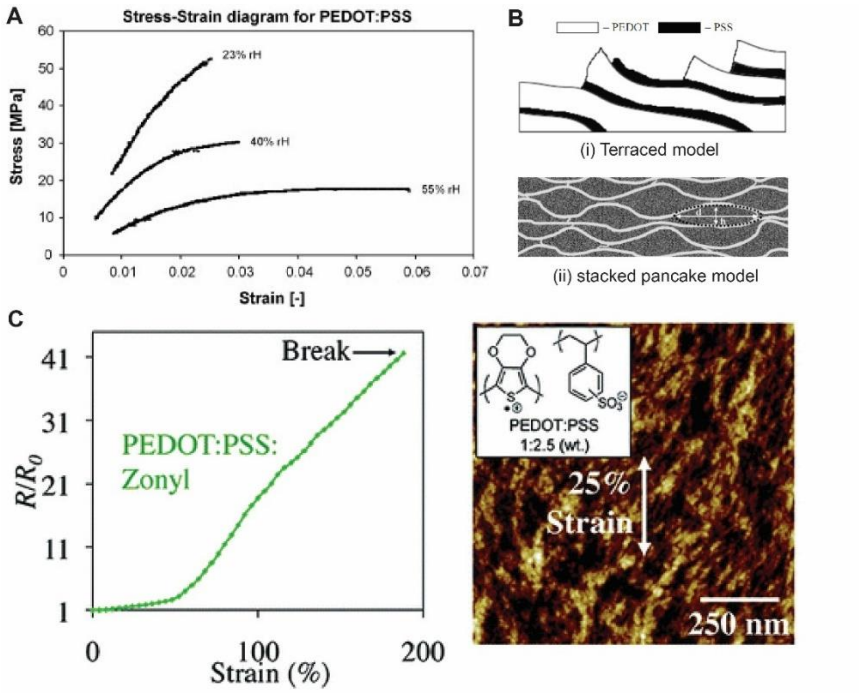

Figure 2-6 Mechanical properties of PEDOT:PSS thin films. A. Stress-strain curves for PEDOT:PSS thin films at different rH[75]. Reprinted with permission. B. Models illustrating the potential hierarchical morphology of PEDOT:PSS thin films[76,77]. Reprinted with permission. C. Normalized resistance of Zonyl-treated PEDOT:PSS thin film stretched from 0 to 200% and atomic force microscope (AFM) image of partially aligned grains after stretching[78]. Reprinted with permission.

Phase segregation is a crucial phenomenon in modifying the properties of spin coated PEDOT:PSS thin films. Proposed by Greczynski et al.[69], the spin coated PEDOT:PSS thin films are nonuniform but with PEDOT and PSS domains within multiple grains. The PSS chains (including both the PSSH and the $PSS^{-}Na^{+}$ components) would aggregate on the very surface of PEDOT:PSS thin films (about 3-4 nm of thickness), and the PSS-to-PEDOT ratio could reach 2.6-3.5, while the overall PSS-to-PEDOT ratio is about 1.2, characterized by X-Ray photoelectron spectroscopy (XPS) of S (2p) and O (1s). Based on the small angle neutron spectroscopy, the length of PSS-enriched domain is about 5-15 nm depending the baking and annealing conditions. Confirmed by high angle annular dark field (HAADF) scanning transmission electron microscopy

(STEM), the granular structure of PEDOT:PSS gel particles maintained during film formation [79]. Based on the observation, there are multiple models illustrating the grain-like morphology of PEDOT:PSS thin films, including the molecular terraced structure proposed by Ionescu-Zanetti et al.[76] and the stacked pancake model proposed by Nardes et al.[77].

Unlike silicon whose atoms are tightly fixed via valence bonds, PEDOT:PSS has relative soft chains with large entropy change when mixing with others. Therefore, the flexibility and stretchability of PEDOT:PSS thin films have been viewed as one of the key benefits over conventional silicon materials. Although the stretchability of intrinsic PEDOT:PSS is limited (~5%)[80], by introducing plasticizer Zonyl (currently change names into Capstone), the PEDOT:PSS thin film on polydimethylsiloxane (PDMS) substrates could be stretched to 30% without introducing significant cracks[78].

2.1.3.4 Optical properties

High optical transparency of PEDOT:PSS have promoted it as an ideal alternative to indium tin oxide (ITO) for flexible display[80-82]. The absorption spectrum of PEDOT:PSS thin films is strongly dependent on the oxidation states of PEDOT. When oxidized, the intermedia polaron or bipolaron states could forms and therefore shifting the absorption peak locations from 2.2 eV into 0.5, 1.4 eV, changing the color of thin films. Such transparency and electrochromic properties might also aid conducting polymer for biomedical applications with its potential to be orthogonally applied with optical modalities.

2.1.4 Typical additives and their effects

Beyond modifying the electrical properties, the additive introduction in PEDOT:PSS could also significantly change the global properties of PEDOT:PSS, including its optical and mechanical properties. Especially for PEDOT:PSS thin film researches, the strategies of introducing additives are frequently adopted given its facile process and high efficacy. The additive introduction

processes could be simply achieved either by adding the liquid or solid organic compounds via directly mixing with PEDOT:PSS suspension before film forming step (for example, spin coating)[68,83-86] or by exposing pre-formed PEDOT:PSS films to the solvent vapor[87]. Chemicals includes water miscible high boiling point solvents, such as, ethylene glycol (EG)[88], and dimethyl sulfoxide (DMSO)[89,90] are commonly utilized. According to the electrical screening theory, it hypothesizes that the introduction of solvent of high dielectric constant might induce screening effect among positively charged PEDOT chains and negatively charged PSS chains[68]. Therefore, the more crystalized PEDOT nanofibrillar structures could be formed as conducting islands and enhance the overall conductance of the thin films[80]. According to the theory mainly considering the conformational change of PEDOT:PSS chains, the conductivity increasement in the final PEDOT:PSS thin film needs two or more polar groups on each additive molecule (DMSO is an exception). Such hypothesis was evaluated by testing a family of materials with different number of polar groups including EG, DMSO, N-methyl-2-pyrrolidone (NMP), acetonitrile, nitromethane, methyl alcohol, pyridine for their independent effects on the conductivity of PEDOT:PSS thin films. The mechanism could be interpreted as the conformational change of PEDOT chains and the interaction between the dipole of one polar group of the additives and the dipoles or the positive charges on the PEDOT chains[72]. As mentioned in previous section, according to polymer physics, PEDOT chains in PEDOT:PSS complex would have various conformations which have macroscopic controls over the overlapping of π-π delocalized electron clouds, therefore, hindering the in-chain and inter-chain free carrier transportation. While the benzoid structures of PEDOT are preferable to form a coil conformation, the quinoid structures tend to form a linear or expanded-coil conformation, which is more favorable for high conductance. After introducing the water miscible high boiling point solvents, for example, EG, one of the polar groups is interacting with PEDOT chains, forming a dipole with the positive charge of doped PEDOT chains, while the other polar group is reaching out for the PSS chains with a potential hydrogel bond. Therefore,

the PEDOT chains are dragged to be adjacent to the rigid PSS chains to enable an expanded-coil or linear conformation. In DMSO case, although there is only one polar group, the potential mechanism may be: the strong dipole moment to PEDOT chains could remain after forming hydrogen bond with PSS chains. Except for such generalized theories for enhancing the electrical, structural or optical properties of PEDOT:PSS thin films, there are also star additives that are more frequently used in PEDOT:PSS researches comparing to others. Here, this thesis would enumerate three chemicals of distinctive functions for PEDOT:PSS engineering.

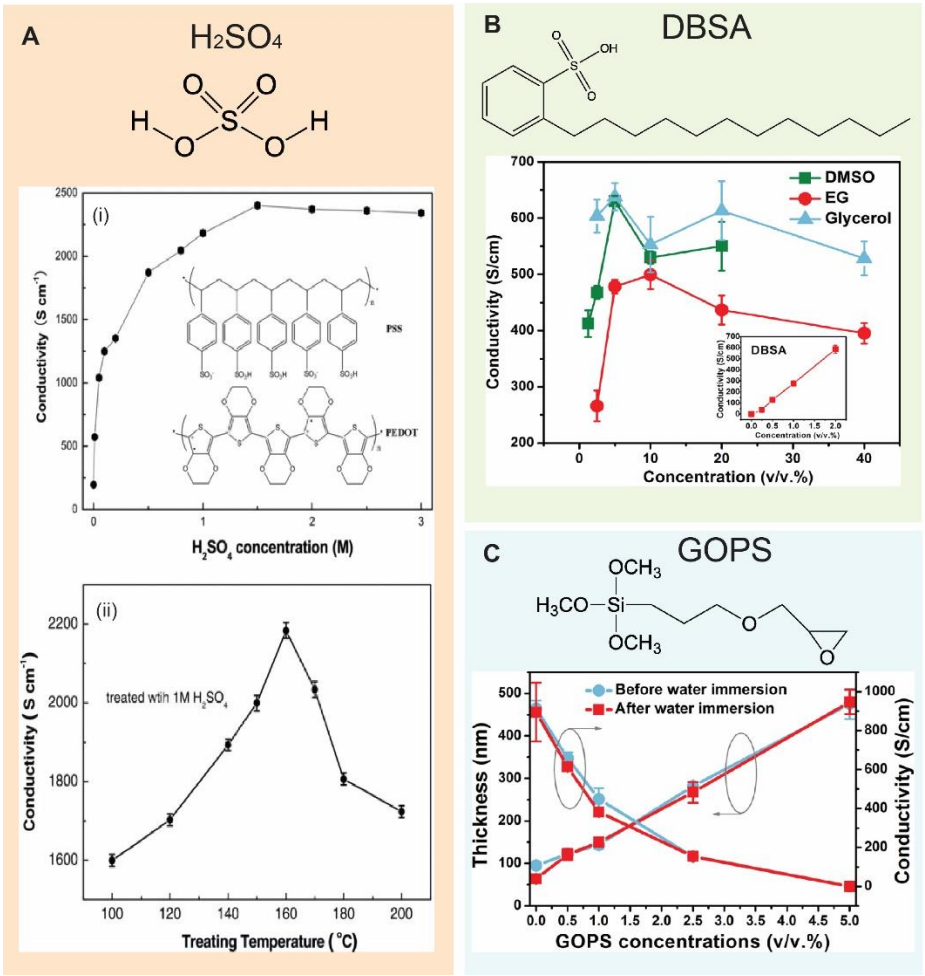

Figure 2-7 Typical additives and their effects on PEDOT:PSS thin films. A. H_2SO_4 treatments on the PEDOT:PSS thin films[91]. Reprinted with permission. The conductivity of PEDOT:PSS thin films as a function of H_2SO_4 concentration (i) and treating temperature (ii). B. DBSA treatments on PEDOT:PSS thin films and their effects on electrical conductivity[92]. C. DBSA treatments on PEDOT:PSS thin films and their effects on the water stability of the films[92]. Reprinted with permission.

Sulfuric acid (H_2SO_4) is adopted to significantly increase the conductivity of PEDOT:PSS thin film. The conductivity of H_2SO_4-treated PEDOT:PSS thin films could reach extremely high-level of 3065 S/cm[91] and 4380 S/cm[5]. The potential mechanism for the enhancement could be explained by the introduction of H^+ and HSO_4^- replacement of negatively charged PSS chains according to the reaction.

$$PSS^- + H^+ = PSSH$$

Since the PSS chains which mostly exhibit coil conformation are expelled from PEDOT domains via electrostatic interaction, the charges on PEDOT are more delocalized, leading to highly crystallized PEDOT nanofibril with extremely high conductivity. However, although only limited amount is needed, normally the H_2SO_4 addition used for such treatment is required to be of high concentration, which is corrosive and dangerous to process especially for biomedical applications. Comparing to other additives that could pre-mix with PEDOT:PSS suspension before spin coating or other film forming process, H_2SO_4 treatment is only limited to soak PEDOT:PSS thin films in high temperature. Given that the hydrophilic PSS chains are expelled from the hydrophobic PEDOT chains, H_2SO_4-treated PEDOT:PSS thin films have limited adhesion to hydrophilic substrates, causing the detachment issues.

Dodecylbenzenesulfonic acid (DBSA) is a viscous, colorless liquid stored avoiding light. Traditionally used as surfactants to facilitate the PEDOT:PSS film processing, DBSA has been widely used in OECT research pioneered by Prof. George G. Malliaras[18,93]. Recently, its effects on electrical conductivity enhancement and stretchability enhancement for PEDOT:PSS thin films are also systematically characterized[92]. For example, film conductivity over 500 S/cm could be reached with 2 v/v% DBSA.

(3-glycidyloxypropyl)trimethoxysilane (GOPS) is reported to be a crosslinker for PEDOT:PSS thin film processing. It can enhance the adhesion between PEDOT:PSS thin film and substrates,

preventing partial dissolution and delamination of PEDOT:PSS thin films[92,94,95]. Therefore, GOPS is frequently adopted to improve the water stability of PEDOT:PSS thin films. But the introduction of GOPS would inevitably degrade the conductivity of PEDOT:PSS thin films, hence in most studies, the addition concentration of GOPS would usually be restricted below 1 v/v%[92].

It's worth noting that the additive effects on PEDOT:PSS discussed in this section mainly limit in those for PEDOT:PSS thin films. When considering different scenario, for example, PEDOT:PSS hydrogels, the additive effects could not be simply generalized, since certain properties enhancing mechanisms are based on the modification of the very interface between PEDOT:PSS thin film and substrates. But such understanding on what the additives would cause might be valuable as a reference to predict the potential modification of the morphological, structural, or chemical properties of PEDOT:PSS chains. For instance, according to its effects on enhancing the morphology and conductivity of PEDOT:PSS thin films, DMSO is also used in PEDOT:PSS hydrogel researches in order to transit into the highly conductive gel state[29].

2.2 Poly(3,4-ethylenedioxythiophene):poly(styrenesulfonate) Hydrogels

2.2.1 Hydrogels for minimizing mismatch

In order to functionally bridge the endogenous tissues and artificial components with reduced irritations on the normal metabolism and of high reliability, since the birth of bioelectronics by Luigi Galvani's landmark experiment, there are rising needs for a conformal electrode-tissue interfaces. The emerging flexible electronics offers an preliminary solution to the challenges by minimizing the mechanical difference[34]. Flexible electronics, which is soft, bendable and stretchable, impressed both academia and industry with not only its own potentials of seamless biointerfacing, but also a generalized idea about the importance of the mechanical resemblances to biological tissues means to biomedical engineering. Hence, the correlation between minimized mechanical

mismatch and enhanced biointerface has been researched in theory and evaluated in multiple cases. From systematic perspectives, the effect of mismatched biointerface could be categorized as following: (1). The difference in Young's modulus and bending stiffness of biological tissues and devices could result in relative dislocations, which would affect the quality of recorded signals, since the recorded amplitude of single neuron unit is inversely proportion to the distance between the source neuron and electrode[96]. By decreasing the feature size and therefore decreasing the bending stiffness in matching biological tissues, microwire-based array also achieved chronic unit recording in cerebral cortex of primates, which could last over weeks[97]. (2) Since they behave differently under micromotion, the rigid devices would constantly scratch biological tissues and cause nearby cell death. (3) Fibrosis and gliosis tend to concentrate around the rigid devices as the main behavior of chronic immune response. For example, in neuroengineering, the response of glial cells, which as a marker for foreign object effect, is profoundly suppressed with interfacing, rationalizing the logic in minimizing mechanical mismatch in achieving chronically implanted neuroprostheses[98]. (4) The constant dislocation increases the chance for device failure. (5) The rigid device could not be compatible with the dynamic deformation of biological tissues, such as growth, therefore, the inner strain would build up on interfaced tissue. (6) Especially on neuroengineering, the blood-brain barrier (BBB) is more vulnerable when inserting rigid neural probes, accelerating the neurodegeneration and immune response.

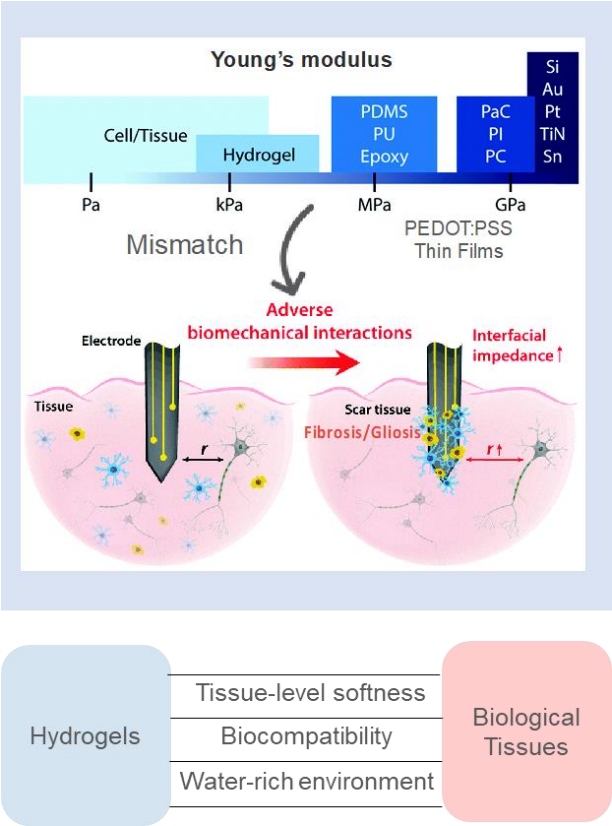

Figure 2-8 Hydrogels and their mechanical resemblances to biological tissues [20]. Polymeric thin films exhibit Young's moduli on the range of MPa to GPa, which are significantly larger than that of biological tissues. The electrodes mechanically mismatching endogenous tissues will severely damage biological tissues and degrade the recording/stimulating quality. Reprinted with permission.

Despite the impressive achievements on flexible-electronics-based biointerface, the intrinsic gap between biological tissues and thin film electronics plays as the main hinderance for further developing materials, structural and topological shapes as seamlessly functional biointerface. The Young's modulus of flexible thin film substrates, such as Parylene C, polyimide (PI) is nearly 10^6 times higher than the interfaced tissues. Even the elastomers which have been frequently used in wearable biosensors, such as PDMS, polyurethane (PU) and epoxy exist huge different in the rigidity. The obvious disparity heralds that there should be another branch of materials adopted to minimize the mechanical mismatch between the artificial components and biological tissues.

Advances in chemistry and bioengineering significantly push the engineering toward materials with more controllable physicochemical and mechanical properties. Hydrogels are the crosslinked

three-dimensional (3D) polymeric network infiltrated with water (water content > 90% by weight). Since they do not dissolve but swell in water, hydrogels play as an ideal carrier for drug delivery[99] and tissue engineering[100]. Recently, given numbers of achievement confirming the exclusive benefits of hydrogels in biomedical engineering, we have witnessed the rise of hydrogel engineering. In light of their resemblances to biological tissues from the mechanical, physical and chemical perspectives[20,21], hydrogels tend to "trick" the endogenous tissues for chronic and seamless interfacing. The tissue-level softness supports the suppressed immune effects and irritation on endogenous tissues, offering an unprecedent opportunities for soft, conformal, and chronic biointerface. Additionally, with their potential biocompatibility as well as the water-rich environment, hydrogels represent an ideal platform for next-generation biointerface.

2.2.2 Poly(3,4-ethylenedioxythiophene) hydrogels

Comparing to the conventional hydrogels engineering for biomedical engineering, where the geometrical structures and pharmacological efficacies are the priority, one of the primary requirements for realizing hydrogel bioelectronics for seamless and chronic interface is developing conducting hydrogels. There are two branches in achieving such conducting hydrogels. The first branch tends to use conducting hydrogel as the interface layer buffering the biological tissues and rigid electrodes. The second branch aims to replace traditional electrodes by directly using bulky conducting hydrogels as electrodes. Considering the conducting mechanism and the free carriers (ions or electrons) adopted to conduct the current, the bulky conducting hydrogels could be further divided into ionically conductive hydrogels and electrically conductive hydrogels. Similar to the electrolytic tissue, ionically conductive hydrogels rely on the ionic transportation in conducting a macroscopic current. The most common methods in synthesizing ionically conductive hydrogels are to dissolve and confine ionic salts, such as NaCl or LiCl, into the hydrogel matrices[101]. However, the extreme high concentration of ionic salts (>1 M) results in high osmotic pressure when interacting with common physiological environments

s(<300 mM for corresponding ion concentration). Therefore, such ionically conductive hydrogels are limited in wearable and epidermal electrodes where the skin itself could be the barrier for ionic invasion, preventing the irritations on normal metabolisms. In order to achieve electrical conductivity in hydrogel materials, the key is to introduce electrically conductive networks in competing with the watery environment which facilitate the ionic conductivity. Incorporating conducting filaments, such as metal nanoparticles, carbon nanotubes (CNT), graphene and conducting polymers when preserving the main matrix structure intact, provide a facile method in granting electrical conductivity to hydrogels. For example, The introduction of the highly conductive CNT into the nonconductive poly(glycerol sebacate): gelatin nanofibrous scaffolds enables the conductive hydrogel for cardiac tissue engineering[102]. PEDOT is also actively adopted as conducting filaments to enhance the electrical conductivity given its solution processability and biocompatibility[61,103]. The forms PEDOT incorporated into the hydrogel matrix could be mainly categorized into EDOT synthesis and PEDOT:PSS suspension addition, which would be discussed in the following section. By mechanically mixing the hot acyl gellan gum (GG) solution and PEDOT:PSS dispersions, PEDOT:PSS is supposed to be evenly distributed in GG matrix solution[104]. After the crosslinking of GG solution triggered by Ca^{2+}, the highly conductive PEDOT:PSS domain tends to be locked in the macroscopic holes within the GG matrix. Processed by this method, such PEDOT:PSS-mixed hydrogels exhibit tissue-level softness (Young's modulus of 1~8 kPa) and decent electrical conductivity (conductivity of ~0.1 S/cm). The main drawbacks of this approach are the limited electrical conductivity, since the main component of such hydrogel is till the nonconductive matrices. Meanwhile, the addition of rigid components would also hinder the intrinsic biocompatibility and mechanical softness of the hydrogel matrix, undermining its strength in reaching seamless and chronic biointerface.

Considering the pros and cons of the methods discussed above in order to achieve the optimal materials for conducting hydrogel, the concept of pure conducting polymer hydrogels has been

explored. In contrast to taking conducting filaments to aid the electrical properties of hydrogels, pure conducting polymer hydrogels manipulate the conducting polymers and crosslink the polymer chains to form an intrinsically conductive three-dimensional network which could store water within the conducting scaffold. However, as one of main aspect of hydrogels or gels, the ability hold large amount of water or solvent is hard to be achieved given the poor solution processability of most conducting polymer. As discussed in previous section, the requirement to maintain the coplanarity of π-π conjugation for the macroscopic electronic transportation ability and the rigidity (steric hinderance) of benzoid or quinoid rings, the entropy change when interacting with most solvent is very small, therefore could not thermodynamically activate the reaction. PEDOT:PSS, with the exceptional solution processability assisted by the hydrophilic and soft PSS counterions, has been viewed as the essential materials to realize the conducting hydrogels. By mixing aqueous PEDOT:PSS suspensions with the volatile additive, DMSO, which has been frequently adopted in PEDOT:PSS thin films researches to enhance the morphology and conductivity, followed by controllable dry-annealing and rehydration process, pure PEDOT:PSS hydrogels show interconnected PEDOT:PSS nanofibrils as well as the ability to hold certain amount of water within[29]. With high electrical conductivity of ~20 S/cm in phosphate-buffered saline (PBS) and ~40 S/cm in deionized water and decent softness (Young's modulus of ~2 MPa), the DMSO-assisted pure PEDOT:PSS hydrogels herald the rise of hydrogel bioelectronics. In order to further strength the mechanical properties of the brittle PEDOT:PSS hydrogels, the idea of interpenetrating a secondary network is developed to further stabilize and support the loosely crosslinked PEDOT:PSS gel[105].

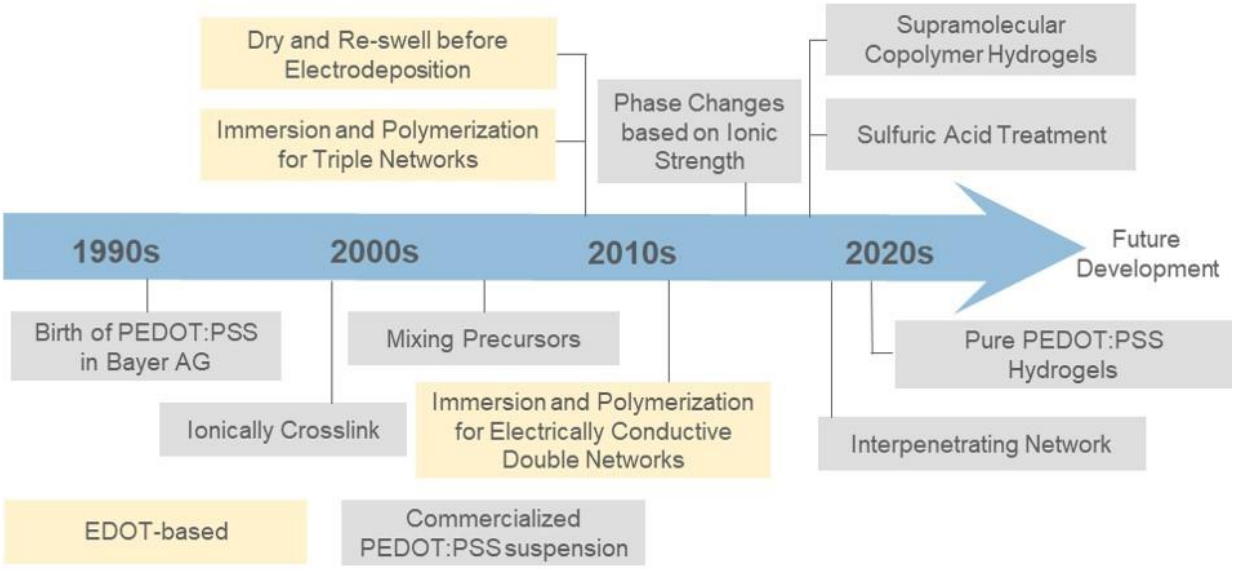

Figure 2-9 Landmarks of PEDOT hydrogels. The development of PEDOT hydrogels are shown on the timeline. The yellow block indicates that the methods are based on EDOT while the grey block indicate the methods are based on commercial PEDOT:PSS suspension.

By categorizing the landmark PEDOT hydrogel synthesis methods (not include the scenario where PEDOT is used as a low concentration dopant), the logic for realizing PEDOT hydrogels for bioelectronics originates from two separate starting points: from the monomer, 3,4-ethylenedioxythiophene (EDOT), and from the commercial PEDOT:PSS suspension. In the following sections, we discuss the benefits as well as the limitations of those approaches by enumerating the selected works of PEDOT hydrogels.

2.2.2.1 Ethylenedioxythiophene-based poly(3,4-ethylenedioxythiophene) hydrogel synthesis

EDOT is the monomer of PEDOT. Unlike PEDOT:PSS, EDOT has a poor solution processability (at 20 ° C, EDOT solubility at water is merely 0.21 g/100 mL water). In order to become conductive, EDOT need to be polymerized into PEDOT. The polymerization could be achieved by loading oxidants (such as $FeCl_3$) into the EDOT aqueous suspension (PSS has to be added into the system to enhance the likelihood for the activation of the reaction), by vapor phase depositing EDOT on oxidant layer (forming thin film), or by electropolymerization[106]. Therefore, the main

drawback of these methods are the complex process and limited repeatability since the overall process have not been standardized.

Based on solution process, the idea of immersion and in situ polymerization for double and triple networks started in the late 2000s[107]. Besides forming double network hydrogels to provide basic mechanical robustness, EDOT and PSS are incorporated into the existed hydrogel networks by diffusion under the concentration gradient during the immersion. When the concentration distribution of EDOT within the macroscopic scaffold reaches the steady state after long time immersion, the sequent exposure to oxidant solution gradually oxidizes the incorporated EDOT is situ along with the nonconducting but structurally supportive hydrogel matrix. Assisted by the well-dispersed EDOT, such networks could avoid phase segregation within the matrix, conducting from a macroscopic perspective. Except for adding chemicals to trigger the oxidation of EDOT to form PEDOT in situ, electropolymerization provide another dimension in achieving PEDOT hydrogels[108]. However, due to the limited electrical field distribution within electrode and electrolyte interface (similar to the phenomena of electrical double layer), by injecting current, the selective in-growth of PEDOT could locally form thin conductive PEDOT films within hydrogel templates[109]. Comparing the conventional process methods which use PEDOT:PSS suspensions (the PEDOT:PSS microgels) as conducting islands, polymerization within hydrogel scaffold supported a highly crosslinked secondary network of newly formed PEDOT, therefore, significantly enhancing the macroscopic conductivity.

By confining EDOT in limited space, a freestanding PEDOT hydrogels could be formed via electropolymerization without the existence of pre-formed hydrogel networks[39]. *In vivo* polymerized PEDOT “cloud” electrode could integrated with tissue surrounding implanted electrode by first injecting EDOT then locally electropolymerizing the EDOT in situ in rodent cerebral cortex. This method acts as a significant foundation for injectable electrodes and in vivo synthesized electrodes[43].

2.2.2.2 Poly(3,4-ethylenedioxythiophene):poly(styrenesulfonate) hydrogels synthesized by commercial PEDOT:PSS suspension

Since its birth and commercialization in late 20th century, PEDOT:PSS is expected to be a branch of basic materials as silicon to conventional semiconductor industry. The versatile of commercial PEDOT:PSS suspension rather than the possibility to synthesize new conducting polymer would be of priority for the translation of the biomedical devices for biointerfacing. Therefore, there are increasing number of initiating projects targeting to use the commercial PEDOT:PSS suspension as the source materials to further investigate its potential in synthesizing new materials of better mechanical, electrical and biochemical properties and fabricating novel devices for seamless and chronic biointerface.

As the most traditional approach, directly mixing the hydrogel precursors and PEDOT:PSS suspension before crosslinking the host hydrogel matrix supports intuitive ways in achieving PEDOT:PSS-entangled hydrogels with decent electrical conductivity[110]. Borrowing the idea of supramolecular engineering, the PEDOT:PSS-doped hydrogels obtain the enhanced mechanical robustness, thermoplasticity, and self-healability, which are favorable for chronic biointerfaces[111].

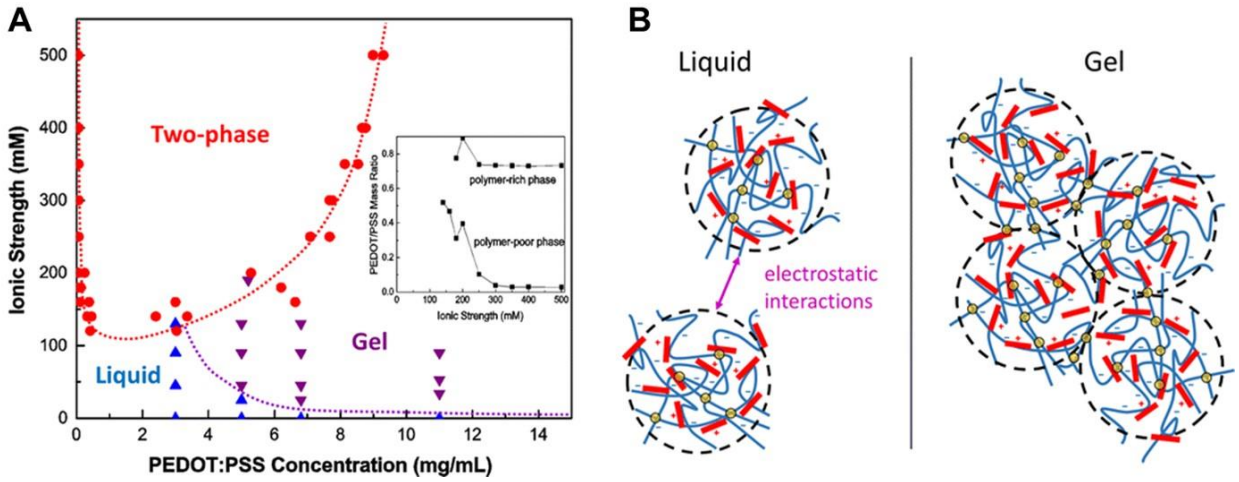

Figure 2-10 Ionic crosslinking PEDOT:PSS suspension[112]. A. Partial phase diagram of PEDOT:PSS toward the gel transition. B. The schematics of morphology of PEDOT:PSS in suspension and in gel. The red bar indicates PEDOT oligomers and the blue bar indicates PSS chains. Reprinted with permission.

The phenomena that PEDOT:PSS suspensions would undergo spontaneous gelation when exposed to high ionic strength was first revealed in 1999 by Prof. Olle Inganäs[113]. In the very first experiment, 0.25 M Mg^{2+} additions are used to ionically crosslink the PEDOT:PSS microgels into the macroscopic hydrogel for supercapacitor applications. The mechanism of the ion triggered gelation behaviors have been systematically researched based on the phase diagram of PEDOT:PSS later published on Macromolecules in 2016 by Michael A. Leaf and Murugappan Muthukumar[112]. Given the background knowledge discussed above in PEDOT:PSS section, in PEDOT:PSS suspension, the existence of PEDOT:PSS is relay on the microgels that float within the aqueous environment. Intrinsically, the microgels are well dispersed and separated by the electrostatic interactions. The size of microgels tends to increase along with the surrounding ionic strength increase, which might be caused by the aggregation of microgels. Therefore, the gel-like behaviors become dominant when the ionic strength increases. To certain extent, the morphology change of PEDOT:PSS thin film when introducing additives, such as DMSO, might also be interpreted by this theory. Guided by the idea in morphologically straightening the polymer chains to enhance the entanglement between different microgels, DMSO and H_2SO_4 can be introduced to crosslink PEDOT:PSS suspension as PEDOT:PSS hydrogel. After H_2SO_4 treatment, PEDOT:PSS hydrogels of high conductivity (~8.8 S/cm) could be achieved[114]. With the aim to strengthen the nanofibrils within the DMSO treated PEDOT:PSS for hydrogel formation, dry-anneal and reswell cycles are adopted to enhance the phase separation for stable and highly conductive PEDOT:PSS hydrogels[29].

Given the fact that most ionically crosslinked PEDOT:PSS hydrogels suffer from brittleness, the concept of interpenetrating network is purposed to enhance the mechanical robustness of as-prepared PEDOT:PSS hydrogels[105]. On the contrary to previous cases where PEDOT:PSS acts as dopant, in interpenetrating network model, PEDOT:PSS hydrogels are pre-formed and then strengthen by incorporating the mechanically robust secondary network to support the inner

PEDOT:PSS framework. Due to the preservation of the ionically crosslinked PEDOT:PSS network, this method supports stretchable PEDOT:PSS hydrogels with high conductivity of 23 S/cm.

2.2.3 Temperature and poly(3,4-ethylenedioxythiophene) hydrogel processing

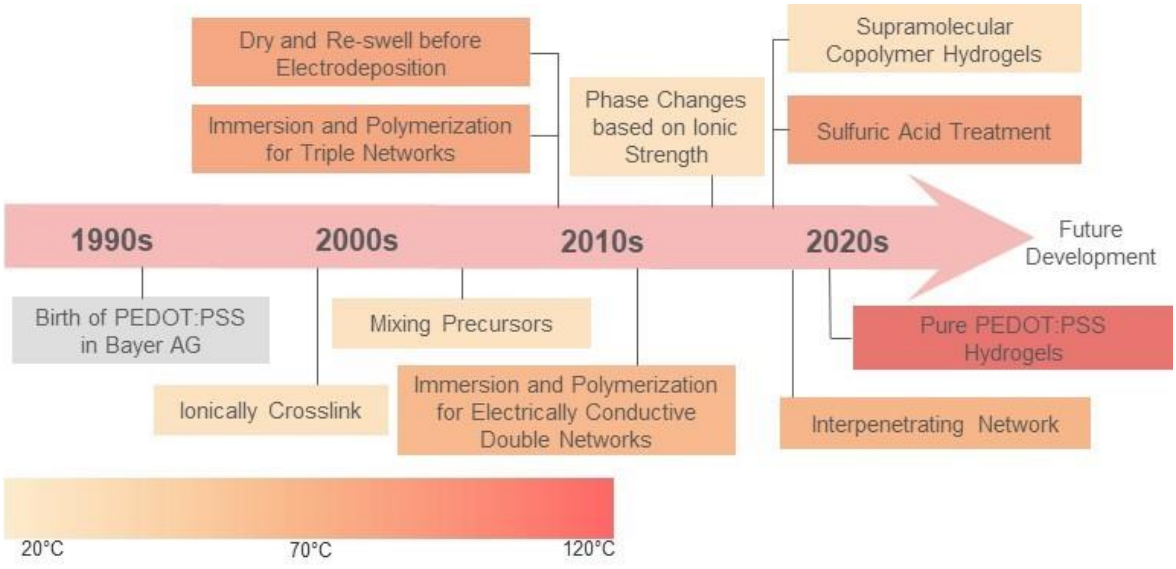

Figure 2-11 Elevating temperature is required in most PEDOT hydrogel synthesis processes. The temperature needed for hydrogel formation is indicated by the color according to the color bar.

Looking back to the goals in realizing seamless and chronic functional interface between biological tissues and electronics, PEDOT:PSS and PEDOT:PSS hydrogels are extensively investigated, given their potential in minimizing the mechanical, electrical, physiological mismatches. However, during this long-term voyage, certain key aspects are missing in researches due to the over-focus on the conductivity and mechanical softness. For example, the tissue-level softness of PEDOT:PSS hydrogels would cause serious problems for manipulation, especially for implanted devices, where the device itself should have decent mechanical strength to penetrate the dura mater and the neural tissues. Therefore, solely decreasing the Young's modulus of PEDOT:PSS hydrogels would result technical issues. Moreover, in wearable application, conformability is one of the key aspects for the stability and reliability of the devices. But simply stretching and conforming the interface for temporary adhesion would inevitably build

inner strain, which would degrade the interface over time. Considering these limitations in pragmatic applications, we argue that a more comprehensive view should be applied to solve the real questions. Since hydrogel itself exhibit the ability for three-dimensional patterning via drop casting or 3D printing as well as the injectability[21], we foresee the importance to realize in situ shaping of PEDOT:PSS hydrogels in targeted areas via injection.

However, in most cases, in order to realize expected mechanical softness, robustness and electrical conductivity, available PEDOT:PSS hydrogels are synthesized in elevated temperature, for example, 60 °C for the interpenetration method[105], 90 °C for H_2SO_4 treatment method[114], 130 °C for DMSO treatment method[29]. Due to the temperature sensitivity of all tissues, heating to high temperature would burn them, resulting in additional trauma during interfacing. Therefore, in vivo applications of such high-temperature-processed PEDOT:PSS hydrogels are only limited to specific realms, precluding the chances to achieve in situ formation of strain-free biointerface. Hence, in order to regain the in situ patternability of hydrogels in PEDOT:PSS researches and therefore realizing the seamless and chronic functional interface, it's of great importance in developing low-temperature-processable PEDOT:PSS hydrogels which are compatible with in vivo manipulation.

2.3 Organic Electrochemical Transistors

The first OECT was invented by Mark S. Wrighton in 1984[115]. The PPy based device enabled the basic functionality in signal amplification supported by channel oxidation (on) and reduction (off) states. In 2007, the ion-to-electron conversion ability of organic conducting polymer has been revealed and modeled, making organic electronics, especially OECTs[116,117], a more pragmatic interface for human–computer interaction. Comparing to traditional inorganic bioelectronics, most of OECTs uses conducting polymer rather than silicon or other inorganic semiconductor as channel and replaced dielectric layer with electrolytes. Therefore, by replacing inorganic rigid

materials with intrinsic soft organic materials and polymers, OECTs have the mechanical strength in realizing flexibility[118], and stretchability[119]. Meanwhile, the adaptation for organic materials, especially conducting polymer thin films, also supports the outstanding biocompatibility and low cytotoxicity of OECTs[93], which it's one of the key problem silicon-based inorganic bioelectronics is facing for implanted devices[98]. In contrast to traditional field-effect transistors (FETs) that use dielectric properties of interlayer materials in forming capacitor for controlling the ultrathin channel layer for conductivity of the device, and electrolyte-gate FETs that use electrical double layers (EDLs) for increasing the capacitance by decreasing the effective thickness of dielectric layer, OECTs takes the advantage of ion transportation and ion injection into the bulk channel layer given the porosity of conducting polymer films. Therefore, the overall conductivity change of OECT devices is controlled by 3-dimensional bulky channel layer rather than the very thin semiconducting channel for FETs, resulting in higher sensitivity for sensing ions and molecules.

The channel of OECTs, as the very active layer that senses and responses according to the external stimulus, is one of the most critical layers for device properties. The materials for OECT channel mainly consist of PEDOT:PSS, PPy, PANi[120]. Although as the first materials adopted in fabricating OECTs, PPy has the major drawbacks in the poor electrochemical properties and stability[115]. PANi is a conducting polymer whose conductivity could be tuned by redox reaction. While in its reduced state (in leucoemeraldine phase), PANi has no or few free carriers in transporting; in its oxidation states (in emeraldine states), holes have been created since the main chain of PANi was ionized, and the π-π stacking structure in PANi could easily conduct holes. PEDOT:PSS is widely utilized in OECTs given its ability and stability in electrochemical and chemical modification in ambient atmosphere[121]. Accompanying with its advantages in water-solubility as well as stability, PEDOT:PSS has become the most popular conducting polymers in organic electronics and has been commercialized as discussed in previous section.

The following section narrowed down to the PEDOT:PSS-based OECTs, in spite that there are numbers of OECTs based on other organic conducting material. Firstly, the mechanism of OECTs as well as its difference with organic field-effect transistors (OFETs) would be discussed. Secondly, current PEDOT:PSS OECTs and their targeted applications are highlighted.

2.3.1 Organic electrochemical transistors device physics

OECTs, as a new branch of organic transistors, consists of organic semiconducting layer (PEDOT:PSS in this section) which is in contact with the electrolyte and bridges the source and drain source. Their architectures are similar to those of FETs. Therefore, the modelling and analysis of OECTs share numbers of theories with FETs, especially OFETs. Hence, in this part, a brief description about basic physics for OFETs would be introduced first before introducing the mechanism for OECTs.

2.3.1.1 From metal–oxide–semiconductor field-effect transistors to organic electrochemical transistors

OFET is the field effect transistor that uses organic semiconductor as its channel. In spite that organic semiconductors had been viewed to be of low and insufficient mobility, which is always lower than 10^{-4} cm^2/Vs, to drive transistors, recently there are many improvements due to the viability for more eligible conducting polymers with less defects, the more controlled processing. And with its strength in intrinsic flexibility and processability in low-cost roll-to-roll fabrication, OFETs have significant potential in active matrix electronic paper displays[122], and soft, flexible, stretchable, wearable electronics[123].

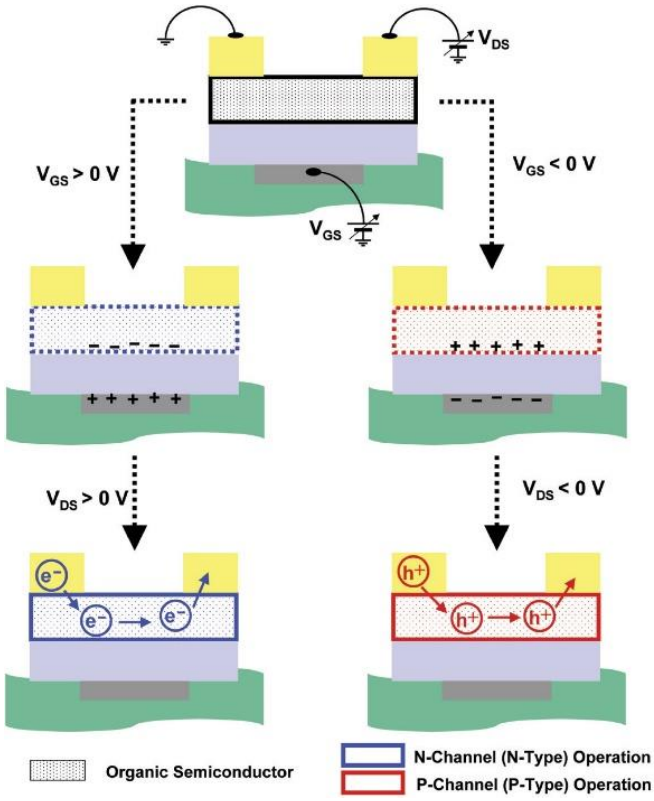

Figure 2-12 OFET. Schematic of p- and n-channel OFET [124]. Reprinted with permission.

The structures of OFETs are same as conventional metal–oxide–semiconductor field-effect transistors (MOSFETs). Organic semiconductors gated by metallic gate electrode, bridge the metallic source and drain electrodes. According to the organic semiconductor applied, the OFETs could be further divided into thin-film transistors (TFTs) where the orientation of organic molecules is in disordered state and single-crystal OFETs where the organic molecules are ideally organized without defects[125]. The discussion in this part would limit in TFTs given their similarity with OECTs.

Principally, OFETs are analogous to the accumulation mode inorganic transistors. When voltage applied on gate electrode, the charge accumulation layers would be induced in the channel region, therefore dramatically increase the conductivity of the channel. Similar to MOSFETs, the physics of OFETs could also be viewed as the integration of source-drain diode and gate-dielectric-channel capacitor. For the diode part, the current is also made up of drift and diffusion current in steady state. For the capacitor part, the model setting is same with MOSFETs, where the gate's

effects on channel layer are achieved by capacity control. By adopting the Poisson Equation and the charge neutrality equation, the spatial relationship between charge density and potential. In order to get the direct relationship between total charge density and surface potential, the assumption that all electrical field are perpendicular to the plane of channel. However, in contrast to MOSFETs whose working mode is in inversion region, OFETs normally work in accumulation region. Assuming the channel of OFET is long enough to preclude short channel effects, the charge density deduced by capacitor effects could be introduced into the diode equation. However, due to complexity of the equation and low carrier concentration in bulky and intrinsic organic semiconductor layer, it's reasonable to follow the charge-sheet approximation, where the number of induced free carriers on the surface of organic semiconductor is in the order of magnitude over that in bulk organic semiconductor. Therefore, when $V_{ds} < V_g - V_t$, as the linear region in output curve of MOSFETs, the current, source-drain voltage and gate voltage relationship in steady state could be simplified and expressed as following:

$$I_{ds} = \mu_{eff} C_d \frac{W}{L} (V_g - V_t) V_{ds}$$

, where I_{ds} is the source-drain current, μ_{eff} is the field effective mobility of organic channel, $C_d$is the capacitance of dielectric layer, $\frac{W}{L}$ is the width-to-length ratio of organic channel, V_g, V_t, V_{ds} are the gate voltage, threshold voltage, and source-drain voltage, respectively. When $V_{ds} > V_g - V_t$, as the saturation region in output curve of MOSFETs, the current, source-drain voltage and gate voltage relationship in steady state could be expressed as following:

$$I_{ds} = \mu_{eff} C_d \frac{W}{2L} (V_g - V_t)^2$$

In order to quantitively evaluate the quality and performance, there are mainly 7 parameters that are referred to: mobility, threshold voltage, contact resistance, on/off ratio, subthreshold swing, hysteresis, stability.

2.3.1.2 From organic field-effect transistors to organic electrochemical transistors

OECTs are a branch of transistors whose source-drain current are modulated by ion injection. Structurally, the configuration of OECTs is similar to that of OFETs, especially to electrolyte-gate FETs. The main difference between the two transistor is the mechanism that gate effects the corresponding transconductance of device.

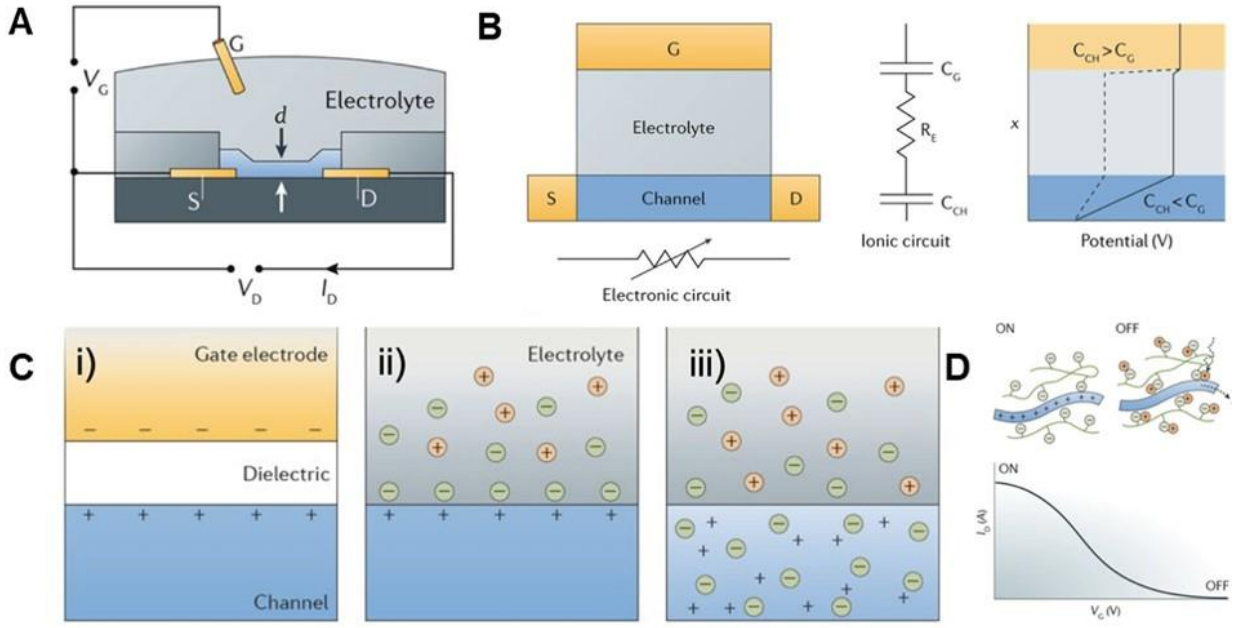

Figure 2-13 OECTs. A. The typical structure of an OECT, where G is gate, S is source, D is drain. B. Ionic and electronic circuits used to model OECTs. C. difference between OFET (i), electrolyte-gate FET (ii), and OECT (iii). D. Transfer curve of an PEDOT-based OECT[126]. Reprinted with permission.

For typical OFETs, the entire gate controlling process is based on the equivalent capacitance that gaps the direct electrical contact between gate and channel. When gate voltage applied, the existence of effective capacitance would result in the charge carrier density change on the interface sheet of organic semiconductor. As surface charges work in MOSFETs, the source-drain current is tuned according to the level of charge filled in, separating into accumulation, depletion, weak inversion, and strong inversion region. Electrolyte-gate FETs are OFETs that utilizes electrolyte rather than dielectric layer as the very gap for gate to amplify its control on

channel. Like typical OFETs, their controllability of gate is still based on the capacitance effects. However, comparing to typical OFETs, electrolyte-gate FETs utilize the spontaneous formation of the nanoscale electrical double layers (EDLs) on the interface of organic semiconductor layer and electrolyte. When gate voltage applied, the ions within the electrolyte would be driven and spontaneously move according to the electrostatic force. Cations would transport towards the surface where electrical potential is relatively lower, while anions would transport towards the surface where electrical potential is relatively high. The mass transfer process would sustain and drive ions towards the very thin region near electrodes, in the case, gate electrode and channel layer, until the equilibrium state reaches. Therefore, in steady state, most ionic charges would stick to the surface of channel layer and forming an effective plane-parallel capacitor whose net charge is the total ionic charge stick on the surface and whose inter-distance is merely the radius of attracted ions. Hence, the effective gate-channel capacitance in electrolyte-gate FETs is much larger than that in typical OFETs, according to the capacitance function of plane-parallel capacitor:

$$C = \frac{\varepsilon S}{4\pi k d}$$

, where ε is the dielectric constant of the gap, S is the effective area of channel surface, k is the Coulomb constant that is fixed to be $9 \times 10^9\ Nm^2C^{-2}$ in the case. Given the approximation function for the current, source-drain voltage and gate voltage relationship deduced in previous part, where $I_{ds} \propto C_d$, it's clear that the controllability of gate on source-drain current has been amplified in electrolyte-gate FETs. However, it's undoubtable that the basic mechanism for the gate controllability still rely on induced charges in channel region under external potential in both typical OFETs and electrolyte-gate FETs.

For OECTs, the gate controllability over channel conductivity originates from direct ion injection into bulky channel layer. In the case of PEDOT:PSS-based OECTs, the devices work in the depletion region. In other words, when no voltage applied, PEDOT:PSS is conductive since it

could generate electron-hole pairs in the main chain and the charge carriers could transport along single chain or hop between multiple chains. Therefore, the device is originally in ON state. After applying gate voltage (positive), the high potential in the region near gate would push cations towards channel. Different from electrolyte-gate FETs, where the ions could merely concentrate on the surface, OECTs enable the ion to directly penetrate the bulky channel layer. The cation would bond with PSS^- due to the electrostatic attraction, electrochemically dedoping PEDOT:PSS, which could be written as:

$$PEDOT^+PSS^- + M^+ + e^- = PEDOT^0 + M^+PSS^-$$

, where $PEDOT^+$ is PEDOT in oxidation and conductive state, M^+ is the cation injected from electrolyte, $PEDOT^0$ is PEDOT in reduced and nonconductive state. The process leads to switch OFF the device.

The parameters to evaluate OECTs normally includes the transfer and output curve, on/off ratio, transconductance, response time, and mobility. Similar to MOSFET and OFET researches, transfer and output curve include the information about on/off ratio, transconductance, mobility, and they are undoubtedly one of the most important properties of OECTs.

On/off ratio is the ratio of current in on state when gate voltage is zero over that in off state when gate voltage is positive. The ratio could be simply calculated based on the transfer curve of OECTs. In PEDOT-based OECTs, the typical methods in improving on/off ratio, therefore the switching ability of OECTs are by increasing the gate voltage to more aggressively electrochemically dedoping PEDOT: PSS channel. However, in actual device, the voltage applied on gate electrode could not be too large since it would inevitably increase the energy consumption of OECTs, and hence precluding its potential in pragmatic bioelectronics. Currently, OECTs could obtain high on/off ratio up to 10^5 [127].

Transconductance is the efficiency of transduction, which is calculated as the ratio of source-drain current deviation and gate voltage deviation extracted from the transfer curve. It can be written as[18]:

$$g_m = \frac{\Delta I_{ds}}{\Delta V_g}$$

Since OECTs permit ion injection from electrolyte directly into organic channel layer and affects not only interface layer but also the bulky organic channel, the transconductance of OECT is thickness-related and is much higher than that of either OFET or electrolyte-gate FET. The OECT transconductance in saturation region could be written as:

$$g_m = \frac{W \times d}{L} \mu C^* \left(V_t - V_g\right)$$

, where d is the thickness of organic channel (PEDOT: PSS in this case), μ is charge-carrier mobility (hole mobility in this case), C^* is the capacitance per unit volume of the channel[128]. However, the high transconductance of OECT leads to slow response, because thick organic channel layer needs to be dedoped via ion transport which is much slower than electron transport.

2.3.2 Applications of organic electrochemical transistors

Given the outstanding ability of OECTs in efficiently transducing ionic signals into electrical signals and in amplifying the sensing signals, OECTs play an important role in sensing. According to the fact whether faradic reaction happens on the gate electrode of OECT, the sensing could be divided into non-faradic sensing and faradic sensing. For gate voltage that is small and cannot excite electrolysis reaction of water or other electrochemical reaction, no net charge transfer between gate electrode and electrolyte would happen, therefore, the OECT sensing mechanism is in the regime of non-faradic sensing[129]. According to the Bernards model, the voltage drop

within gate and organic channel is controlled by the formation of EDL formation[116]. It could be written as:

$$V_{sol} = \frac{V_g}{1+\gamma}$$

, where $\gamma = \frac{C_c}{C_g}$ is defined to be the ratio of capacitance of channel over that of gate. However, when relatively active molecules are added into electrolyte or the gate voltage is large enough to drive electrochemical reaction, additional voltage drop would exist on the interface of gate electrode and electrolyte in order to support the electrochemical reaction processing[130]. Based on the Nernst Equation, the very voltage drops taken by electrochemical reaction could be written as:

$$V_{g,reaction} = \frac{kT}{ze} ln \frac{a_{ox}}{a_{red}}$$

, where k is the Boltzmann constant, T is temperature, z is the electron transferred per reactant being oxidized, e is the elementary charge, a_{ox}, a_{red} are the activity of the oxidized form and the reduced form, respectively. Assuming the solution is ideal, where activity of components quantitively equals their concentration, the overall voltage drop could be written as:

$$V_{sol} = \frac{V_g}{1+\gamma} + (\frac{kT}{ze} \ln c_{analyte} + constant)$$

, where $c_{analyte}$ is the concentration of analyte. Hence, when analyte concentration changes, the effective voltage applied on channel, therefore the charge carrier density, must change, resulting in the source-drain current change. Nowadays, there are already numbers of applications based on the sensitivity and the amplification functions published, including glucose[131,132], DNA[133], dopamine[134].

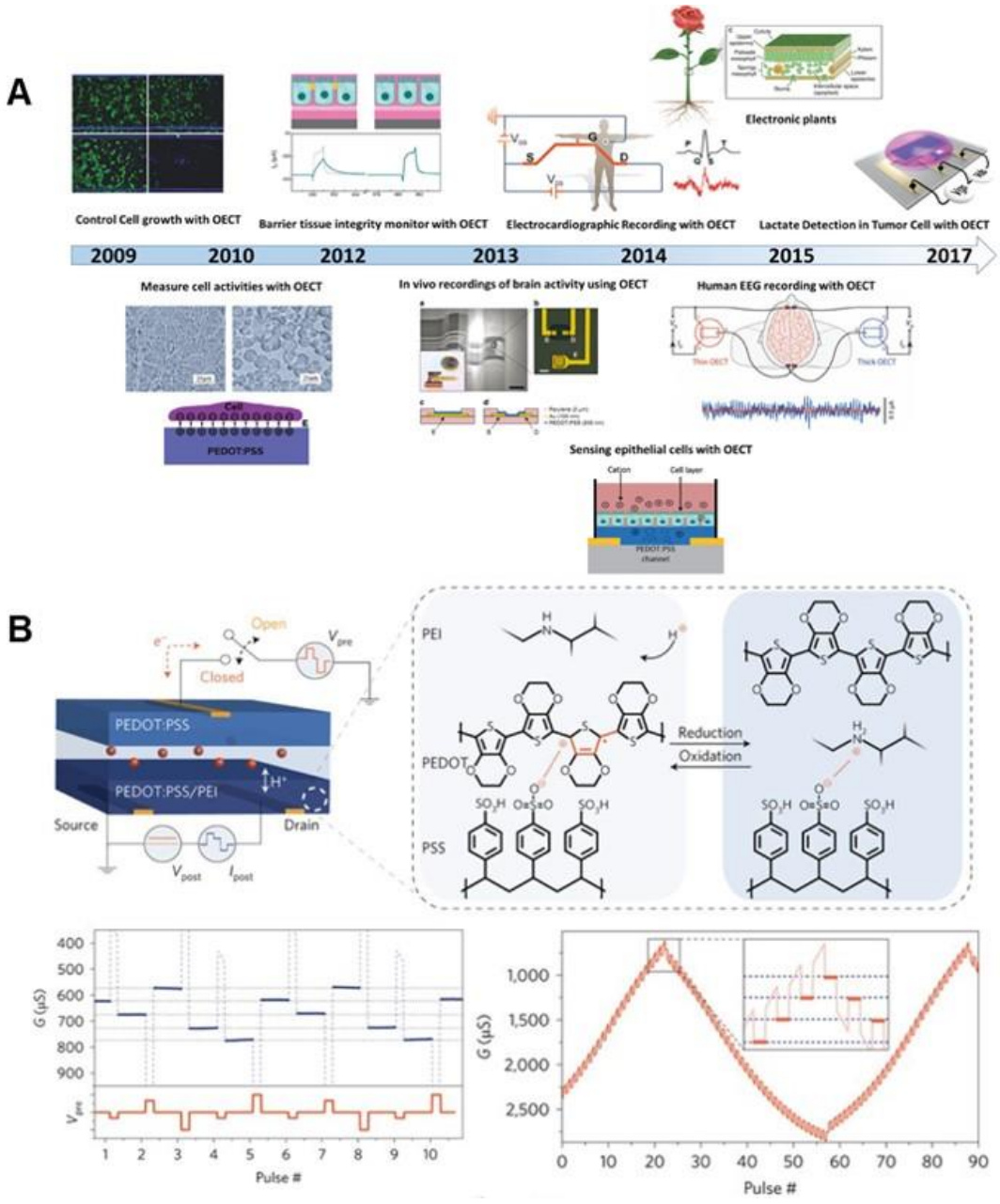

Figure 2-14 Applications of OECT. a) OECTs research progress in bioelectronics[135]. b) PEDOT-based OECT artificial synapses[136]. Reprinted with permission.

Bioelectronics is the major field that OECTs are designed to be, since OECTs are sensitive to external signals and they have significant potential in producing flexible and wearable electronics. According to the problems bioelectronics target to solve, OECTs could be utilized for electrophysiological activity sensing[93], impedance sensing[137], and analyte detection[138]. Moreover,

OECTs could be applied to monitor cell culture condition[139] especially its coverage over the substrate[137]. The basic mechanism for the process is that the thin layer of proliferating cells formed above the channel within culture media, which could also be viewed as electrolyte[140,141]. The changes including cells growth or inner-properties could induce corresponding change in overall impedance for electrolyte[142]. OECTs could then amplify the impedance change via charge carrier density in channel and record the fluctuations with current signals. Analyte detection in OECT bioelectronics is similar to conventional OECT for sensing. However, for bioelectronics, flexibility and biocompatibility shall also be considered for pragmatic clinical applications. Therefore, the voltage applied and materials in OECT are more cautiously selected. Currently, there are many successful OECT-based biosensors in saline solution including breath[143], sweat[144], saliva[145], cell culture media[146].

Memory and neuromorphic devices are also field that OECT could adopt. Since the doping process of OECT is realized via electrochemical reaction, OECT devices have long-term memory for the conductivity that applied before. In one way, by providing sufficient voltage with long period, OECT can be used memory. Otherwise, by dynamically doping the channel region, neuromorphic devices with a multi-state could be achieved. In 2017, Salleo et al. has fabricated a flexible artificial synapse based on OECTs, which could switch at low voltage and energy and mimic long-term potentiation and depression in biological synapses[16].

Chapter 3 Room-Temperature Formation of Poly(3,4-ethylenedioxythiophene):poly(styrenesulfonate) Hydrogels

3.1 Introduction

Poly(3,4-ethylenedioxythiophene) doped with poly(styrenesulfonate) (PEDOT:PSS) has earned tremendous success in the past years owing to its excellent biocompatibility, high electrical conductivity, and water stability[147]. Among the applications covering solar cells[4,148], light-emitting diodes[149], transparent electrodes[150], electrochemical transistors[53], neuromorphic computing[16,151], and supercapacitors[152], PEDOT:PSS has proven its potentials to be adopted as a generalized materials for electronics. With the rise of biomedical engineering, the electrical biointerface with human body has become an emerging trend to reliably monitor the health status of human body and to offer personized platform for precision medicine[153]. In recent years, owing to the superior flexibility comparing to silicon-based materials, PEDOT:PSS acts as a key role in developing soft bioelectronics for the seamless biointerface[30]. However, the real applications of PEDOT:PSS thin films, which most PEDOT:PSS bioelectronics researches relied on, reveal the huge intrinsic mismatches with endogenous tissues due to the mechanical rigidity (Young's moduli on the scale of MPa~GPa). Besides the risks of detachment which would degrade the input and output of the devices, such physical and mechanical mismatches may constantly irritate the normal metabolism of targeted regions, inducing immune effects which kill the local cells[29,105]. Therefore, PEDOT:PSS of tissue-level softness is of profound interests toward seamless and chronic bioelectronic interface.

PEDOT:PSS hydrogels are the optimal biointerfacing alternatives given its tissue-like mechanical properties, water-rich environment and biocompatibility. Except for acting as a extracellular matrix for cell growth and differentiation, PEDOT:PSS hydrogels provide a platform to investigate cellular

causality when exposed to electrical stimulations[154,155]. With the intention to synthesize and modify the PEDOT:PSS hydrogels for biointerface of minimized mismatches, tremendous research projects have focused on the fundamental properties of PEDOT:PSS hydrogels. Shi et al. used concentrated H_2SO_4 at 90 °C in processing PEDOT:PSS dispersion for synthesizing conductive PEDOT:PSS hydrogels which acted as electrodes in supercapacitors applications[114]. Bao et al. interpenetrated a secondary network within pre-formed PEDOT:PSS hydrogels to tune the mechanical properties in matching biological tissues[105]. Zhao et al. claimed pure PEDOT:PSS hydrogels by controlled dry-annealing and rehydration of PEDOT:PSS thin films[29].

However, most PEDOT:PSS hydrogels fabricated yet required elevated temperatures (> 60 °C) which are beyond the tolerance limit of biological tissues. While the additional needs for high temperature thermodynamically enable the hydrogel matrix formation or conductivity enhancement, the *in situ* processability, which are one of the key benefits of hydrogel engineering, is eliminated due to the inevitable damages to endogenous tissues. Therefore, in real applications, PEDOT:PSS hydrogels have to pre-form the geometries and then conform to the targeted shapes, which introduces inner strains and undermines the long-term stability of the seamless biointerface. With the intention to customize the PEDOT:PSS hydrogel shapes for seamless and chronic interface, PEDOT:PSS hydrogels that could be synthesize and processed completely at room temperature (RT-PEDOT:PSS hydrogels) are thus of significant importance. Besides the direct benefit for processing in situ, RT-PEDOT:PSS hydrogels offer a generalized platform for injectable applications where crosslinking and shaping can be controlled occurring at the exact locations where PEDOT:PSS liquid is injected. Accordingly, such hydrogels are of great medical demand, especially for nerve regeneration and brain stimulation or recording. Considering the swelling properties of hydrogels, RT-PEDOT:PSS hydrogels may also enable their application as water-healable electronics, an emerging field of PEDOT:PSS researches[156].

In this chapter, we demonstrated the first injectable and water-healable PEDOT:PSS hydrogels enabled by RT-PEDOT:PSS hydrogels. With no need for any further treatment, the RT-PEDOT:PSS hydrogels could gelate spontaneously after syringe-injecting PEDOT:PSS/surfactant mixture of liquid phase. Containing ultrahigh water content (~95 wt%), the RT-PEDOT:PSS hydrogels exhibit tissue-level softness (Young's modulus of kPa scale) and excellent patternability in shaping self-standing and patterned structures. Due to the interconnected PEDOT:PSS chains as the matrix, the RT-PEDOT:PSS hydrogels have ultralow electrical resistance in circuits. Moreover, owing to the high swelling ratios, the RT-PEDOT:PSS hydrogels obtain water-healability which could further strengthen its potential in real applications.

3.2 Room-temperature gelation of poly(3,4-ethylenedioxythiophene): poly(styrenesulfonate)

By mixing PEDOT:PSS suspension with the widely used surfactant DBSA, spontaneous gelation could occur at room temperature without the need for any other treatment when the concentration of DBSA is above the threshold (2 v/v.%). The formation of hydrogel is confirmed with the vial inversion test, which has been widely used as the criterion in judging the macroscopic phase transition in hydrogel engineering[157]. The mechanism of gelation would be discussed later in the following section.

The obtained RT-PEDOT:PSS hydrogels have ultrahigh water content (95 wt%). Since the entire synthesis process is in liquid states, the RT-PEDOT:PSS hydrogels could be customized and patterned into various of three-dimensional shapes by molding. It's worth noting that the gelation is not an instant transition from liquid to hydrogel, but an evolving process where the storage modulus and loss modulus are both increasing overtime. After transited into hydrogel states (the transition is confirmed by inversion test or rheological characterization), the synthesized RT-

PEDOT:PSS hydrogels would slightly shrink after leaving overnight, which significantly benefit for the demolding process by minimizing the chance in damage the hydrogels.

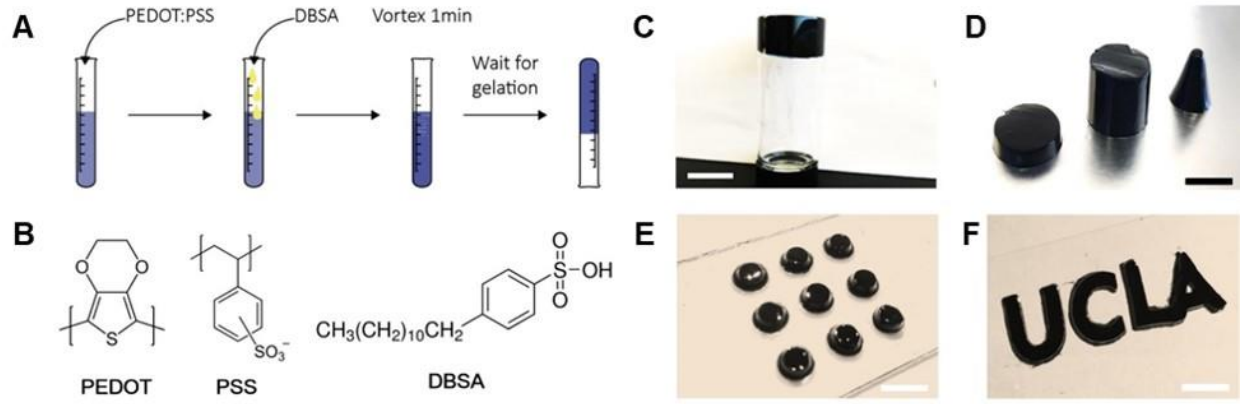

Figure 3-1 A. Schematic illustration of gelation processes of RT-PEDOT:PSS hydrogels; B. Chemical structures of PEDOT:PSS and DBSA; C. RT-PEDOT:PSS hydrogel formed within 10 min: the gel adhered at the bottom when flipping the vial; D. Demonstrations of self-standing RT-PEDOT:PSS hydrogels of different shapes; E-F. Various patterns of the RT-PEDOT:PSS hydrogel after removing PMMA molds. Scale bar: 5 mm.

3.2.1 Gelation mechanism

The spontaneous gelation process of the RT-PEDOT:PSS hydrogels at room temperature is tentatively attributed to the physical crosslinking between $PEDOT^+$ polymer chains[112,114], enabled by the addition of DBSA. As discussed in the PEDOT:PSS section, commercial PEDOT:PSS product is the suspension of PEDOT:PSS microgels in water environment supported by the hydrophilicity of PSS chains and dispersed by the electrostatic repulsion between charged microgels[112]. Within the microgels, coiled hydrophobic $PEDOT^+$ chains entangle with each other and act as the main component of the core of the domain, while the hydrophilic PSS^- chains forming the sheath to stabilize the existence of microgels within water[158]. For pristine PEDOT:PSS PH 1000, the medium number of the microgel size is 0.03 µm according to the information from Clevios™, the manufacturer. And in order to rule out the effects from intrinsic large PEDOT:PSS microgels, PEDOT:PSS suspension are filtered with 0.45-µm PVDF filter right after mixing with

surfactant, the initial size of PEDOT:PSS microgels is significantly smaller than that of macroscopic hydrogels.

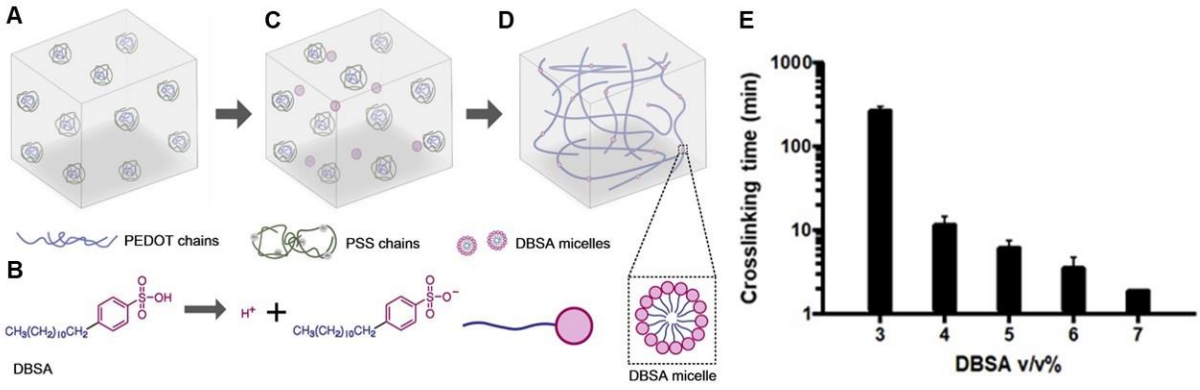

Figure 3-2 Crosslinking mechanism of our RT-PEDOT:PSS hydrogel: A. Schematic of core-shell structure of the PEDOT:PSS grains ($PEDOT^+$ core and PSS^- shell); B. Schematic of the hydrophilic head (pink) and hydrophobic tail (blue) of a DBSA molecule; C. The addition of the DBSA micelle into the suspension, which weakens electrostatic attraction between $PEDOT^+$ and PSS^-, exposing the $PEDOT^+$ chains to water; D. The exposed $PEDOT^+$ chains undergo a conformational change from a confined coiled to an expanded-linear structure and subsequently physically crosslinked due to π–π stacking and hydrophobic attractions. E. Gelation time of PEDOT:PSS hydrogels with different DBSA concentration. Error bars represent standard deviation (N=4).

DBSA is an acidic surfactant. When its concentration in water solvent is larger than the critical micelle concentration (0.04 v/v%), DBSA tends to be electrolyzed and form well-defined micellar structures in water, where the negatively charged sulfuric acid groups (SO_3^-) are facing out. The presence of sufficient DBSA molecules in the final RT-PEDOT:PSS hydrogels has been confirmed by Fourier-transform infrared spectroscopy (FTIR) (Figure 3-3). And by changing the adding amount of DBSA, the gelation time of RT-PEDOT:PSS hydrogels could be controlled, indicating the active roles of DBSA in the hydrogel formation process. With strong negative charges, electrolyzed DBSA molecules are likely to protonate PSS^- chains, screening the electrostatic attractions between $PEDOT^+$ chains and PSS^- counterions. Therefore, the soft and hydrophilic PSS long chains are released from PEDOT:PSS complexes and dissolved in water. The $PEDOT^+$ chains which originally coiled as the core of PEDOT:PSS microgels are coupling with DBSA anions, undergoing the conformational change towards a more expanded and linear

structure[72]. Such spreading structure of $PEDOT^+$ chains promotes the interchain interactions in forming three-dimensionally crosslinked $PEDOT^+$ networks facilitated by the physical interaction induced by π-π stacking and hydrophobic interactions. This mechanism based on physical crosslinking could be further evaluated by the complex viscosity of as-prepared RT-PEDOT:PSS hydrogels. The trend of complex viscosity decreasing when increasing the shear frequency from 0.1 to 10 rad/s indicates a typical behavior of physically crosslinked elastic hydrogels[159,160].

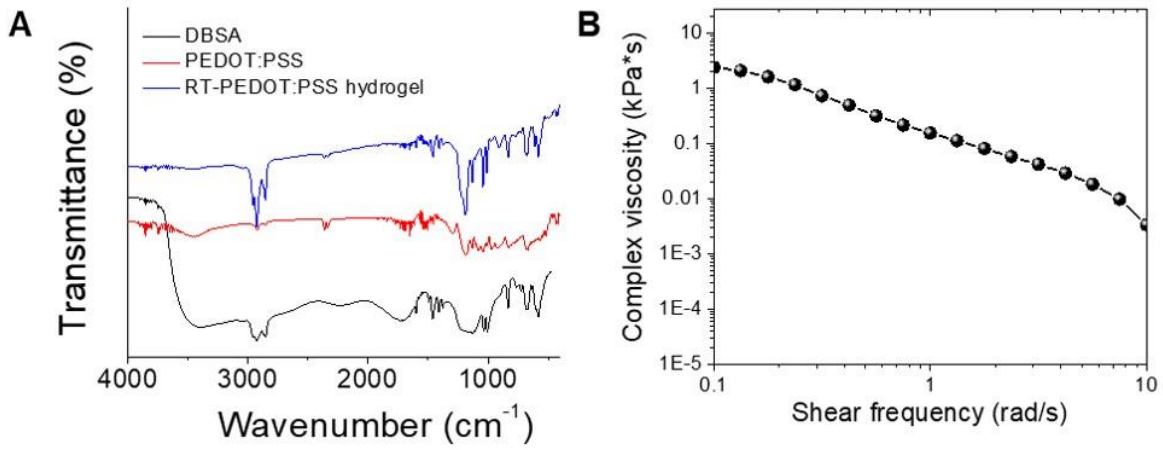

Figure 3-3 A. FTIR of pure DBSA, pure PEDOT:PSS and RT-PEDOT:PSS hydrogel. In RT-PEDOT:PSS hydrogel, the strong peaks from 2800 to 2950 cm^{-1} is attributed to (C-H) stretching vibration in benzene ring and aliphatic chain from DBSA. The peaks around 1000–1200 cm^{-1} are assignable to the vibration of sulfone groups in both PSS and DBSA. Peaks in range from 600 to 1000 cm^{-1} are contributed from vibration modes of C–S bond in the thiophene ring in PEDOT:PSS and C-H bending in disubstituted benzene ring in DBSA. B. Complex viscosity of RT-PEDOT:PSS hydrogel as a function of shear rate.

3.2.2 Mechanical properties

The as-prepared RT-PEDOT:PSS hydrogels exhibited tissue-level softness. In order to preserve the integrity and mechanical properties intact, the RT-PEDOT:PSS hydrogels were manipulated with special care. The RT-PEDOT:PSS hydrogels were molded in standardized PMMA wells with two designed holding pads and one effective stretching region. Because of the extreme softness and water-rich nature, the as-prepared RT-PEDOT:PSS hydrogels were slippery and vulnerable when directly clamped by INSTRON tensile tester. Customized polymethyl methacrylate (PMMA)

clamps were designed and patterned by CO_2 laser cutter. The molded RT-PEDOT:PSS hydrogel samples were left in wet atmosphere (by putting some water in a small petri dish within the sealed container with as-prepared RT-PEDOT:PSS hydrogels) overnight to stabilize the mechanical and physical properties of the hydrogels (the evolving mechanical properties could be proved by the real-time modulus change during the very first 30 min of gelation). The RT-PEDOT:PSS hydrogel testing sample was carefully transferred to the PMMA clamps by the gravity and the momentum introduced by water drops. After restricting the RT-PEDOT:PSS hydrogel samples within the PMMA clamps by screwing, the two PMMA clamps confining the two holding pads of the tested hydrogels were tapped in order to preserve the original length of the RT-PEDOT:PSS hydrogel sample and to prevent the damage to the effective testing region of the sample. The tapes were cut right before initiating the tensile test. From the stress-strain curve, the Young's modulus of the RT-PEDOT:PSS hydrogels was ~1 kPa, which reached the tissue-level softness. As the targeted interfacing tissues, the brain (although the dura mat is very rigid, for implanted device, dura mater would be removed during the scalp removal, therefore is not considered here.) shows the Young's modulus of 1-4 kPa[22], where the RT-PEDOT:PSS hydrogels have the potential in behaving identically with the endogenous brain tissues without introducing any stress on surrounding cells when undergoing constant motions driven by the respiration and acceleration (for example, head shaking).

The rheological measurements were applied to further evaluate the hydrogel nature of RT-PEDOT:PSS (25-mm sandblasted steel plate geometry and 1-mm gap distance). Real-time gelation rheological measurements were performed by using time sweeps of 1% strain and 1 Hz at 25 °C, after loading 500 µL precursor solution (4 v/v% DBSA) which has been stirred for 2 min and filtered through 0.45 µm PVDF filters to preclude the effect from intrinsically large microgels in commercial PEDOT:PSS suspension. The gelation time (~10 min) defined by the crossing point of G' and G'' agreed with the vial inversion test[105]. After stabilizing the as-prepared PEDOT:PSS

hydrogels overnight, oscillatory time sweeps of PEDOT:PSS hydrogel were performed at 1% strain, 1 Hz, 25 °C, after loading PEDOT:PSS hydrogels, indicating the RT-PEDOT:PSS reached steady state overnight.

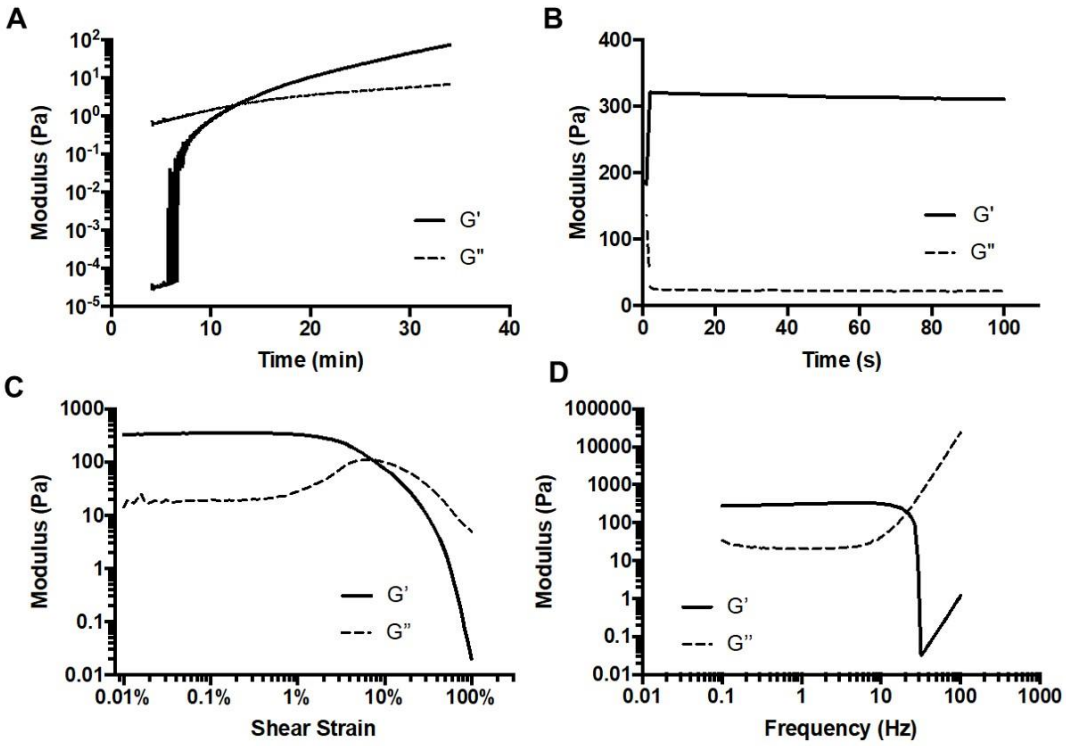

Figure 3-4 Rheological properties of RT-PEDOT:PSS hydrogels. A. Real time gelation in rheometer. Constant 1% strain, 1 Hz, at 25 °C; B. Oscillatory time sweep. Constant 1% strain, 1 Hz, at 25 °C; C. Oscillatory strain sweep. Constant 1 Hz, at 25 °C; (strain 0.01-100%); D. Oscillatory frequency sweep. Constant strain 1 Hz, 25 °C. (frequency 0.01-100 Hz); The rheological measurements were performed using an MCR 302 Rheometer (Anton Paar, Graz, Austria) with 25 mm steel plate geometry at 1 mm gap distance. G' (solid line) and G'' (dashed line) mean storage and loss modulus, respectively.

3.2.3 Electrical properties

The RT-PEDOT:PSS hydrogels exhibit decent conductivity of ~0.1 S/cm. Although the conductivity is lower than that of PEDOT:PSS thin film (>1 S/cm) since the π-π stacking in three-dimensionally crosslinked PEDOT networks is not so dense as in two-dimensional plane, considering the scenario where RT-PEDOT:PSS hydrogels would be applied, such conductivity has already orders of larger than those of biological tissues[161]. For instance, the cerebrospinal fluid (CSF) holds the highest conductivity among human tissues, but the conductivity (15.38 ×

10^{-3} S/cm) is still much lower than that of RT-PEDOT:PSS hydrogels. Therefore, RT-PEDOT:PSS hydrogels are electrically applicable for seamless electrical biointerface in vivo. Moreover, since in real application, as a three-dimensional material, RT-PEDOT:PSS hydrogels would have the dimension of thickness. According the Pouillet's law:

$$R = \rho \cdot \frac{l}{A} = \frac{l}{\sigma \cdot W \cdot H}$$

, where R is the overall resistance, $l, A, W, H$are the length, cross section area, width and height of the resistor, respectively. The resistance would significantly decrease when the bulky hydrogels are of large cross section or height, which are common for the targeted biointerface application. An as-prepared bulky RT-PEDOT:PSS hydrogel (length × width × thickness: 15 mm × 5 mm × 5 mm) have resistance of ~100 Ω. Long-term resistance of PEDOT:PSS hydrogels were tested by directly putting the bulky RT-PEDOT:PSS hydrogels between the two adjacent gold electrodes (There would be significant contact resistance given the watery and microporous structure of hydrogels) and then biasing at a constant direct current (DC) voltage of 0.1 V. When exposed to air and naturally dehydrating the RT-PEDOT:PSS hydrogels, the dramatic conductance increase would occur since the π-π stacking degree is enhanced. Moreover, the bulky RT-PEDOT:PSS hydrogels can also play as conductive interconnects to drive a light-emitting diode (LED) circuit as a demonstration for its potential for bioelectronic applications. Interestingly, attributable to their favorable viscoelastic property, the brightness of the LED was insensitive to external cuts in the hydrogel interconnects, indicating that the RT-PEDOT:PSS hydrogels can remain the high conductivity level even after single cutting. The current flow through RT-PEDOT:PSS hydrogel interconnects could only be interrupted by removing a bulky segment of the original hydrogel to result in the macroscopic loss of conductor. Simply by reuniting the removed RT-PEDOT:PSS hydrogel segment, the current could successfully recover to its original state, demonstrated by the brightness of the LED.

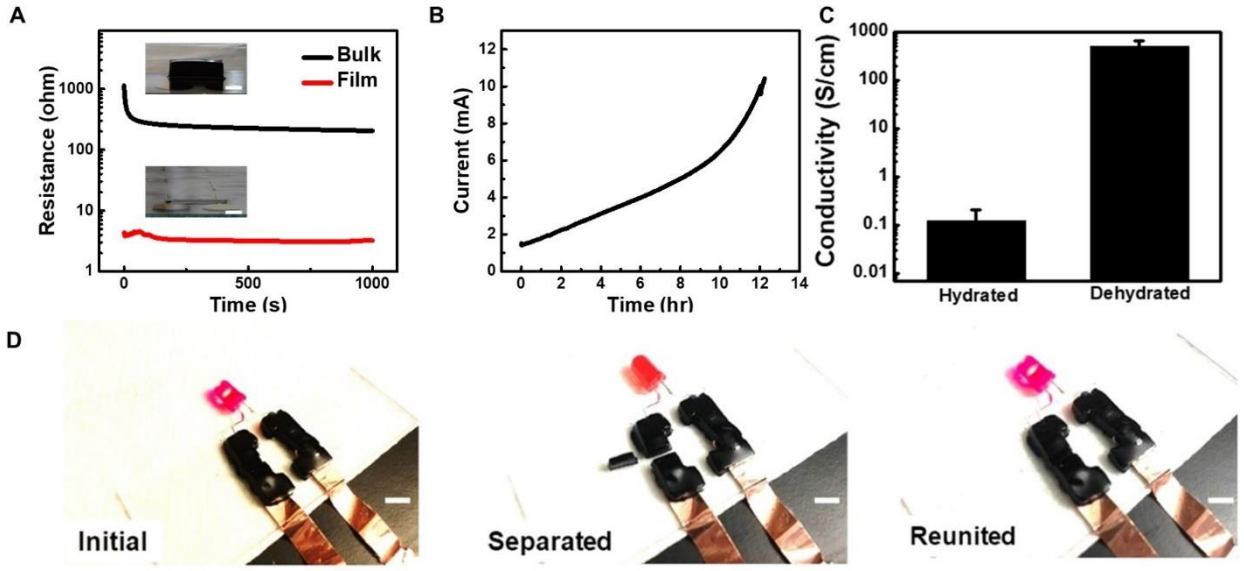

Figure 3-5 A-B. Long-term resistance of RT-PEDOT:PSS hydrogels and PEDOT:PSS films was tested by biasing at a constant direct current (DC) voltage of 0.1 V. RT-PEDOT:PSS hydrogels (length × width × thickness: 15 mm × 5 mm × 5 mm) were directly placed between Au electrodes whose inter-distance was 12 mm. PEDOT:PSS films were fabricated by heating RT-PEDOT:PSS mentioned above in 140 °C for 4 hours. C. Conductivity of RT-PEDOT:PSS hydrogels under hydration and dehydration states (100 °C, 4 hours). D. RT-PEDOT:PSS hydrogels acting as conductive interconnects to drive a LED via a "cut and stick" approach. Scale bar: 5 mm.

3.2.4 Biocompatibility

Given the RT-PEDOT:PSS hydrogels' potential applications in electromyography (EMG) interface, the biocompatibility of RT-PEDOT:PSS hydrogels were evaluated on the myoblast of *Mus musculus* from mouse (C2C12). Since the RT-PEDOT:PSS hydrogels have the PSSH and DBSA residues which are of high acidity. The intrinsic biocompatibility of RT-PEDOT:PSS hydrogels might be undermined. In order to remove the acidity of RT-PEDOT:PSS hydrogels, the hydrogel-coated polyethylene teraphthalate (PET) was rinsed thoroughly with Dulbecco's phosphate-buffered saline (DPBS). The viability of C2C12 exhibited no significant different from the control groups (no hydrogel coated PET films). Therefore, the RT-PEDOT:PSS hydrogels allow the cellular growth, supporting the chronic biointerface.

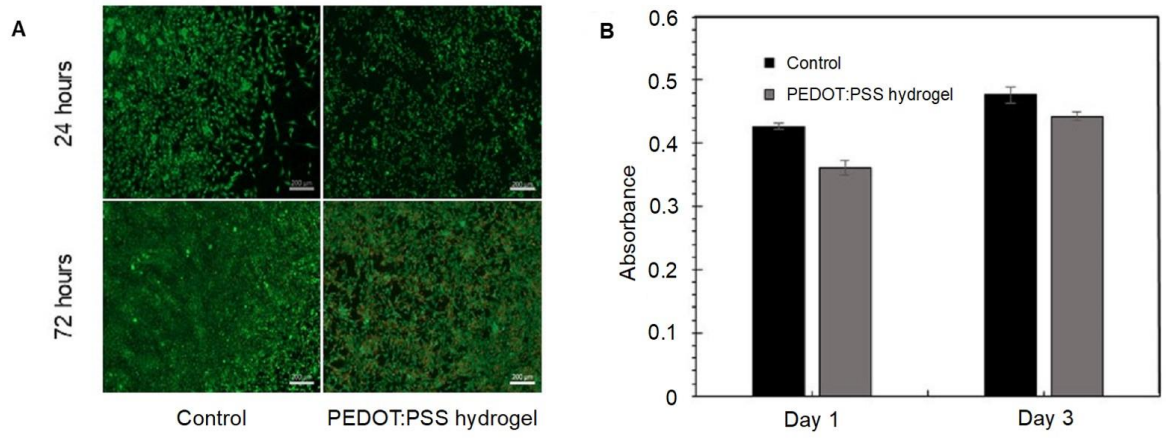

Figure 3-6 A. A representative image of live/dead assay of mouse muscle cells (C2C12) cultured on control (without RT-PEDOT:PSS hydrogels) and RT-PEDOT:PSS hydrogel substrates for 24 and 72 hours; B. quantitative analysis of cell proliferation: absorbance (at 570 nm) of cells after Presto Blue staining. Error bars represent standard deviation (N=3).

3.3 Injectable room-temperature-formed PEDOT:PSS hydrogels

Injection is a well-recognized approach in biomedical engineering and clinical usage due to its easy and minimally invasive access to the targeted region supported by the background knowledge of anatomy. Lieber et al. proposed the one of the first idea to combine the concepts of injectable and bioelectronics by directly syringe-injecting the nanofabricated mesh electronics into the targeted brain tissues for chronic biointerface[162,163]. However, the extremely flexible electronics is vulnerable to crumple when injecting into the tissue because of the excess water injection needed to push mesh electronics into the body[164]. Moreover, the pre-patterned input/output (I/O) pads of μm-scale mesh electronics also accompany with serious challenges in align the single electrodes with the flexible flat cable (FFC) or amplifier[164]. On the contrary to the method which requires superior dexterity, injectable hydrogels can be simply applied for biomedical applications in drug delivery, 3D printing and tissue engineering, due to the excellent patternability in vivo[165]. Additionally, the hydrophilicity and biocompatibility of hydrogel materials could not only passively allow their existence within endogenous minimizing the foreign body effects, but also actively acts as the scaffold for cell regeneration. Inspired by the benefits of

injectable electronics and hydrogels, we argue that the RT-PEDOT:PSS hydrogels could be manipulated as injectable conductive hydrogels.

3.3.1 Room-temperature-formed PEDOT:PSS hydrogels as injectable fillers

To evaluate its injectability, we demonstrated the RT-PEDOT:PSS hydrogels can be used as injectable fillers in a void and be patterned into different three-dimensional shapes. The injectable molding process only required a minimized puncture with the size of needles. During the 10-min window before gelation, the pre-mixed PEDOT:PSS/DBSA liquid could be conveniently prepared even in the surgery room and be injected into the targeted region in situ adjusting the designed three-dimensional geometries without introducing any stress on the endogenous tissues.

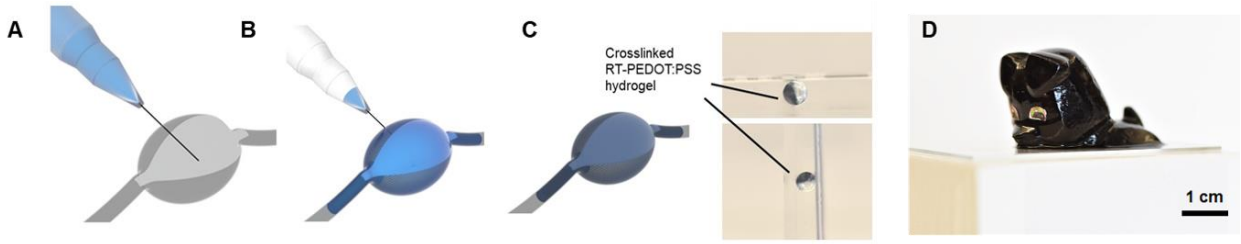

Figure 3-7 A-C. Schematic of injectable RT-PEDOT:PSS hydrogels: A. Puncturing the soft tissue with syringe; B. Syringe-injecting PEDOT:PSS suspension (w/DBSA) into the cavity; C. RT-PEDOT:PSS hydrogel formed spontaneously after 10 min; The optical images show the RT-PEDOT:PSS hydrogel attached to the wall of the cavity even we flipped the mold; D. Freestanding complex three-dimensional shaped RT-PEDOT:PSS hydrogels (PEDOT:PSS hydrogel dog) could be obtained by injecting PEDOT:PSS/DBSA mixture into PDMS void. The eyes of the PEDOT:PSS hydrogel dog was drawn on paper and manually stuck to the location.

PDMS molds with void are used as the phantoms for the in-body lumens where the biointerface would be applied, such as thoracic cavity or peritoneal cavity. By partially filling the void with filtered PEDOT:PSS/DBSA liquid, the RT-PEDOT:PSS hydrogels could spontaneously form after 10 min gelation window, which could be confirmed by the vial inversion test (The injected components could remain its integrity even after flipping the PDMS molds). Considering the real scenarios where the targeted regions are normally of more complex two-dimensional and three-dimensional structures, we fabricated a monolithic PDMS mold by casting a dog toy to mimic the

complexity for in situ shaping. As expected, the injectable RT-PEDOT:PSS hydrogels replicated the geometric features of the original shape with high fidelity. The results indicate the possibility to reliably molded by the endogenous tissues and forming the customized, stress-free contact for chronic biointerface.

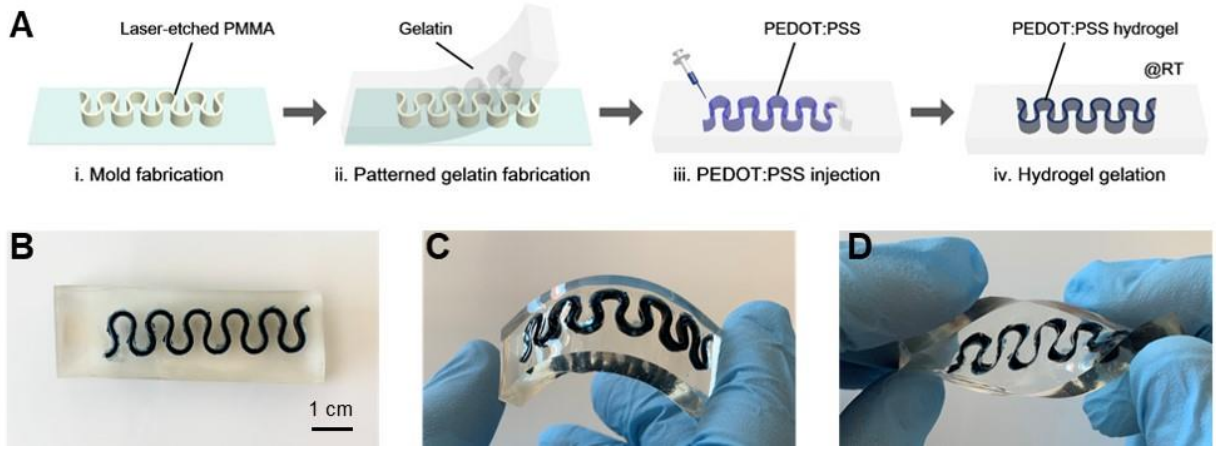

Figure 3-8 A. Schematic of inject-patterning RT-PEDOT:PSS hydrogel on temperature-sensitive gelatin substrate with pre-defined serpentine structures. B-D. Optical images of the injected RT-PEDOT:PSS hydrogel inside gelatin substrates (B), under bending (C) and twisting (D).

Another requirement for injectable hydrogels in biomedical engineering is the capability to be synthesized and processed with no need to significantly increase the temperature which would burn the endogenous tissues. Comparing to available methods of PEDOT:PSS hydrogels where elevated temperature is required to enable the formation or enhancement of the hydrogels, the RT-PEDOT:PSS hydrogels could be directly fabricated and functionalize on temperature-sensitive substrates in situ. Gelatin is a branch of skin-derived biocompatible hydrogels. Similar to the physical properties of skin, gelatin could not tolerate high temperature, since its melting point is around body temperature (~37 °C). Therefore, we demonstrated that the RT-PEDOT:PSS hydrogels forming in situ could act as conductive interconnects within temperature-sensitive gelatin channels. Gelatin with serpentine hollow channels were first created by casting. After sealing gelatin channels by attaching gelatin sheets, PEDOT:PSS/DBSA liquid was syringe-injected into these channels (note that another puncture site for venting is needed.). The RT-

PEDOT:PSS hydrogels could gelate spontaneously after 10 min with the identical shape of the serpentine channels. Interestingly, the RT-PEDOT:PSS hydrogel interconnects could tolerate multiple mechanical deformation such as bending and twisting without any breakings, indicating its robustness when interfacing endogenous biological tissues. The current flow through the RT-PEDOT:PSS hydrogel maintained 80% of its initial value even after strained up to 50% (gelatin rupture), demonstrating its potential for chronic and stable biointerface.

3.3.2 Stiffening room-temperature-formed PEDOT:PSS hydrogels

The pristine RT-PEDOT:PSS hydrogels (~1 kPa) perfectly fit in the young's modulus range covering brain, bone marrow, making it an ideal material for seamless and chronic biointerface. However, there are still electroactive tissues whose young's modulus is larger, for example, heart and kidney. With the intention to open up the interface window to a broader spectrum, we designed our formulation in stiffening our injectable RT-PEDOT:PSS hydrogels merely in a room temperature treatment.

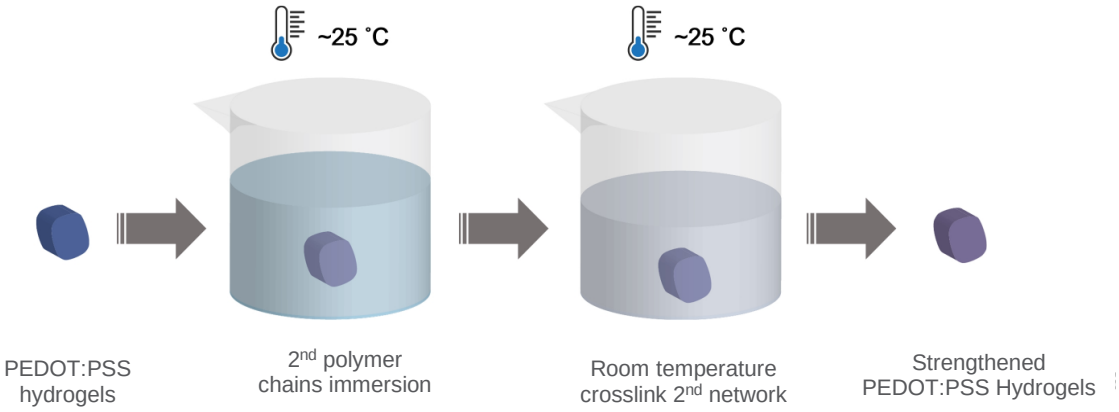

Figure 3-9 Schematics of room-temperature interpenetrating 2nd network within RT-PEDOT:PSS hydrogels.

We use the interpenetration method to stiffen our gel, because it would not significantly affect the conductivity of our PEDOT:PSS hydrogel, since the crosslinked PEDOT networks would not be significantly affected by the add-on secondary networks[105]. As an example, polyacrylamide (PAAm) system was adopted due to its excellent mechanical properties[166,167]. More importantly,

we chose ammonium persulfate (APS) as our initiator, since its best activation temperature is just room temperature (~25 °C), which is proven by many other works[168,169]. The overall process could be divided into two main steps. In the first step, the pristine RT-PEDOT:PSS hydrogels are immersed in the solution of aqueous PAAm precursor solution (or injecting aqueous PAAm precursor solution into the void where the RT-PEDOT:PSS was interfacing). The exchange of water content with surround atmosphere would help the RT-PEDOT:PSS infiltrate with monomers, crosslinkers, and accelerators. After removing the remainder molecular on the surface of RT-PEDOT:PSS hydrogels (or ejecting the remaining solution within the void), the AAm-infiltrated hydrogels were then immersed in APS solution to initiate the crosslinking of PAAm in situ within the crosslinked PEDOT networks (or injecting APS solution). Comparing to pristine RT-PEDOT:PSS hydrogels, the PAAm-treated hydrogels exhibit similar level of conductivity, since the conducting networks are intact. However, it's worth noting that the immersion in PAAm precursor solution would induce slight shrinking of RT-PEDOT:PSS hydrogels.

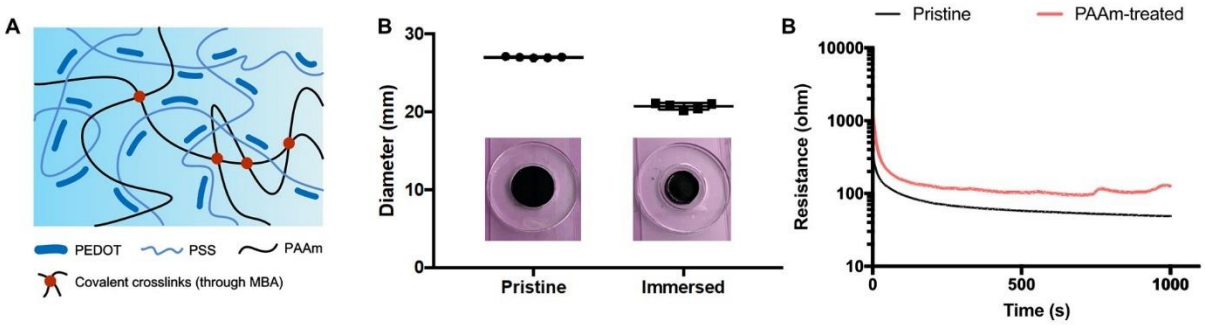

Figure 3-10 A. Schematic of introducing PAAm hydrogel network to injectable RT-PEDOT:PSS hydrogel for mechanical strength improvement. B. deformation after PAAm interpenetration (N=3). C. Resistance of pristine and PAAm-infiltrated PEDOT:PSS hydrogels.

Assisted by the secondary networks, the mechanical rigidity of RT-PEDOT:PSS hydrogels gained significant increase. The Young's modulus of PAAm-infiltrated RT-PEDOT:PSS hydrogels reached ~10 kPa, which is similar to the mechanical rigidity of pristine PAAm hydrogels of synthesized with same concentration (without PEDOT network)[170]. Therefore, except for the direct conclusion that the PAAm-infiltrated RT-PEDOT:PSS hydrogels could follow the logic of fully

injection-processable RT-PEDOT:PSS hydrogels and in situ modify its mechanical properties, which are comparable to that of heart tissues[22], we argue that the approach of interpenetrating mechanically robust networks in concreting the physically crosslinked PEDOT networks could be applied as a general method in maintaining the conductivity but adjusting mechanical properties for a broader spectrum of biointerface.

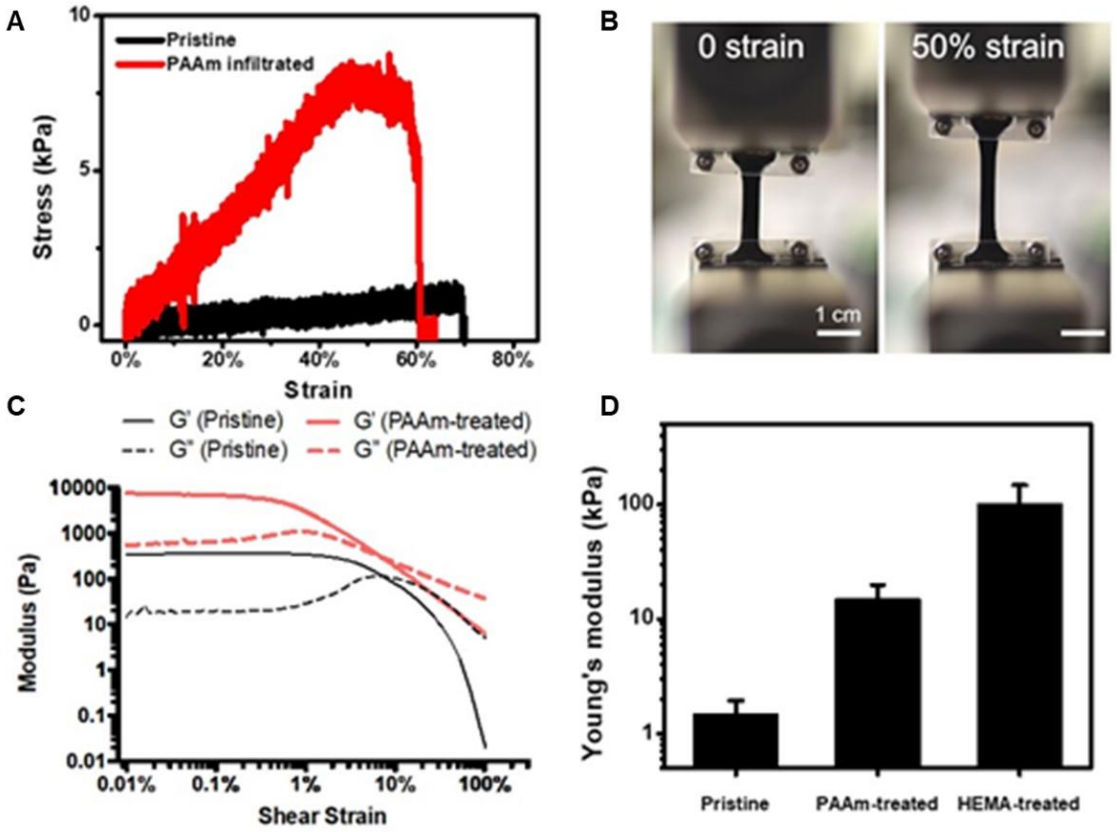

Figure 3-11 A. Stress-strain curves of PEDOT:PSS hydrogels with and without infiltrated PAAm network. B. Digital photos of PAAm-infiltrated PEDOT:PSS hydrogels under different strain levels (0 and 50%). C. Oscillatory strain sweeps of pristine and PAAm-treated PEDOT:PSS hydrogel. Sweeps were performed at 1 Hz. G' (solid line) and G'' (dashed line) mean storage and loss modulus, respectively. D. Young's moduli of PEDOT:PSS hydrogels with and without infiltrated PAAm and HEMA network. Error bars represent standard deviation (N=3).

In order to evaluate the idea could be adopted as a general rule, we tested the HEMA-treated RT-PEDOT:PSS hydrogels. As expected, HEMA-treated PEDOT:PSS hydrogels shared the electrical properties with pristine RT-PEDOT:PSS hydrogels, while the mechanical properties moved

toward to those of pristine poly(HEMA) hydrogels. According to the rheological measurement, the mechanically stiffened RT-PEDOT:PSS remained the nature of hydrogels with G'>G''.

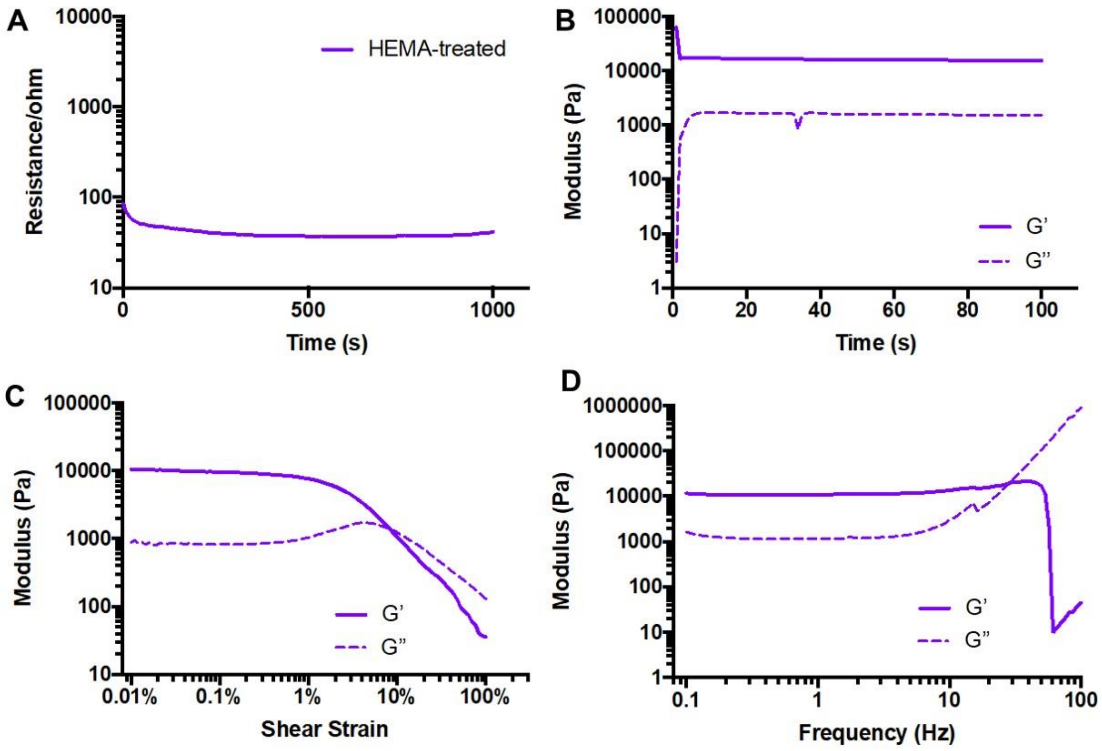

Figure 3-12 HEMA-infiltrated RT-PEDOT:PSS hydrogels. A. Resistance of pristine and HEMA-infiltrated PEDOT:PSS hydrogels. B. Oscillatory time sweep of HEMA-infiltrated PEDOT:PSS hydrogels. Constant 1% strain, 1 Hz, at 25 °C; C. Oscillatory strain sweep of HEMA-infiltrated PEDOT:PSS hydrogels. Constant 1 Hz, at 25 °C; (strain 0.01-100%); D. Oscillatory frequency sweep of HEMA-infiltrated PEDOT:PSS hydrogels. Constant strain 1 Hz, 25 °C. (frequency 0.01-100 Hz); The rheological measurements were performed using an MCR 302 Rheometer (Anton Paar, Graz, Austria) with 25 mm steel plate geometry at 1 mm gap distance. G' (solid line) and G'' (dashed line) mean storage and loss modulus, respectively.

3.4 Self-healing room-temperature-formed PEDOT:PSS hydrogels

Human body is a precise machine. Especially for implanted biomedical devices, after the initial insertion process, no further alternation could be applied to the very implanted device unless holding another surgeon to grant new access to the regions of interest. Therefore, it is of great importance to grant self-healability to the materials and devices implanted to minimize the trauma during therapeutics[171]. Recently, it was reported that PEDOT:PSS thin films (thickness of ~1 μm) exhibited mechanical and electrical healability when exposing to water due to the swelling of

PEDOT:PSS. Accordingly, we investigated the swelling properties and the self-healability of our RT-PEDOT:PSS hydrogels in order to achieve chronically stable biointerfaces.

3.4.1 Swelling properties

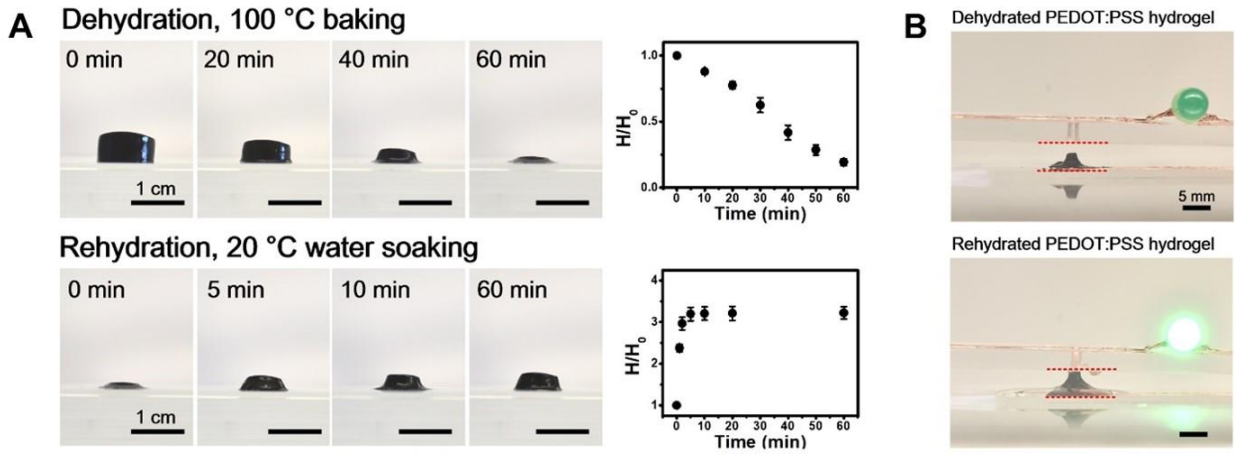

Figure 3-13 A. Shrinking and swelling properties of the RT-PEDOT:PSS hydrogels under mild dehydration; B. Application of the swellable RT-PEDOT:PSS hydrogel as a water-controllable switch for LED.

In order to test the possibility for swelling and rehydration, we first tested RT-PEDOT:PSS hydrogels undergoing severe dehydration (100 °C) process. The height of RT-PEDOT:PSS hydrogel were used as the indicator of the degree toward swelling and rehydrating. After 1 hr dehydration (mild dehydration) at 100 °C isothermal oven, the RT-PEDOT:PSS hydrogels could shrink to 20% of original size. Because of the contact between hydrogels and substrates and gravity, the RT-PEDOT:PSS hydrogels exhibited anisotropic shrinking. When exposed to water, the partially dried PEDOT:PSS hydrogels quickly absorbed water and swell 300% within the first 5 min. Inspired by the swelling behavior and fast response, we demonstrated a humidity-sensitive switch based on the RT-PEDOT:PSS hydrogels. The partially dried RT-PEDOT:PSS hydrogels were placed between two conductive cooper tapes which were adhered to glass slides. 0.2 V voltage is applied in order to drive the LED circuit when the circuit is in ON state. Initially, the partially dried RT-PEDOT:PSS hydrogels were in dry atmosphere, therefore, the macroscopic gap (1 mm) between the copper electrodes prohibited current flow through, and LED is OFF.

When exposed to water, RT-hydrogels could response quickly to physically connect the circuit, enabling current flow indicated by the LED shining.

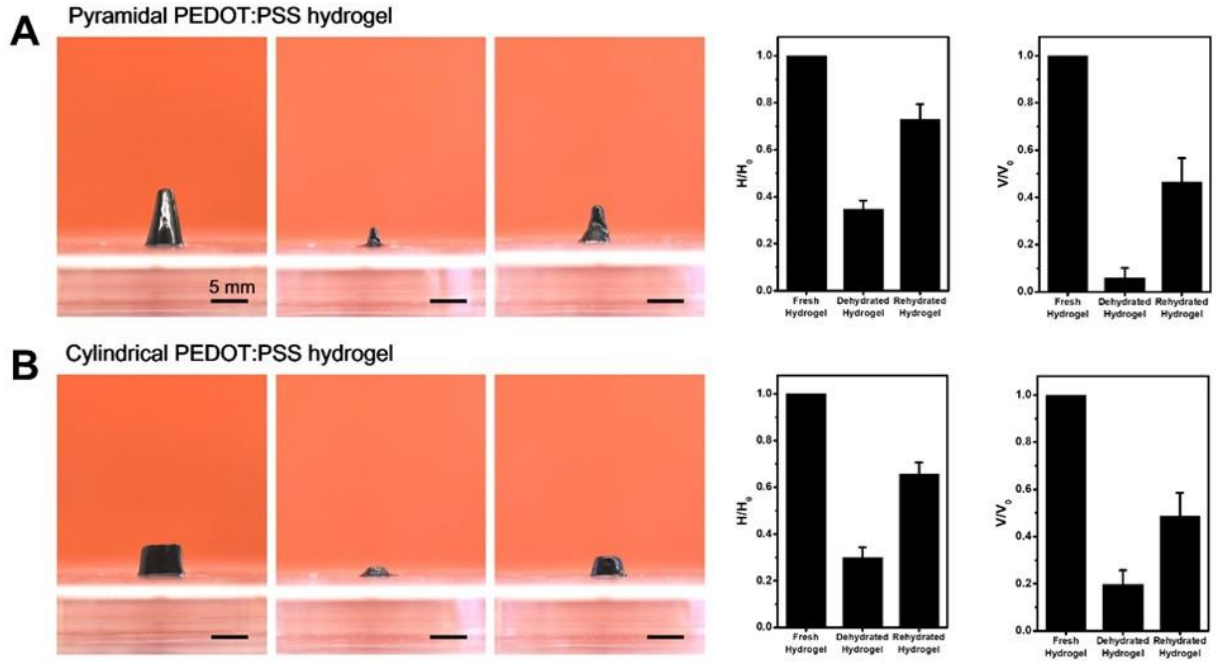

Figure 3-14 Optical images showing the shrinking and swelling of RT-PEDOT:PSS hydrogels dehydrated at room temperature (overnight), with a) pyramid and b) cylinder geometries. H0 denotes the initial height of the hydrogel (before dehydration). The rehydration (swelling) images were taken after immersing the dehydrated samples in water for 5 min. In both cases, the dehydrated hydrogels show a remarkable increase in height after rehydration. Error bars represent standard deviation (N=3).

Supported by the preliminary results, we evaluated the swelling and rehydration ability of RT-PEDOT:PSS hydrogels dehydrated at room-temperature (overnight). Regardless of the initial shapes of RT-PEDOT:PSS hydrogels, the partially dried PEDOT:PSS hydrogels were capable of swelling to 70% of their initial height. The mechanism here could be interpreted as the crosslinked PEDOT networks remained even after solvent molecules evaporate and escape from the hydrogel networks[29].

However, deep dehydration would disable the RT-PEDOT:PSS hydrogels to swell. After dehydrating the RT-PEDOT:PSS hydrogels in severe dehydration (100 °C) process for long time (2 hrs), the fully dried RT-PEOT:PSS hydrogels could no longer swell even by immersing the

bulky dry gels within in water for over 30 hr. We argue that after fully dehydration, the physically crosslinked PEDOT networks completely collapse, therefore, there is no room to uptake water molecular and macroscopic swelling. Although in a bulky gel state, the overall process during complete dehydration is similar to the PEDOT:PSS thin film forming process where the microgels tend to aggregate and phase segregate into dense PEDOT-rich and PSS-rich domains of highly hierarchy.

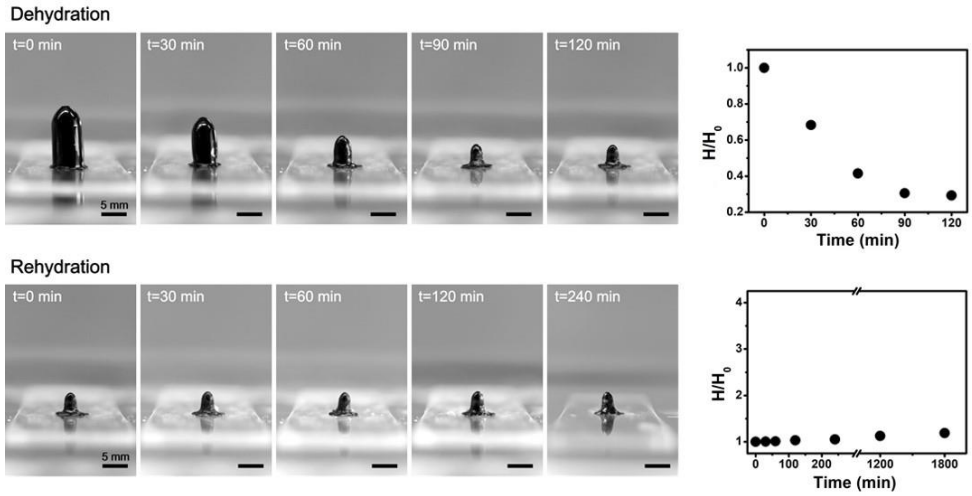

Figure 3-15 RT-PEDOT:PSS hydrogels lost the ability to rehydration after fully dehydration. The dehydration is achieved via 2-hr drying in oven.

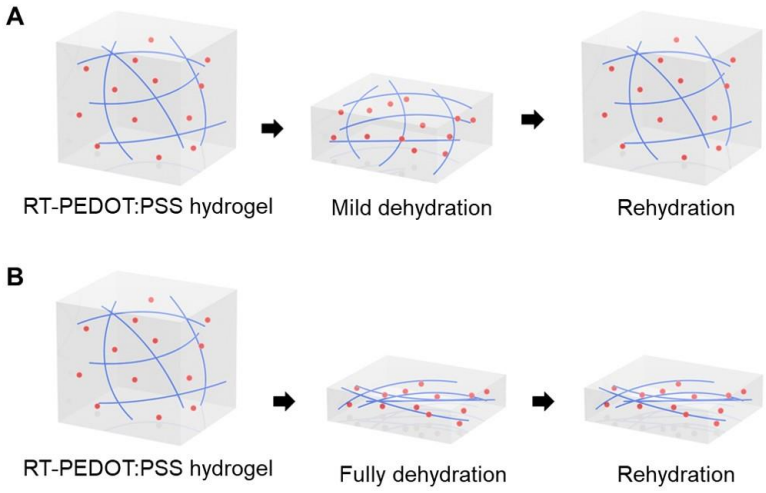

Figure 3-16 Schematics of RT-PEDOT:PSS hydrogels undergoing mild dehydration (A) and fully dehydration (B).

3.4.2 Water healability

Inspired by the phenomena that PEDOT:PSS thin films (thickness of ~1 µm) could self-heal due to the microscopic volumetric swelling, we argue that the macroscopic volumetric swelling behaviors of RT-PEDOT:PSS hydrogels could also enable their applications as water-healable bioelectronics.

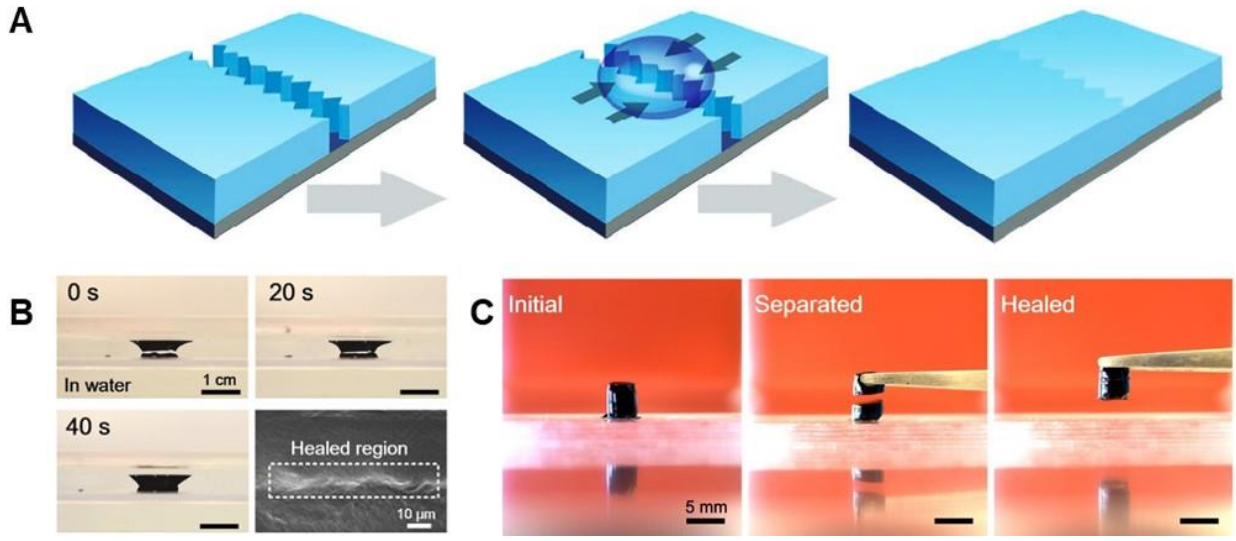

Figure 3-17 A. water-healability of PEDOT:PSS thin films. PEDOT:PSS films swell when exposed to water, causing the expansion and reunion of cutting edges[156]. Reprinted with permission. B. Optical images of the healing processes of the damaged RT-PEDOT:PSS hydrogel, and SEM images of the healed region. C. Mechanical healing of the RT-PEDOT:PSS hydrogel by placing two separated RT-PEDOT:PSS hydrogels (mildly dehydrated) together for 5 min.

In order to demonstrate the capability of RT-PEDOT:PSS hydrogels healing the macroscopic damages, partially dried RT-PEDOT:PSS hydrogels were cut with a razor blade. By adhering the two segments of hydrogels onto separated glass slides, an air gap of ~1 mm was created to evaluate the water-healability. Interestingly, the presence of water healed the gap within merely 40 s due to the rapid swelling of the RT-PEDOT:PSS hydrogels. The interface between the healed regions of RT-hydrogels was also characterized by scanning electron microscope (SEM), after freeze dying the healed hydrogel samples. A clear overlapping region between the two segments could be clearly distinguished, indicating the good adhesions in between. Except for the healability

identified visually, the healed regions also have decent mechanical strength to maintain the healed segment as integrity. The two separated RT-PEDOT:PSS hydrogels healed together could be lifted with tweezers against the gravity. Overall, these results demonstrate that these RT-PEDOT:PSS hydrogels are promising candidates for self-healing electronics.

3.5 Conclusion

In conclusion, we have demonstrated injectable RT-PEDOT:PSS hydrogels with a strategy of using room-temperature synthesized PEDOT:PSS hydrogels (RT-PEDOT:PSS hydrogels). In spite that these RT-PEDOT:PSS hydrogels contained a high-water content of 95 wt.%, they showed high conductivity of ~10^{-1} S/cm and tunable tissue-level mechanical properties. We also demonstrated the potentials of RT-PEDOT:PSS hydrogels to be utilized as injectable conductive hydrogels for the in-situ formation of seamless and chronic biointerface. Compared to other injectable methods, our approach allows facile injection of biocompatible PEDOT:PSS hydrogels, which can reduce immune response of the human body. Except for the potentials in minimally invasive therapeutics such as nerve regeneration and brain stimulation and recording, they also provide the possibility to serve as drug-carriers for developing injectable drug delivery hydrogels. Moreover, we showed that these RT-PEDOT:PSS hydrogels are good candidates to develop water-healable conductors for self-healing bioelectronic applications by taking advantage of their high swelling ratios.

3.6 Experimental section

3.6.1 Materials

PEDOT:PSS (Clevios™ PH1000) was purchased from Haraeus Electronic Materials, Germany. DBSA, Gelatin from porcine skin, and Gallium–Indium eutectic (EGaIn) were purchased from Sigma Aldrich, USA. Dulbecco's phosphate-buffered saline (DPBS) was purchased from Gibco,

USA. Acrylamide (AAm), alginate, N,N′-methylenebisacrylamide (MBA or bis) as the crosslinker and ammonium persulphate (APS) as the thermal initiator were purchased from Sigma Aldrich. 2-hydroxyethyl methacrylate (HEMA), the crosslinker, ethylene glycol dimethacrylate (EGDMA) , and the thermal initiator, benzoyl peroxide (BP) were purchased from Sigma-Aldrich. Deionized (DI) water was obtained by Aqua Solutions Lab Water Systems. PDMS (SYLGARD 184) was purchased from the Dow Chemical Company.

3.6.2 Synthesis of RT-PEDOT:PSS hydrogels

The PEDOT:PSS hydrogels were obtained by adding 4 v/v% of DBSA solution into the PEDOT:PSS suspension, followed by a 2-min agitation. Then, the mixture was poured into pre-patterned molds and then placed in a desiccator or centrifuged to remove bubbles induced by vortex. PEDOT:PSS hydrogels formed spontaneously within about 10 min after mixing DBSA with PEDOT:PSS suspension.

3.6.3 Patterning of RT-PEDOT:PSS hydrogels

Patterning in PDMS: To create the mold, poly(methyl methacrylate) (PMMA) was laser ablated to the desired shapes (VLS 2.30, Universal Laser, USA). PDMS (SYLGARD 184) base was mixed with the curing agent in a 10:1 weight ratio and the mixture was poured onto a petri dish containing the laser cut PMMA shapes. Following degassing in a desiccator, the PDMS was cured in an oven at 80 °C for 1 hour.

Patterning in temperature-sensitive substrates: In order to mimic skin and temperature-sensitive substrates, gelatin and DPBS were mixed in the ratio of 1:4 by weight and stirred on the hot plate (65 °C, 200 rpm) for 2 hours. The mixture was then left to stand on the hot plate for 10 minutes for natural debubbling and instantly poured into the PMMA molds. Bubbles on the surface of solution were manually removed by the pipette tip. Gelatin was then solidified at 4 °C in the refrigerator. Next, gelatin was peeled from the PMMA mold and a patterned gelatin substrate with

embedded channel was obtained. PEDOT:PSS solution (with 4 v/v.% DBSA) was quickly syringe-injected into the microchannels in gelatin substrate. PEDOT:PSS hydrogels formed spontaneously in gelatin microchannels within 10 min after injection.

3.6.4 Stiffening of PEDOT:PSS hydrogels

Stiffening PEDOT:PSS hydrogel via introducing polyacrylamide (PAAm) or poly-2-hydroxyethyl methacrylate (poly(HEMA)) network. The as-fabricated PEDOT:PSS hydrogel was soaked in the PAAm precursor solution, consisting of acrylamide 20% (w/v), N,N'-methylenebisacrylamide 0.03% (w/v) and N,N,N',N'-tetramethylethylenediamine 10% (v/v). After an overnight soaking, the PEDOT:PSS hydrogel was taken out and rinsed with DI water. Next, the hydrogel was soaked in an ammonium persulphate (10% (w/v)) solution bath for another hour to crosslink the PAAm network. To note that, the ammonium persulphate can be activated at room temperature (~25 ℃) to initiate the polymerization of the PAAm network, which is consistent with the room temperature forming property of the PEDOT:PSS hydrogel reported in this manuscript. For comparing the conductivity difference between PAAm-treated PEDOT:PSS hydrogels and pristine PEDOT:PSS hydrogels, the samples (length × width × thickness: 8 mm × 3 mm × 3 mm) were tested between Au electrodes whose inter-distance was 6 mm at constant DC voltage of 0.1 V.

3.6.5 Characterization of RT-PEDOT:PSS hydrogels

Gelation time was defined by tube inversion method. DBSA of calculated volume was added to 10 mL PEDOT:PSS solution in 50 mL centrifuge tube. After manually stirring for 2 mins, 1 mL mixed precursor solution was loaded to 2 mL centrifuge tubes at room temperature for inversion test. Inversion test of the precursors whose DBSA concentration higher than 3% was performed every 1 min after loading to 2 mL tubes, while that of 3% DBSA was set to be every 15 min. The gelation time was determined as the time when DBSA was added to PEDOT:PSS solution. The experiments were quadruplicated.

The tensile test of the RT-PEDOT:PSS hydrogel was implemented with the INSTRON tensile tester (INSTRON 5943, USA) in extension mode (extension rate of 1 mm/min).

Rheology tests were performed with the Anton-Paar rheometer (MCR 302, Austria). If not specifically declared, all samples had a diameter of 8 mm and height of 3 mm. The samples were cut by a circular blade and had a diameter of 8 mm. The storage and loss modulus as well as complex viscosity were measured via small amplitude shear oscillation with constant shear rates (0.1-10 rad/s) in the linear region.

The conductivity of RT-PEDOT:PSS hydrogel was characterized by biasing the hydrogel at a constant direct current (DC) voltage of 1 V with the source measure unit Agilent B2901A (Keysight Technologies, USA). Conductive copper tape and EGaIn were used to connect the PEDOT:PSS hydrogel (length × width × thickness: 20 mm × 20 mm × 5 mm) to the source measure unit. The current was collected after biasing the PEDOT:PSS hydrogel for 100 seconds at 1 V, which allowed us to extract a stable DC conductance. Conductivity of the dehydrated PEDOT:PSS hydrogel was measured after oven-baking the gel at 100 °C for 1 hour. The length, width and thickness of RT-PEDOT:PSS hydrogels for conductivity characterization are 20 mm, 20 mm and 5 mm, respectively.

The electromechanical properties of patterned PEDOT:PSS hydrogel on gelatin substrates were tested with a tensile tester. Liquid metal (EGaIn) and conductive tape (3M 9703) were used to facilitate the electrical connection to the samples.

3.6.6 Biocompatibility evaluation of RT-PEDOT:PSS hydrogels

Cell culture was performed with C2C12 cells (mouse muscle cells). Cells were seeded on RT-PEDOT:PSS hydrogel coated and uncoated surfaces as control. A Live/Dead calcein AM/ethidium homodimer assay (Thermo Scientific) was used to quantify the viability of the cells according to the manufacturer instruction until day 3. Cell proliferation was quantified using Presto

Blue (Thermo Scientific) by measuring the metabolic activity of cells until day 7. 100 µL of staining solution for each condition was transferred into ELISA (enzyme-linked immunosorbent assay) microplates (96-wells plates, Corning Life Sciences, Lowell, MA, USA) for spectrophotometric measurement. The absorbance of the solutions was measured spectrophotometrically at 570 nm.

Chapter 4 Room-Temperature-Formed Poly(3,4-ethylenedioxythiophene):poly(styrenesulfonate) Hydrogel Fibers

4.1 Introduction

Owing to the extremely large aspect ratio (length/diameter), fibers are favorable for biomedical engineers and clinicians with the potential to achieve minimally invasive therapeutics[172]. The minimized footprint of fiber-based biomedical tools could protect endogenous tissues from exposure to external environments, therefore minimizing the risk of infection. With the rise of optogenetics, fibers, especially optical fibers, are gaining more focus due to their exclusive benefit for deep brain modulation on specific regions. Because of the softness and minimized volume occupation, the utilization of fiber materials could also support a compact and light weight head stage, which is essential for neuroscience research to rule out the side effects and hence enhance the reliability in behavioral experiments. In recent years, there are increasing needs to incorporate optical and electrical modalities through fibers to simultaneously modulate (via optogenetics) and record (via electrode) for evaluating the causality of experiments[173,174]. However, most fibers available have poor electrical conductivity with high Young's moduli, which would trigger immune responses at long-term interfaces. Considering the needs of biomedical engineering, we argue that conductive hydrogel fibers would offer unprecedent opportunities to realize multi-functional biointerface.

However, due to micro and sub-micro scale sizes, hydrogel fibers would be hard to manipulate for biomedical engineering where seamless and macroscopic biointerfaces should be achieved. For example, the ultra-flexibility would significantly hinder fibers' direct applications as neural probes. According to the equation:

$$K = \frac{F}{\Delta x} = \frac{4E \cdot w \cdot t^3}{L^3}$$

where K is the bending stiffness, F is the force applied, Δx is the deflection, E is the Young's modulus of the material, L, w, t is the length, width and thickness of the beam or probe, respectively, Therefore, bending stiffness, which represents the resistance of a probe against bending deformation, is proportional to Young's modulus E and the cubic power of the thickness t of the structure. Therefore, with the Young's modulus of tissue-level, the bending stiffness of hydrogel fibers would even be profoundly lower than that of brain tissues, accompanying with serious challenge in delivering and manipulating the devices in vivo.

RT-PEDOT:PSS hydrogels exhibits tissue-level softness and moderate electrical conductivity for bioelectronics applications. Moreover, the injectability of RT-PEDOT:PSS hydrogels also grants the hydrogels with the ability to form arbitrary shapes in situ within the biological lumens or designed structures, circumventing the need to directly manipulate extremely soft hydrogel itself. By borrowing a tube as a transient shuttle in delivery RT-PEDOT:PSS hydrogels, we argue that RT-PEDOT:PSS hydrogels could be elegantly engineered as injectable conductive hydrogel fibers in solving the two contemporary challenges of biomedical engineering.

In this chapter, we focus on a special form of RT-PEDOT:PSS hydrogels: injectable RT-PEDOT:PSS hydrogel fibers. A facile method for large-scale production of extrudable PEDOT:PSS hydrogel fibers was presented by injecting and crosslinking the PEDOT:PSS suspension in situ within a confined cylinder tube. With superior mechanical and electrical properties, we further demonstrated that these hydrogel fibers can be used as electroactive materials to develop organic bioelectronic devices such as organic electrochemical transistors (OECTs). Foreseeing the potentials of such injectable and conductive hydrogel fibers, we also proposed the promising applications where RT-PEDOT:PSS hydrogel fibers could be actively involved in.

4.2 Extrudable room-temperature-formed PEDOT:PSS fibers

4.2.1 Room-temperature-formed PEDOT:PSS hydrogel conducting fibers

In spite that currently there are numbers of methods in creating PEDOT:PSS nanofibers via electrospinning the PEDOT:PSS suspension under external fields [64,175], it remains a challenge to fabricate large-scale, low-cost, and mechanically robust conductive hydrogel fibers needed by next-generation bioelectronics.

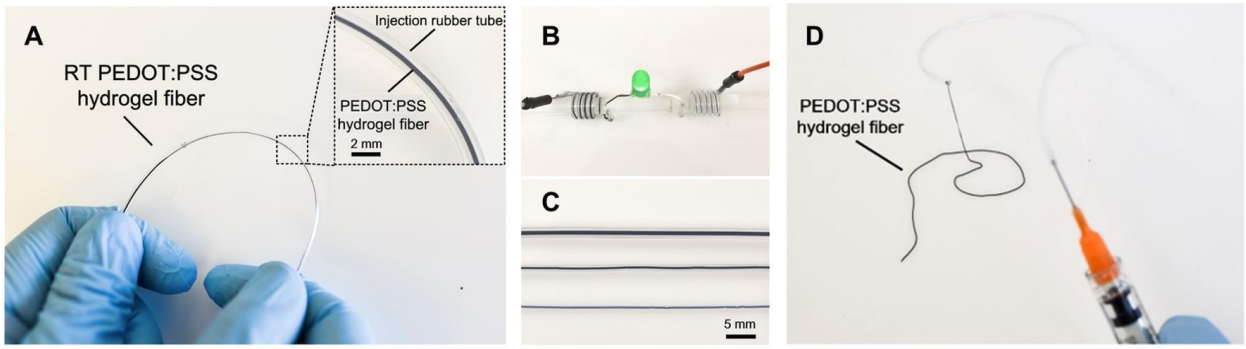

Figure 4-1 A. Formation of the RT-PEDOT:PSS hydrogel in a plastic tube via syringe injection. Inset: enlarged view of the RT-PEDOT:PSS hydrogel in tube; B. Application of RT-PEDOT:PSS hydrogel fibers for driving an LED; C. Injectable RT-PEDOT:PSS hydrogel fibers with different diameters of 875, 480, and 400 µm; D. Extruded fiber-like RT-PEDOT:PSS hydrogel with a syringe.

Inspired by the injectability of RT-PEDOT:PSS hydrogels, we presented an open method to enable large-scale production of conductive hydrogel fibers with customized diameter. Similar to the process in synthesizing RT-PEDOT:PSS hydrogels, PEDOT:PSS suspension was pre-mixed with 4 v/v% DBSA and vigorously agitated for 2 min. Since the hydrogel fibers are of micrometer scale diameter, the existence of microbubbles would separate monolithic fiber into two segments because of the surface tension. Hence, special cares should be paid on bubbles for high-quality RT-PEDOT:PSS hydrogel fiber production. After the mixing process, centrifuging was needed to primarily remove the bubbled introduced during agitation. The PEDOT:PSS mixture was then carefully loaded onto syringe. If bubbles introduced, manual bubble removal was required. Otherwise, more PEDOT:PSS mixture must be injected into the tube to expel the bubble. The

diameter of the final hydrogel fibers could be controlled by the inner diameter of the plastic tube adopted for molding the injected RT-PEDOT:PSS hydrogels. It's worth noting that after gelation, RT-PEDOT:PSS hydrogels would slightly shrink. Therefore, the actual size of RT-PEDOT:PSS hydrogel fibers were slight smaller than the inner diameter of plastic tubes. These RT-PEDOT:PSS hydrogel fibers of different diameters were sufficiently to conduct the circuit in lighting LED. Interestingly, the injected RT-PEDOT:PSS hydrogel fibers could simply be extruded by pressurizing the tube with controlled speed while maintaining their structural integrity because of their good mechanical properties, the slight shrinking after gelation, and the lubricating effect of the DBSA.

4.2.2 Room-temperature-formed PEDOT:PSS hydrogel fiber writing

Figure 4-2 A. Optical images of injected RT-PEDOT:PSS hydrogel fiber into water-filled petri-dish; B. direct writing of "PEDOT" by manually extruding the hydrogel fibers; C. Optical microscopic images of RT-PEDOT:PSS hydrogel fiber before (top) and after (bottom) dehydration at room temperature. The diameter of the hydrogel fiber shrunk from 200 µm to 30 µm.

Owing to the mechanical robustness and their capability to be extruded while maintaining the integrity, we demonstrated that the hydrogel fibers could also be patterned by writing. By gently pressurizing the as-prepared RT-PEDOT:PSS hydrogel fiber within the plastic tube via water-loaded syringe, the hydrogels fiber could be extruded gradually at constant speed, which was similar to the phenomena in wet spinning. The hydrogel fibers could be easily untangled as a straight fiber by pulling it above the water-air surface, even after multiple hydrogels fibers were

entangled with each other. Simultaneous movement in XY plane while gradually extruding RT-PEDOT:PSS hydrogel fibers (Z direction), could also mimic the 3D printing scenario, heralding its potential to be facilitated by the 3D printing techniques[176,177]. As a demonstration, RT-PEDOT:PSS hydrogel writing of words “PEDOT” could be simply achieved. Comparing to the bulky RT-PEDOT:PSS hydrogels, the RT-PEDOT:PSS hydrogel fibers have limited ability to swell when dehydrated. It might be explained by the extremely high aspect ratios would cause the hydrogels to reach the “fully dehydrated” state more easily, resulting in a complete collapse of crosslinked PEDOT networks. Therefore, the as-prepared RT-PEDOT:PSS hydrogel fibers should be carefully stored in wet environment, which could be naturally met in biological applications since the interfaced cells and tissues within body are also required to be exposed to water.

4.3 Hydrogel OECTs

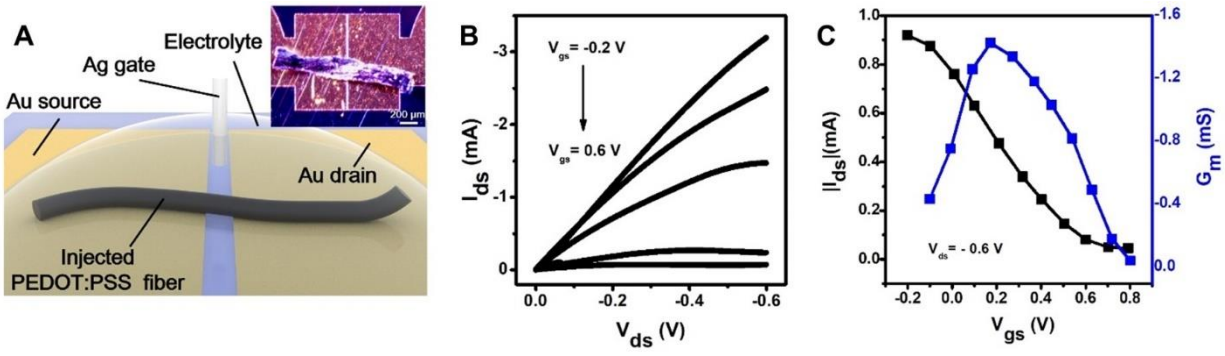

Figure 4-3 A. Schematic of the fabricated OECTs with injected RT-PEDOT:PSS hydrogel fiber; the inset shows the real optical image of the fiber on the source-drain electrodes. B-C. Output and transfer curves of the OECTs with RT-PEDOT:PSS hydrogel fibers as the channel.

As a potential application, we exploited the possibility of using RT-PEDOT:PSS hydrogel fibers as channel material for the fabrication of organic bioelectronic devices, such as OECTs, which has been widely used for in vivo bioelectronics studies. The hydrogel OECTs were fabricated by simply syringe-injecting a piece of RT-PEDOT:PSS hydrogel fibers between two metallic

electrodes, followed by a freeze-drying process (in order to effectively deplete the channel when positive gate voltage applied). As illustrated in the output and transfer curves of the hydrogel OECTs, the OECTs showed typical transistor behavior working in the depletion mode. The resultant hydrogel OECTs had a maximum transconductance of ~1.4 mS (V_{ds}=0.6 V, V_{gs}=-0.2 V), which was comparable to conventional OECTs based on PEDOT:PSS thin films. These results demonstrate good electrochemical properties of these PEDOT:PSS hydrogel fibers, indicating their potential applications for organic and hydrogel bioelectronics.

4.4 Conclusion

In conclusion, we developed a facile method to produce extrudable RT-PEDOT:PSS hydrogel fibers with customized diameters. The fabricated hydrogel fibers were electrically conductive and were actively used as channel materials for OECTs. Owing to the mechanical robustness, multiple manipulation methods could be adopted to pattern the fiber, for example, writing, or potentially 3D printing. Further investigations and optimization of the electrical and mechanical properties of these PEDOT:PSS hydrogel fibers will promote their uses toward biomedical applications.

4.4.1 Outlook

There is a tremendous need for developing advanced materials technology to seamless interface with brain and record neural activity, including local field potentials (LFP) and single-unit signals. The conform interface between electrodes and endogenous neural tissues could not only minimize the space occupation in vivo therefore suppressing the immune effects and neuron loss, but also provide a possibility for in vivo single-unit recording. Conventionally, most in vivo electrodes could merely record noisy extracellular signals owing to the transmembrane current of all adjacent neurons (~100 μm range) which are firing. However, by geometrically shrinking the distance between targeted neurons and electrodes, the signal-to-noise ratio (SNR) could increase, enabling reliable spike detection for chronic in vivo single units recording. For example, although

conventional electrocorticography (ECoG) electrode could merely access the LFP signals, NeuroGrid, an ultra-conformable, biocompatible and scalable neural interface array by using organic materials, could record both LFP and single-unit signals without the need to penetrate the brain surface [178].

Currently, the prevailing ideas creating the conformal interface are to engineer the neural probes from materials or geometric perspectives, according to the definition of bending stiffness. Both methods share the presumption that the devices should be first fabricated and then transferred to the targeted regions. Therefore, the to-be-transferred conformal devices, which are mechanically flexible, were technically hard to be delivered locations of interests with high spatial resolution as silicon probes. Moreover, even though the devices are conformal, the spatial bending would inevitably introduce strain to both functional materials within and interfaced tissues, which could cause unreliable recording and detachments. Therefore, we propose a in situ forming RT-PEDOT:PSS hydrogel probe which could locally gelate after interfacing the targeted region via a catheter as transient shuttle. Comparing to the “fabricate-deliver” approaches, we argue that the “deliver-fabricate” approaches could act as a conformal and strain-free platform in vivo neural interface.

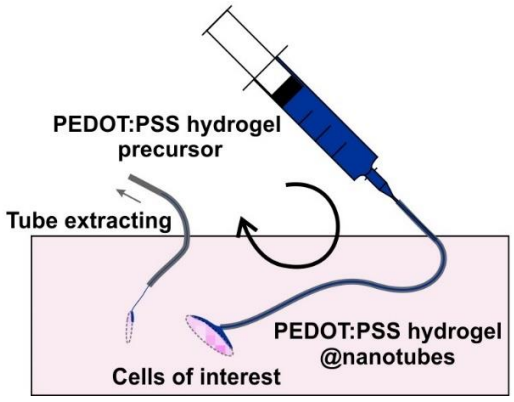

Figure 4-4 The concept of in situ formed RT-PEDOT:PSS hydrogel probe for seamless and strain-free biointerface.

Advanced by the facile fabrication and injectability, the concept of RT-PEDOT:PSS hydrogel fibers could be the optimal materials in realizing the proposal. By simply inserting a plastic tube or catheter with the diameter of micrometer or even nanometer scale, the access to targeted region could be achieved via a minimally invasive surgeon leaving minimal footprint on endogenous tissues. Controlling the injecting amount of PEDOT:PSS/DBSA mixture, a size-controllable interface pad could spontaneous encapsulate the targeted neurons since the injection component is in liquid state. After 10 min for in situ gelation, RT-PEDOT:PSS hydrogel fibers with conformal and strain-free hydrogel interfacing pad could securely fixed in the region of interest for chronically and reliably recording the undisturbed metabolic electrophysiological signals. It's also worth noting that, by genetically encoded neurons with surface proteins to specifically attract and gelate PEDOT:PSS, it could provide cell-type specificity for electrical recording, which is one of the main challenges in electrical neural interface.

Another interesting frontier of this concept is the usage of tubes. For neuroengineering, especially in electrical modalities, the insulation of electrical circuits is a primary concern. Although in silicon probes, the problem could be solved by patterning and depositing SiO_2 layer by nanofabrication processes, flexible electrodes have to utilize other materials in order to maintain the flexibility required. In this case, we argue that soft but highly dielectric hydrogels could be adopted as the implanted tubes to secure the signal transfer within RT-PEDOT:PSS hydrogel fibers (cables). To be published by our group soon, poly(HEMA) hydrogels could be engineered to have microchannels by 3D printing and replication. Considering the superior biocompatibility (poly(HEMA) is used as contact lens) and insulating properties, we believe the combination of poly(HEMA) microtube and RT-PEDOT:PSS hydrogel fiber could offer a technically simple but effective solution to the dilemma.

4.5 Experimental section

4.5.1 Materials

PEDOT:PSS (Clevios™ PH1000) was purchased from Haraeus Electronic Materials, Germany. DBSA was purchased from Sigma Aldrich. Acetone. IPA were purchased from Sigma Aldrich. Deionized (DI) water was obtained by Aqua Solutions Lab Water Systems. SU8 was purchased from Microchem. Parylene C was purchased from Specialty Coating Systems Inc.

4.5.2 Fabrication of RT-PEDOT:PSS hydrogel fibers

4 v/v.% DBSA was added to 10 mL PEDOT:PSS suspension in 50 mL centrifuge tube. After manually stirring for 2 mins, the mixture was carefully extracted via a 5 mL syringe. In order to prevent bubble introduction when loading PEDOT:PSS and DBSA mixture, the timing of the process was controlled to be finished in 1 min. To prevent bubbles injected into PEDOT:PSS fibers, the very first PEDOT:PSS and DBSA mixture was manually removed. After adjusting the microfluidic tubes onto the tip of syringe, gradually pressed the pistol of syringe, avoiding introducing visible bubbles into the lumen of microfluidic tubes. The microfluidic tubes with PEDOT:PSS and DBSA mixture were left in ambient pressure, and room temperature overnight for the hydrogel fiber crosslinking and stabilizing.

To extrude the PEDOT:PSS hydrogel fibers, a syringe was preloaded with DI water. After attaching the needle of the syringe onto the microfluidic tube, pressure was gradually applied to gently flush PEDOT:PSS hydrogel fibers without affecting their mechanical integrity.

4.5.3 Freeze-drying RT-PEDOT:PSS hydrogel fibers

A freshly extruded PEDOT:PSS hydrogel fiber was collected and suspended in DI water or free stood on petri dish. The fibers were then transferred into -80 °C refrigerator and stored overnight to preserve the crosslinked polymeric network. The parameters of freeze-drier were set to be -

60 °C and <1 Pa. The frozen PEDOT:PSS hydrogel fibers were then dried by freeze-drier for 2-3 days. After retrieval of freeze-dried PEDOT:PSS hydrogel fibers, the samples were carefully stored in a desiccator avoiding light exposure.

4.5.4 Fabrication and characterization of OECTs with RT-PEDOT:PSS hydrogel fibers

Silicon substrates were pre-cleaned with acetone, IPA and DI water. Then photoresist (SPR 700 1.2) was spin-coated on top of the substrates, followed by UV exposure under an optical shadow mask to define the desired patterns. After photoresist developing (MA-26A, 30s), Ti/Au (10 nm / 100 nm) was deposited. Patterned source and drain electrodes were obtained after stripping the photoresist with acetone in a sonication bath. Next, parylene C was selectively deposited on top of the electrodes as insulating layer. The fiber-like RT-PEDOT:PSS hydrogel was subsequently syringe-injected in between the source and drain electrode as the transistor channel. The channel length is 10 µm, the channel width is 1000 µm, and the diameter of the RT-PEDOT:PSS hydrogel is about 200 µm which shrinks to 20 µm after baking (100 °C, 1 hour). Before transistor measurements, chitosan solution was coated on top of the RT-PEDOT:PSS hydrogel to prevent delamination during the experiments. Finally, a silver wire was inserted into CTAB solution as gate electrode. The characterization of the OECTs was performed with Agilent B2902A, controlled with LabVIEW software for output and transfer cures measurements.

Chapter 5 Conclusions

The work presented in this thesis focuses on PEDOT:PSS hydrogels, which could be synthesized and processed with no need to elevate temperature to meet the needs of biomedical engineering. The majority of the work is targeting on the PEDOT:PSS hydrogels that can be formed spontaneously at room temperature (RT-PEDOT:PSS hydrogels).

Our first step was acknowledging the designs, experiments and theories developed. Starting from materials, we summarized the history of PEDOT:PSS and discussed the mechanism of its conductivity. With the aim of minimizing the mismatch between biological tissues and electronics, we rationalized the strength of hydrogels and the challenges of PEDOT:PSS hydrogels. Considering the possibility to be adopted and modified in situ for minimally invasive therapeutics, we specifically discussed the biological needs for low-temperature processing in biomedical engineering. We also recognized the demands of device-level biomedical applications and summarized OECT, one of the most promising bioelectronic devices, with its mechanism and potential for functionalizing the PEDOT:PSS hydrogel for electrical biointerface.

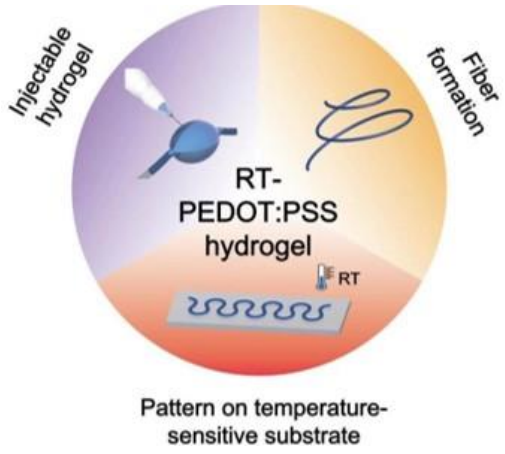

Figure 5-1 PEDOT: PSS hydrogels enable injectable, soft, and healable organic bioelectronics in situ with no need to elevate temperature.

Chapter 3 presented the PEDOT:PSS hydrogels that can be formed spontaneously at room temperature. From materials perspective, we characterized the mechanical, electrical properties

of the hydrogels as well as the gelation mechanism that enables its room-temperature processability. The RT-PEDOT:PSS hydrogels exhibited tissue-level softness and moderate conductivity (~10^{-1} S/cm). Aided by interpenetrating secondary networks, the hydrogels could be further stiffened without sacrificing its electrical conductivity. We then highlight two main benefits of the RT-PEDOT:PSS hydrogels injectability and self-healability, with targeted demonstrations to claim their potentials form seamless and chronic biointerface. In Chapter 4, we foresaw the potential of fibers in biomedical engineering and specifically discussed the benefits of RT-PEDOT:PSS hydrogel fibers with corresponding demonstrations. Based on the conductive hydrogel fibers, hydrogel OECTs were fabricated by simply syringe-injecting a piece of RT-PEDOT:PSS hydrogel fibers between two metallic electrodes. With excellent transistor properties, the hydrogel OECTs worked in depletion mode with maximum transconductance of 1.4 mS, indicating the potential of RT-PEDOT:PSS hydrogels to be utilized as electroactive materials for biointerfaces.

5.1 Outlook

Hydrogels and organic electronics are hot research fields with tremendous new advances. Researchers are utilizing these concepts as a panacea treating every possible existing problem. However, when applied in real life, the solutions to single challenges do not necessarily mean the solution is applicable. Therefore, given the potential of PEDOT:PSS hydrogels and their room-temperature processability, we argue that close collaboration with clinicians and neuroscientists would profoundly advance the applications of RT-PEDOT:PSS in solving real problems. From a challenge-oriented perspective, we highlight that there would two directions for the future development of low-temperature-processed PEDOT:PSS hydrogels.

1. The acute and chronic interactions between hydrogels and endogenous tissue. Although hydrogels are claimed to be biocompatible and most importantly, could minimize mechanical

mismatch, the exact reaction during and after implanting hydrogel as probe in brain tissues has not been modelled or tested experimentally. Systematic works about the effect of hydrogels insertion would be of key interest to neuroscientists and clinicians for translational products that benefit people.

2. Insulation. As discussed in chapter 4, insulation would be a serious issue for hydrogel materials given their extremely high water content. Ionic conductance would leak the current recorded in neural probes, and lead to low-quality signals. Although for silicon probes, nanofabrication could help by depositing a thin insulating layer, hydrogels are not compatible with these processes where vacuum is required. Therefore, a good insulating layer for hydrogel neural probes would be required for reliable and safe biointerfaces.

With targeted real biomedical problems, PEFOT:PSS and PEDOT:PSS hydrogels could help to solve basic and practical issues of neuroscience research and clinical use.

Chapter 6 References

1 Shirakawa, H., Louis, E. J., MacDiarmid, A. G., Chiang, C. K. & Heeger, A. J. Synthesis of electrically conducting organic polymers: Halogen derivatives of polyacetylene, (CH). *Journal of the Chemical Society, Chemical Communications*, 578-580, doi:10.1039/c39770000578 (1977).

2 Ghasemi-Mobarakeh, L. *et al.* Application of conductive polymers, scaffolds and electrical stimulation for nerve tissue engineering. *J Tissue Eng Regen Med* **5**, e17-35, doi:10.1002/term.383 (2011).

3 Bolin, M. H. *et al.* Nano-fiber Scaffold Electrodes Based on PEDOT for Cell Stimulation. *Sensors and Actuators B: Chemical* **142**, 451-456, doi:10.1016/j.snb.2009.04.062 (2009).

4 Kim, Y. H. *et al.* Highly Conductive PEDOT:PSS Electrode with Optimized Solvent and Thermal Post-Treatment for ITO-Free Organic Solar Cells. *Advanced Functional Materials* **21**, 1076-1081, doi:10.1002/adfm.201002290 (2011).

5 Kim, N. *et al.* Highly Conductive PEDOT:PSS Nanofibrils Induced by Solution-Processed Crystallization. *Advanced Materials* **26**, 2268-2272, doi:10.1002/adma.201304611 (2014).

6 Zhang, S. *et al.* Water stability and orthogonal patterning of flexible micro-electrochemical transistors on plastic. *Journal of Materials Chemistry C* **4**, 1382-1385, doi:10.1039/C5TC03664J (2016).

7 Liang, J., Li, L., Niu, X., Yu, Z. & Pei, Q. Elastomeric polymer light-emitting devices and displays. *Nature Photonics* **7**, 817-824, doi:10.1038/nphoton.2013.242 (2013).

8 Sun, K. *et al.* Review on application of PEDOTs and PEDOT:PSS in energy conversion and storage devices. *Journal of Materials Science: Materials in Electronics* **26**, 4438-4462, doi:10.1007/s10854-015-2895-5 (2015).

9 Po, R., Carbonera, C., Bernardi, A., Tinti, F. & Camaioni, N. Polymer-and carbon-based electrodes for polymer solar cells: Toward low-cost, continuous fabrication over large area. *Solar Energy Materials and Solar Cells* **100**, 97-114 (2012).

10 Okuzaki, H., Takagi, S., Hishiki, F. & Tanigawa, R. Ionic liquid/polyurethane/PEDOT:PSS composites for electro-active polymer actuators. *Sensors and Actuators B: Chemical* **194**, 59-63, doi:https://doi.org/10.1016/j.snb.2013.12.059 (2014).

11 Roh, E., Hwang, B.-U., Kim, D., Kim, B.-Y. & Lee, N.-E. Stretchable, Transparent, Ultrasensitive, and Patchable Strain Sensor for Human–Machine Interfaces Comprising a Nanohybrid of Carbon Nanotubes and Conductive Elastomers. *ACS Nano* **9**, 6252-6261, doi:10.1021/acsnano.5b01613 (2015).

12 Lipomi, D. J., Dhong, C., Carpenter, C. W., Root, N. B. & Ramachandran, V. S. Organic Haptics: Intersection of Materials Chemistry and Tactile Perception. *Advanced Functional Materials*, 1906850, doi:10.1002/adfm.201906850 (2019).

13 Isaksson, J. *et al.* Electronic control of Ca2+ signalling in neuronal cells using an organic electronic ion pump. *Nature Materials* **6**, 673-679, doi:10.1038/nmat1963 (2007).

14 Simon, D. T. *et al.* Organic electronics for precise delivery of neurotransmitters to modulate mammalian sensory function. *Nature Materials* **8**, 742-746, doi:10.1038/nmat2494 (2009).

15 Ludwig, K. A., Uram, J. D., Yang, J., Martin, D. C. & Kipke, D. R. Chronic neural recordings using silicon microelectrode arrays electrochemically deposited with a poly(3,4-ethylenedioxythiophene) (PEDOT) film. *Journal of neural engineering* **3**, 59-70, doi:10.1088/1741-2560/3/1/007 (2006).

16 van de Burgt, Y. *et al.* A non-volatile organic electrochemical device as a low-voltage artificial synapse for neuromorphic computing. *Nature Materials* **16**, 414-418, doi:10.1038/nmat4856 (2017).

17 Zhang, S. *et al.* Hydrogel-Enabled Transfer-Printing of Conducting Polymer Films for Soft Organic Bioelectronics. *Advanced Functional Materials* **30**, 1906016, doi:10.1002/adfm.201906016 (2020).

18 Khodagholy, D. *et al.* High transconductance organic electrochemical transistors. *Nature Communications* **4**, 2133, doi:10.1038/ncomms3133 (2013).

19 Malaga, K. A. *et al.* Data-driven model comparing the effects of glial scarring and interface interactions on chronic neural recordings in non-human primates. *Journal of neural engineering* **13**, 016010 (2015).

20 Yuk, H., Lu, B. & Zhao, X. Hydrogel bioelectronics. *Chemical Society Reviews* **48**, 1642-1667, doi:10.1039/C8CS00595H (2019).

21 Zhang, Y. S. & Khademhosseini, A. Advances in engineering hydrogels. *Science* **356**, eaaf3627, doi:10.1126/science.aaf3627 (2017).

22 Handorf, A. M., Zhou, Y., Halanski, M. A. & Li, W.-J. Tissue Stiffness Dictates Development, Homeostasis, and Disease Progression. *Organogenesis* **11**, 1-15, doi:10.1080/15476278.2015.1019687 (2015).

23 Li, J. & Mooney, D. J. Designing hydrogels for controlled drug delivery. *Nature Reviews Materials* **1**, 16071, doi:10.1038/natrevmats.2016.71 (2016).

24 Naahidi, S. *et al.* Biocompatibility of hydrogel-based scaffolds for tissue engineering applications. *Biotechnology Advances* **35**, 530-544, doi:10.1016/j.biotechadv.2017.05.006 (2017).

25 Caló, E. & Khutoryanskiy, V. V. Biomedical applications of hydrogels: A review of patents and commercial products. *European Polymer Journal* **65**, 252-267, doi:https://doi.org/10.1016/j.eurpolymj.2014.11.024 (2015).

26 Stejskal, J. Conducting polymer hydrogels. *Chemical Papers* **71**, 269-291, doi:10.1007/s11696-016-0072-9 (2016).

27 Abidian, M. R. *et al.* Hybrid Conducting Polymer–Hydrogel Conduits for Axonal Growth and Neural Tissue Engineering. *Advanced healthcare materials* **1**, 762-767, doi:10.1002/adhm.201200182 (2012).

28 Han, L. *et al.* Mussel-Inspired Adhesive and Conductive Hydrogel with Long-Lasting Moisture and Extreme Temperature Tolerance. *Advanced Functional Materials* **28**, 1704195, doi:10.1002/adfm.201704195 (2018).

29 Lu, B. *et al.* Pure PEDOT:PSS hydrogels. *Nature Communications* **10**, 1043, doi:10.1038/s41467-019-09003-5 (2019).

30 Kayser, L. V. & Lipomi, D. J. Stretchable Conductive Polymers and Composites Based on PEDOT and PEDOT:PSS. *Advanced Materials* **31**, 1806133, doi:10.1002/adma.201806133 (2019).

31 Ni, J. *et al.* Three-dimensional printing of metals for biomedical applications. *Materials Today Bio* **3**, 100024, doi:https://doi.org/10.1016/j.mtbio.2019.100024 (2019).

32 Duan, X., Fu, T.-M., Liu, J. & Lieber, C. M. Nanoelectronics-biology frontier: From nanoscopic probes for action potential recording in live cells to three-dimensional cyborg tissues. *Nano Today* **8**, 351-373, doi:https://doi.org/10.1016/j.nantod.2013.05.001 (2013).

33 Hong, G. & Lieber, C. M. Novel electrode technologies for neural recordings. *Nature Reviews Neuroscience* **20**, 330-345, doi:10.1038/s41583-019-0140-6 (2019).

34 Someya, T., Bao, Z. & Malliaras, G. G. The rise of plastic bioelectronics. *Nature* **540**, 379-385, doi:10.1038/nature21004 (2016).

35 Hubel, D. H. Single unit activity in lateral geniculate body and optic tract of unrestrained cats. *The Journal of Physiology* **150**, 91-104 (1960).

36 Wise, K. D., Angell, J. B. & Starr, A. An integrated-circuit approach to extracellular microelectrodes. *IEEE Transactions on Biomedical Engineering* **17**, 238-247, doi:10.1109/tbme.1970.4502738 (1970).

37 Nordhausen, C. T., Maynard, E. M. & Normann, R. A. Single unit recording capabilities of a 100 microelectrode array. *Brain Research* **726**, 129-140 (1996).

38 Jun, J. J. *et al.* Fully integrated silicon probes for high-density recording of neural activity. *Nature* **551**, 232-236 (2017).

39 Ouyang, L., Shaw, C. L., Kuo, C.-c., Griffin, A. L. & Martin, D. C. In vivo polymerization of poly (3, 4-ethylenedioxythiophene) in the living rat hippocampus does not cause a significant loss of performance in a delayed alternation task. *Journal of Neural Engineering* **11**, 026005 (2014).

40 Liu, Y. *et al.* Morphing electronics enable neuromodulation in growing tissue. *Nature Biotechnology*, doi:10.1038/s41587-020-0495-2 (2020).

41 Lecomte, A., Descamps, E. & Bergaud, C. A review on mechanical considerations for chronically-implanted neural probes. *Journal of Neural Engineering* **15**, 031001, doi:10.1088/1741-2552/aa8b4f (2018).

42 Niu, J. *et al.* Engineering live cell surfaces with functional polymers via cytocompatible controlled radical polymerization. *Nature Chemistry* **9**, 537-545, doi:10.1038/nchem.2713 (2017).

43 Liu, J. *et al.* Genetically targeted chemical assembly of functional materials in living cells, tissues, and animals. *Science* **367**, 1372-1376, doi:10.1126/science.aay4866 (2020).

44 Dewhirst, M. W., Viglianti, B. L., Lora-Michiels, M., Hanson, M. & Hoopes, P. J. Basic principles of thermal dosimetry and thermal thresholds for tissue damage from hyperthermia. *International Journal of Hyperthermia* **19**, 267-294, doi:10.1080/0265673031000119006 (2003).

45 Dickerson, E. B. *et al.* Gold nanorod assisted near-infrared plasmonic photothermal therapy (PPTT) of squamous cell carcinoma in mice. *Cancer Lett* **269**, 57-66, doi:10.1016/j.canlet.2008.04.026 (2008).

46 Zhang, S. *et al.* Room-Temperature-Formed PEDOT:PSS Hydrogels Enable Injectable, Soft, and Healable Organic Bioelectronics. *Advanced Materials* **32**, 1904752, doi:10.1002/adma.201904752 (2020).

47 Gerard, M., Chaubey, A. & Malhotra, B. D. Application of conducting polymers to biosensors. *Biosensors and Bioelectronics* **17**, 345-359, doi:https://doi.org/10.1016/S0956-5663(01)00312-8 (2002).

48 MacDiarmid, A. G. “Synthetic Metals”: A Novel Role for Organic Polymers (Nobel Lecture). *Angewandte Chemie International Edition* **40**, 2581-2590, doi:10.1002/1521-3773(20010716)40:14<2581::Aid-anie2581>3.0.Co;2-2 (2001).

49 Skotheim, T. A. & Reynolds, J. *Handbook of Conducting Polymers*. (CRC press, 2007).

50 Lipomi, D. J., Tee, B. C., Vosgueritchian, M. & Bao, Z. Stretchable organic solar cells. *Advanced Materials* **23**, 1771-1775, doi:10.1002/adma.201004426 (2011).

51 Gustafsson, G. *et al.* Flexible light-emitting diodes made from soluble conducting polymers. *Nature* **357**, 477-479, doi:10.1038/357477a0 (1992).

52 Kee, S. *et al.* Highly Deformable and See-Through Polymer Light-Emitting Diodes with All-Conducting-Polymer Electrodes. *Advanced Materials* **30**, 1703437, doi:10.1002/adma.201703437 (2018).

53 Rivnay, J. *et al.* Organic electrochemical transistors. *Nature Reviews Materials* **3**, 17086 (2018).

54 Zhang, S. & Cicoira, F. Flexible self-powered biosensors. *Nature* **561**, 466 (2018).

55 Asen, P., Shahrokhian, S. & zad, A. I. Ternary nanostructures of Cr2O3/graphene oxide/conducting polymers for supercapacitor application. *Journal of Electroanalytical Chemistry* **823**, 505-516, doi:10.1016/j.jelechem.2018.06.048 (2018).

56 Kee, S. *et al.* Highly Deformable and See‐Through Polymer Light‐Emitting Diodes with All‐Conducting‐Polymer Electrodes. *Advanced Materials* **30**, 1703437 (2018).

57 Skotheim, T. A. & Reynolds, J. *Handbook of Conducting Polymers, 2 Volume Set*. (CRC press, 2007).

58 Bredas, J. L. & Street, G. B. Polarons, bipolarons, and solitons in conducting polymers. *Accounts of Chemical Research* **18**, 309-315, doi:10.1021/ar00118a005 (1985).

59 Elschner, A., Kirchmeyer, S., Lovenich, W., Merker, U. & Reuter, K. *PEDOT: Principles and Applications of an Intrinsically Conductive Polymer*. (CRC press, 2010).

60 Jonas, F., Krafft, W. & Muys, B. Poly(3, 4-ethylenedioxythiophene): Conductive coatings, technical applications and properties. *Macromolecular Symposia* **100**, 169-173, doi:10.1002/masy.19951000128 (1995).

61 Xu, Y. *et al.* Cytocompatible, Injectable, and Electroconductive Soft Adhesives with Hybrid Covalent/Noncovalent Dynamic Network. *Advanced Science* **6**, 1802077, doi:10.1002/advs.201802077 (2019).

62 Bodart, C. *et al.* Electropolymerized Poly(3,4-ethylenedioxythiophene) (PEDOT) Coatings for Implantable Deep-Brain-Stimulating Microelectrodes. *ACS Applied Materials & Interfaces* **11**, 17226-17233, doi:10.1021/acsami.9b03088 (2019).

63 Andersson Ersman, P. *et al.* All-printed large-scale integrated circuits based on organic electrochemical transistors. *Nature Communications* **10**, 5053, doi:10.1038/s41467-019-13079-4 (2019).

64 Liu, N. *et al.* Electrospun PEDOT:PSS–PVA nanofiber based ultrahigh-strain sensors with controllable electrical conductivity. *Journal of Materials Chemistry* **21**, 18962-18966, doi:10.1039/C1JM14491J (2011).

65 Meng, Q., Jiang, Q., Cai, K. & Chen, L. Preparation and thermoelectric properties of PEDOT:PSS coated Te nanorod/PEDOT:PSS composite films. *Organic Electronics* **64**, 79-85, doi:https://doi.org/10.1016/j.orgel.2018.10.010 (2019).

66 Youn, H., Jeon, K., Shin, S. & Yang, M. All-solution blade–slit coated polymer light-emitting diodes. *Organic Electronics* **13**, 1470-1478, doi:https://doi.org/10.1016/j.orgel.2012.04.008 (2012).

67 Liu, Y. *et al.* High-Performance Flexible All-Solid-State Supercapacitor from Large Free-Standing Graphene-PEDOT/PSS Films. *Scientific Reports* **5**, 17045, doi:10.1038/srep17045 (2015).

68 Kim, J. Y., Jung, J. H., Lee, D. E. & Joo, J. Enhancement of electrical conductivity of poly(3,4-ethylenedioxythiophene)/poly(4-styrenesulfonate) by a change of solvents. *Synthetic Metals* **126**, 311-316, doi:https://doi.org/10.1016/S0379-6779(01)00576-8 (2002).

69 Greczynski, G., Kugler, T. & Salaneck, W. R. Characterization of the PEDOT-PSS system by means of X-ray and ultraviolet photoelectron spectroscopy. *Thin Solid Films* **354**, 129-135, doi:https://doi.org/10.1016/S0040-6090(99)00422-8 (1999).

70 Bodart, C. *et al.* Electropolymerized Poly(3,4-ethylenedioxythiophene) (PEDOT) Coatings for Implantable Deep-Brain-Stimulating Microelectrodes. *ACS Applied Materials & Interfaces* **11**, 17226-17233, doi:10.1021/acsami.9b03088 (2019).

71 Poverenov, E., Li, M., Bitler, A. & Bendikov, M. Major Effect of Electropolymerization Solvent on Morphology and Electrochromic Properties of PEDOT Films. *Chemistry of Materials* **22**, 4019-4025, doi:10.1021/cm100561d (2010).

72 Ouyang, J. *et al.* On the mechanism of conductivity enhancement in poly(3,4-ethylenedioxythiophene):poly(styrene sulfonate) film through solvent treatment. *Polymer* **45**, 8443-8450, doi:https://doi.org/10.1016/j.polymer.2004.10.001 (2004).

73 Zuppiroli, L., Bussac, M. N., Paschen, S., Chauvet, O. & Forro, L. Hopping in disordered conducting polymers. *Physical Review B* **50**, 5196-5203, doi:10.1103/physrevb.50.5196 (1994).

74 Aleshin, A. N., Williams, S. R. & Heeger, A. J. Transport properties of poly(3,4-ethylenedioxythiophene)/poly(styrenesulfonate). *Synthetic Metals* **94**, 173-177, doi:https://doi.org/10.1016/S0379-6779(97)04167-2 (1998).

75 Lang, U., Naujoks, N. & Dual, J. Mechanical characterization of PEDOT:PSS thin films. *Synthetic Metals* **159**, 473-479, doi:https://doi.org/10.1016/j.synthmet.2008.11.005 (2009).

76 Ionescu-Zanetti, C., Mechler, A., Carter, S. A. & Lal, R. Semiconductive Polymer Blends: Correlating Structure with Transport Properties at the Nanoscale. *Advanced Materials* **16**, 385-389, doi:10.1002/adma.200305747 (2004).

77 Nardes, A. M. *et al.* Microscopic Understanding of the Anisotropic Conductivity of PEDOT:PSS Thin Films. *Advanced Materials* **19**, 1196-1200, doi:10.1002/adma.200602575 (2007).

78 Lipomi, D. J. *et al.* Electronic Properties of Transparent Conductive Films of PEDOT:PSS on Stretchable Substrates. *Chemistry of Materials* **24**, 373-382, doi:10.1021/cm203216m (2012).

79 Lang, U., Müller, E., Naujoks, N. & Dual, J. Microscopical Investigations of PEDOT:PSS Thin Films. *Advanced Functional Materials* **19**, 1215-1220, doi:10.1002/adfm.200801258 (2009).

80 Wang, Y. *et al.* A highly stretchable, transparent, and conductive polymer. *Science Advances* **3**, e1602076, doi:10.1126/sciadv.1602076 (2017).

81 McCarthy, J. E., Hanley, C. A., Brennan, L. J., Lambertini, V. G. & Gun'ko, Y. K. Fabrication of highly transparent and conducting PEDOT:PSS films using a formic acid treatment. *Journal of Materials Chemistry C* **2**, 764-770, doi:10.1039/C3TC31951B (2014).

82 Lipomi, D. J. *et al.* Skin-like pressure and strain sensors based on transparent elastic films of carbon nanotubes. *Nature Nanotechnology* **6**, 788-792, doi:10.1038/nnano.2011.184 (2011).

83 Pettersson, L. A. A., Ghosh, S. & Inganäs, O. Optical anisotropy in thin films of poly(3,4-ethylenedioxythiophene)–poly(4-styrenesulfonate). *Organic Electronics* **3**, 143-148, doi:https://doi.org/10.1016/S1566-1199(02)00051-4 (2002).

84 Kim, W. H. *et al.* Molecular organic light-emitting diodes using highly conducting polymers as anodes. *Applied Physics Letters* **80**, 3844-3846, doi:10.1063/1.1480100 (2002).

85 Jönsson, S. K. M. *et al.* The effects of solvents on the morphology and sheet resistance in poly(3,4-ethylenedioxythiophene)–polystyrenesulfonic acid (PEDOT–PSS) films. *Synthetic Metals* **139**, 1-10, doi:https://doi.org/10.1016/S0379-6779(02)01259-6 (2003).

86 Crispin, X. *et al.* Conductivity, morphology, interfacial chemistry, and stability of poly(3,4-ethylene dioxythiophene)–poly(styrene sulfonate): A photoelectron spectroscopy study. *Journal of Polymer Science Part B: Polymer Physics* **41**, 2561-2583, doi:10.1002/polb.10659 (2003).

87 Dimitriev, O. P., Grinko, D. A., Noskov, Y. V., Ogurtsov, N. A. & Pud, A. A. PEDOT:PSS films—Effect of organic solvent additives and annealing on the film conductivity. *Synthetic Metals* **159**, 2237-2239, doi:https://doi.org/10.1016/j.synthmet.2009.08.022 (2009).

88 Liu, Z. *et al.* Transparent conductive electrodes from graphene/PEDOT:PSS hybrid inks for ultrathin organic photodetectors. *Advanced Materials* **27**, 669-675, doi:10.1002/adma.201403826 (2015).

89 Lingstedt, L. V. *et al.* Effect of DMSO Solvent Treatments on the Performance of PEDOT:PSS Based Organic Electrochemical Transistors. *Advanced Electronic Materials* **5**, 1800804, doi:10.1002/aelm.201800804 (2019).

90 Chou, T.-R., Chen, S.-H., Chiang, Y.-T., Lin, Y.-T. & Chao, C.-Y. Highly conductive PEDOT:PSS films by post-treatment with dimethyl sulfoxide for ITO-free liquid crystal display. *Journal of Materials Chemistry C* **3**, 3760-3766, doi:10.1039/C5TC00276A (2015).

91 Xia, Y., Sun, K. & Ouyang, J. Solution-processed metallic conducting polymer films as transparent electrode of optoelectronic devices. *Advanced Materials* **24**, 2436-2440, doi:10.1002/adma.201104795 (2012).

92 Zhang, S. *et al.* Solvent-induced changes in PEDOT:PSS films for organic electrochemical transistors. *APL Materials* **3**, 014911, doi:10.1063/1.4905154 (2014).

93 Khodagholy, D. *et al.* In vivo recordings of brain activity using organic transistors. *Nature Communications* **4**, 1575, doi:10.1038/ncomms2573 (2013).

94 Yang, S. Y. *et al.* Electrochemical transistors with ionic liquids for enzymatic sensing. *Chemical Communications* **46**, 7972-7974, doi:10.1039/C0CC02064H (2010).

95 Kergoat, L. *et al.* Detection of Glutamate and Acetylcholine with Organic Electrochemical Transistors Based on Conducting Polymer/Platinum Nanoparticle Composites. *Advanced Materials* **26**, 5658-5664, doi:10.1002/adma.201401608 (2014).

96 Gold, C., Henze, D. A., Koch, C. & Buzsaki, G. On the origin of the extracellular action potential waveform: A modeling study. *Journal of Neurophysiology* **95**, 3113-3128, doi:10.1152/jn.00979.2005 (2006).

97 Jackson, A. & Fetz, E. E. Compact Movable Microwire Array for Long-Term Chronic Unit Recording in Cerebral Cortex of Primates. *Journal of Neurophysiology* **98**, 3109-3118, doi:10.1152/jn.00569.2007 (2007).

98 Salatino, J. W., Ludwig, K. A., Kozai, T. D. Y. & Purcell, E. K. Glial responses to implanted electrodes in the brain. *Nature Biomedical Engineering* **1**, 862-877, doi:10.1038/s41551-017-0154-1 (2017).

99 Wang, J. *et al.* Core–Shell Microneedle Gel for Self-Regulated Insulin Delivery. *ACS Nano* **12**, 2466-2473, doi:10.1021/acsnano.7b08152 (2018).

100 Bertassoni, L. E. *et al.* Hydrogel bioprinted microchannel networks for vascularization of tissue engineering constructs. *Lab on a Chip* **14**, 2202-2211, doi:10.1039/C4LC00030G (2014).

101 Keplinger, C. *et al.* Stretchable, Transparent, Ionic Conductors. *Science* **341**, 984-987, doi:10.1126/science.1240228 (2013).

102 Kharaziha, M. *et al.* Tough and flexible CNT-polymeric hybrid scaffolds for engineering cardiac constructs. *Biomaterials* **35**, 7346-7354, doi:10.1016/j.biomaterials.2014.05.014 (2014).

103 Xu, Y. *et al.* Noncovalently Assembled Electroconductive Hydrogel. *ACS Applied Materials & Interfaces* **10**, 14418-14425, doi:10.1021/acsami.8b01029 (2018).

104 Warren, H. & Panhuis, M. i. h. Electrically Conducting PEDOT:PSS – Gellan Gum Hydrogels. *MRS Proceedings* **1569**, 219-223, doi:10.1557/opl.2013.1101 (2013).

105 Feig, V. R., Tran, H., Lee, M. & Bao, Z. Mechanically tunable conductive interpenetrating network hydrogels that mimic the elastic moduli of biological tissue. *Nature Communications* **9**, 2740, doi:10.1038/s41467-018-05222-4 (2018).

106 Ali, M. A., Wu, K.-H., McEwan, J. & Lee, J. Translated structural morphology of conductive polymer nanofilms synthesized by vapor phase polymerization. *Synthetic Metals* **244**, 113-119, doi:https://doi.org/10.1016/j.synthmet.2018.07.007 (2018).

107 Dai, T., Qing, X., Lu, Y. & Xia, Y. Conducting hydrogels with enhanced mechanical strength. *Polymer* **50**, 5236-5241, doi:https://doi.org/10.1016/j.polymer.2009.09.025 (2009).

108 Abidian, M. R. & Martin, D. C. Multifunctional Nanobiomaterials for Neural Interfaces. *Advanced Functional Materials* **19**, 573-585, doi:10.1002/adfm.200801473 (2009).

109 Sekine, S., Ido, Y., Miyake, T., Nagamine, K. & Nishizawa, M. Conducting polymer electrodes printed on hydrogel. *Journal of the American Chemical Society* **132**, 13174-13175, doi:10.1021/ja1062357 (2010).

110 Aouada, F. A. *et al.* Electrochemical and mechanical properties of hydrogels based on conductive poly(3,4-ethylene dioxythiophene)/poly(styrenesulfonate) and PAAm. *Polymer Testing* **25**, 158-165, doi:https://doi.org/10.1016/j.polymertesting.2005.11.005 (2006).

111 Wu, Q. *et al.* A robust, highly stretchable supramolecular polymer conductive hydrogel with self-healability and thermo-processability. *Scientific Reports* **7**, 41566, doi:10.1038/srep41566 (2017).

112 Leaf, M. A. & Muthukumar, M. Electrostatic Effect on the Solution Structure and Dynamics of PEDOT:PSS. *Macromolecules* **49**, 4286-4294, doi:10.1021/acs.macromol.6b00740 (2016).

113 Ghosh, S. & Inganäs, O. Conducting Polymer Hydrogels as 3D Electrodes: Applications for Supercapacitors. *Advanced Materials* **11**, 1214-1218, doi:10.1002/(sici)1521-4095(199910)11:14<1214::Aid-adma1214>3.0.Co;2-3 (1999).

114 Yao, B. *et al.* Ultrahigh-Conductivity Polymer Hydrogels with Arbitrary Structures. *Advanced Materials* **29**, 1700974, doi:10.1002/adma.201700974 (2017).

115 White, H. S., Kittlesen, G. P. & Wrighton, M. S. Chemical derivatization of an array of three gold microelectrodes with polypyrrole: fabrication of a molecule-based transistor. *Journal of the American Chemical Society* **106**, 5375-5377, doi:10.1021/ja00330a070 (1984).

116 Bernards, D. A. & Malliaras, G. G. Steady-State and Transient Behavior of Organic Electrochemical Transistors. *Advanced Functional Materials* **17**, 3538-3544, doi:10.1002/adfm.200601239 (2007).

117 Owens, R. M. & Malliaras, G. G. Organic Electronics at the Interface with Biology. *MRS Bulletin* **35**, 449-456, doi:10.1557/mrs2010.583 (2010).

118 Yao, C., Li, Q., Guo, J., Yan, F. & Hsing, I. M. Rigid and flexible organic electrochemical transistor arrays for monitoring action potentials from electrogenic cells. *Advanced healthcare materials* **4**, 528-533, doi:10.1002/adhm.201400406 (2015).

119 Zhang, S. *et al.* Patterning of Stretchable Organic Electrochemical Transistors. *Chemistry of Materials* **29**, 3126-3132, doi:10.1021/acs.chemmater.7b00181 (2017).

120 Zeglio, E. & Inganas, O. Active Materials for Organic Electrochemical Transistors. *Advanced Materials* **30**, e1800941, doi:10.1002/adma.201800941 (2018).

121 Nilsson, D. *et al.* Bi-stable and Dynamic Current Modulation in Electrochemical Organic Transistors. *Advanced Materials* **14**, 51-54, doi:10.1002/1521-4095(20020104)14:1<51::Aid-adma51>3.0.Co;2-# (2002).

122 Peng, B. *et al.* High performance organic transistor active-matrix driver developed on paper substrate. *Scientific Reports* **4**, 6430, doi:10.1038/srep06430 (2014).

123 Bao, Z. & Chen, X. Flexible and Stretchable Devices. *Advanced Materials* **28**, 4177-4179, doi:10.1002/adma.201601422 (2016).

124 Facchetti, A. Semiconductors for organic transistors. *Materials Today* **10**, 28-37, doi:https://doi.org/10.1016/S1369-7021(07)70017-2 (2007).

125 Xu, Y., Liu, C., Khim, D. & Noh, Y. Y. Development of high-performance printed organic field-effect transistors and integrated circuits. *Phys Chem Chem Phys* **17**, 26553-26574, doi:10.1039/c4cp02413c (2015).

126 Rivnay, J. *et al.* Organic electrochemical transistors. *Nature Reviews Materials* **3**, 17086, doi:10.1038/natrevmats.2017.86 (2018).

127 Rivnay, J. *et al.* Organic electrochemical transistors with maximum transconductance at zero gate bias. *Advanced Materials* **25**, 7010-7014 (2013).

128 Rivnay, J. *et al.* High-performance transistors for bioelectronics through tuning of channel thickness. **1**, e1400251, doi:10.1126/sciadv.1400251 %J Science Advances (2015).

129 Contat-Rodrigo, L., Pérez-Fuster, C., Lidón-Roger, J. V., Bonfiglio, A. & García-Breijo, E. Characterization of Screen-Printed Organic Electrochemical Transistors to Detect Cations of Different Sizes. *Sensors (Basel, Switzerland)* **16**, 1599, doi:10.3390/s16101599 (2016).

130 Bernards, D. A. *et al.* Enzymatic sensing with organic electrochemical transistors. *Journal of Materials Chemistry* **18**, 116-120, doi:10.1039/B713122D (2008).

131 Shim, N. Y. *et al.* All-plastic electrochemical transistor for glucose sensing using a ferrocene mediator. *Sensors (Basel, Switzerland)* **9**, 9896-9902, doi:10.3390/s91209896 (2009).

132 Bihar, E. *et al.* A fully inkjet-printed disposable glucose sensor on paper. *npj Flexible Electronics* **2**, 30, doi:10.1038/s41528-018-0044-y (2018).

133 Tao, W. *et al.* A sensitive DNA sensor based on an organic electrochemical transistor using a peptide nucleic acid-modified nanoporous gold gate electrode. *RSC Advances* **7**, 52118-52124, doi:10.1039/C7RA09832D (2017).

134 Gualandi, I. *et al.* Selective detection of dopamine with an all PEDOT:PSS Organic Electrochemical Transistor. *Scientific Reports* **6**, 35419, doi:10.1038/srep35419 (2016).

135 Zhang, S. *Processing and Patterning of Conducting Polymer Films for Flexible, Stretchable and Healable Electronics*, École Polytechnique de Montréal, (2017).

136 van de Burgt, Y. *et al.* A non-volatile organic electrochemical device as a low-voltage artificial synapse for neuromorphic computing. *Nature Materials* **16**, 414-418, doi:10.1038/nmat4856 (2017).

137 Rivnay, J. *et al.* Organic electrochemical transistors for cell-based impedance sensing. *Applied Physics Letters* **106**, 043301, doi:10.1063/1.4906872 (2015).

138 Gualandi, I. *et al.* Selective detection of dopamine with an all PEDOT:PSS Organic Electrochemical Transistor. *Scientific Reports* **6**, 35419, doi:10.1038/srep35419

https://www.nature.com/articles/srep35419#supplementary-information (2016).

139 Pitsalidis, C. *et al.* Transistor in a tube: A route to three-dimensional bioelectronics. *Science Advances* **4**, eaat4253, doi:10.1126/sciadv.aat4253 (2018).

140 Tria, S. A., Ramuz, M., Jimison, L. H., Hama, A. & Owens, R. M. Sensing of barrier tissue disruption with an organic electrochemical transistor. *Journal of visualized experiments : JoVE*, e51102-e51102, doi:10.3791/51102 (2014).

141 Ramuz, M., Hama, A., Rivnay, J., Leleux, P. & Owens, R. M. Monitoring of cell layer coverage and differentiation with the organic electrochemical transistor. *Journal of Materials Chemistry B* **3**, 5971-5977, doi:10.1039/C5TB00922G (2015).

142 Cicoira, F. *et al.* Influence of Device Geometry on Sensor Characteristics of Planar Organic Electrochemical Transistors. *Advanced Materials* **22**, 1012-1016, doi:10.1002/adma.200902329 (2010).

143 Ghittorelli, M. *et al.* High-sensitivity ion detection at low voltages with current-driven organic electrochemical transistors. *Nature Communications* **9**, 1441, doi:10.1038/s41467-018-03932-3 (2018).

144 Kim, Y. *et al.* Organic electrochemical transistor-based channel dimension-independent single-strand wearable sweat sensors. *NPG Asia Materials* **10**, 1086-1095, doi:10.1038/s41427-018-0097-3 (2018).

145 Liao, C., Mak, C., Zhang, M., Chan, H. L. W. & Yan, F. Flexible Organic Electrochemical Transistors for Highly Selective Enzyme Biosensors and Used for Saliva Testing. *Advanced Materials* **27**, 676-681, doi:10.1002/adma.201404378 (2015).

146 Piro, B. *et al.* Fabrication and Use of Organic Electrochemical Transistors for Sensing of Metabolites in Aqueous Media. *Applied Sciences* **8**, doi:10.3390/app8060928 (2018).

147 Groenendaal, L., Jonas, F., Freitag, D., Pielartzik, H. & Reynolds, J. R. Poly(3,4-ethylenedioxythiophene) and Its Derivatives: Past, Present, and Future. *Advanced Materials* **12**, 481-494, doi:10.1002/(sici)1521-4095(200004)12:7<481::Aid-adma481>3.0.Co;2-c (2000).

148 Lipomi, D. J., Tee, B. C.-K., Vosgueritchian, M. & Bao, Z. Stretchable Organic Solar Cells. *Advanced Materials* **23**, 1771-1775, doi:10.1002/adma.201004426 (2011).

149 Liu, Y.-s. *et al.* Ultrasmooth, highly conductive and transparent PEDOT:PSS/silver nanowire composite electrode for flexible organic light-emitting devices. *Organic Electronics* **31**, 247-252, doi:https://doi.org/10.1016/j.orgel.2016.01.014 (2016).

150 Crispin, X. *et al.* The Origin of the High Conductivity of Poly(3,4-ethylenedioxythiophene)−Poly(styrenesulfonate) (PEDOT−PSS) Plastic Electrodes. *Chemistry of Materials* **18**, 4354-4360, doi:10.1021/cm061032+ (2006).

151 Fuller, E. J. *et al.* Parallel programming of an ionic floating-gate memory array for scalable neuromorphic computing. *Science* **364**, 570-574, doi:10.1126/science.aaw5581 (2019).

152 Gund, G. S. *et al.* MXene/Polymer Hybrid Materials for Flexible AC-Filtering Electrochemical Capacitors. *Joule* **3**, 164-176, doi:https://doi.org/10.1016/j.joule.2018.10.017 (2019).

153 Patel, S. R. & Lieber, C. M. Precision electronic medicine in the brain. *Nature Biotechnology* **37**, 1007-1012, doi:10.1038/s41587-019-0234-8 (2019).

154 Spencer, A. R. *et al.* Electroconductive Gelatin Methacryloyl-PEDOT:PSS Composite Hydrogels: Design, Synthesis, and Properties. *ACS Biomaterials Science & Engineering* **4**, 1558-1567, doi:10.1021/acsbiomaterials.8b00135 (2018).

155 Tondera, C. *et al.* Highly Conductive, Stretchable, and Cell-Adhesive Hydrogel by Nanoclay Doping. *Small* **0**, 1901406, doi:10.1002/smll.201901406 (2019).

156 Zhang, S. & Cicoira, F. Water-Enabled Healing of Conducting Polymer Films. *Advanced Materials* **29**, 1703098, doi:10.1002/adma.201703098 (2017).

157 Poolman, J. M. *et al.* Variable gelation time and stiffness of low-molecular-weight hydrogels through catalytic control over self-assembly. *Nature Protocols* **9**, 977-988, doi:10.1038/nprot.2014.055 (2014).

158 Zhou, J. *et al.* The temperature-dependent microstructure of PEDOT/PSS films: insights from morphological, mechanical and electrical analyses. *Journal of Materials Chemistry C* **2**, 9903-9910, doi:10.1039/C4TC01593B (2014).

159 Song, G. *et al.* Rheological Behavior of Tough PVP-in Situ-PAAm Hydrogels Physically Cross-Linked by Cooperative Hydrogen Bonding. *Macromolecules* **49**, 8265-8273, doi:10.1021/acs.macromol.6b01448 (2016).

160 Gaharwar, A. K. *et al.* Physically Crosslinked Nanocomposites from Silicate-Crosslinked PEO: Mechanical Properties and Osteogenic Differentiation of Human Mesenchymal Stem Cells. *Macromolecular Bioscience* **12**, 779-793, doi:10.1002/mabi.201100508 (2012).

161 Ramon, C., Schimpf, P. H. & Haueisen, J. Influence of head models on EEG simulations and inverse source localizations. *BioMedical Engineering OnLine* **5**, 10, doi:10.1186/1475-925X-5-10 (2006).

162 Liu, J. *et al.* Syringe-injectable electronics. *Nature Nanotechnology* **10**, 629-636, doi:10.1038/nnano.2015.115 (2015).

163 Fu, T.-M. *et al.* Stable long-term chronic brain mapping at the single-neuron level. *Nature Methods* **13**, 875-882, doi:10.1038/nmeth.3969 (2016).

164 Hong, G. *et al.* Syringe Injectable Electronics: Precise Targeted Delivery with Quantitative Input/Output Connectivity. *Nano Letters* **15**, 6979-6984, doi:10.1021/acs.nanolett.5b02987 (2015).

165 Avery, R. K. *et al.* An injectable shear-thinning biomaterial for endovascular embolization. *Science translational medicine* **8**, 365ra156-365ra156, doi:10.1126/scitranslmed.aah5533 (2016).

166 Goding, J., Gilmour, A., Martens, P., Poole-Warren, L. & Green, R. Interpenetrating Conducting Hydrogel Materials for Neural Interfacing Electrodes. *Advanced Healthcare Materials* **6**, 1601177, doi:10.1002/adhm.201601177 (2017).

167 Sun, J.-Y. *et al.* Highly stretchable and tough hydrogels. *Nature* **489**, 133-136, doi:10.1038/nature11409 (2012).

168 Huang, S. H. *et al.* Whispering gallery mode resonator sensor for in situ measurements of hydrogel gelation. *Optics Express* **26**, 51-62, doi:10.1364/OE.26.000051 (2018).

169 Zhang, E., Bai, R., Morelle, X. P. & Suo, Z. Fatigue fracture of nearly elastic hydrogels. *Soft Matter* **14**, 3563-3571, doi:10.1039/C8SM00460A (2018).

170 Liu, H. *et al.* Spatially modulated stiffness on hydrogels for soft and stretchable integrated electronics. *Materials Horizons* **7**, 203-213, doi:10.1039/C9MH01211G (2020).

171 Liu, Y. *et al.* Morphing electronics enable neuromodulation in growing tissue. *Nature Biotechnology*, doi:10.1038/s41587-020-0495-2 (2020).

172 Yoo, P. B. & Grill, W. M. Minimally-invasive electrical stimulation of the pudendal nerve: a pre-clinical study for neural control of the lower urinary tract. *Neurourol Urodyn* **26**, 562-569, doi:10.1002/nau.20376 (2007).

173 Anikeeva, P. *et al.* Optetrode: a multichannel readout for optogenetic control in freely moving mice. *Nature Neuroscience* **15**, 163, doi:10.1038/nn.2992 (2012).

174 Canales, A. *et al.* Multifunctional fibers for simultaneous optical, electrical and chemical interrogation of neural circuits in vivo. *Nature Biotechnology* **33**, 277-284, doi:10.1038/nbt.3093 (2015).

175 Laforgue, A. All-textile flexible supercapacitors using electrospun poly(3,4-ethylenedioxythiophene) nanofibers. *Journal of Power Sources* **196**, 559-564, doi:https://doi.org/10.1016/j.jpowsour.2010.07.007 (2011).

176 Knowlton, S. *et al.* 3D-printed microfluidic chips with patterned, cell-laden hydrogel constructs. *Biofabrication* **8**, 025019, doi:10.1088/1758-5090/8/2/025019 (2016).

177 Khademhosseini, A. & Langer, R. Microengineered hydrogels for tissue engineering. *Biomaterials* **28**, 5087-5092 (2007).

178 Khodagholy, D. *et al.* NeuroGrid: recording action potentials from the surface of the brain. *Nature Neuroscience* **18**, 310-315, doi:10.1038/nn.3905 (2015).